The Impact of the Predictability of Continental Tropical Lows on Hydrological Modelling: Current State and Future Projections

Report to the
Water Research Commission

by

Liesl Dyson[1], Elizabeth Webster[1,2], Christina Botai[2], Jaco de Wit[2] and Francois Engelbrecht[3,4]

1. University of Pretoria
2. South African Weather Service
3. Council for Scientific and Industrial Research
4. University of the Witwatersrand

WRC Report No. 2510/1/21
ISBN 978-0-6392-0294-5

October 2021

Obtainable from
Water Research Commission
Private Bag X03
Gezina, 0031
Pretoria

orders@wrc.org.za or download from www.wrc.org.za

Executive Summary

This report deals with Continental Tropical Low (CTL) pressure systems which occur fairly regularly in late summer over southern Africa. Before the commencement of this research it was known that these weather systems have in the past been responsible for widespread and heavy rainfall over South Africa. In this report the character of CTLs are explored by creating a synoptic climatology and also to quantify the rainfall contributions of these systems to South African rainfall.

An objective, repeatable method was developed to identify CTLs over southern Africa. The identification method places strict constrains on the atmospheric circulation in order to eliminate weaker low pressure system such as the Angola Low. The objective method was applied to NCEP reanalysis data from 1979-2018 from December to March in order to create a synoptic climatology of CTLs. This climatology is the first of its kind over southern Africa and advances knowledge of synoptic scale weather systems over South Africa.

The results show that CTLs occur most frequently occur over southern Angola and Zambia. There is an average of 19 CTL days per year across the domain, however, over the central interior of South Africa, the return period 78 years. CTLs occur most often during January with 36% of CTL events while CTLs seldom occur in December with only 15%. It was also found that CTL events do not show any real diurnal trends, however, they do occur most regularly at 18Z. The average life-span of a CTL is between 1-3 days, although there are rare occasions when they last for more than 13 days. The longest a CTL existed during the study period was in January 2017, when it lasted for 19-days. There is an increasing trend in CTLs over southern Africa with the most significant trend being in January. Warm ENSO events are associated with below normal CTL events and during cold ENSO events there is an increase in the number of CTLs.

The geographical area where rainfall is influenced by CTLs is enormous. In this research an area of 10 x 10 degrees surrounding the position of the CTL was investigated for rainfall occurrence. This is an area of approximately 1 million square kilometres. It was found that the heaviest, most widespread rainfall occur to the east of the CTL and although the rainfall amounts west of the CTLS are generally less it can still cause rainfall some 500 km west of the CTL.

The highest CTL rainfall occur during January, also the month with the highest number of CTLs. The geographical distribution of CTL rainfall in December months is mainly confined to the north-eastern parts of South Africa with the highest rainfall recorded when a CTL is positioned over north-eastern KwaZulu-Natal. By February months, the CTL rainfall distribution spreads further towards the west and by

March the rainfall reaches the western interior of the country. This demonstrates that the CTL rainfall has a clear westward shift from December to March and plays an extremely important role in bringing rainfall to the arid western half of South Africa. Major rain events (MREs) are defined as an event where the average rainfall over a NCEP rain area exceeds 10 mm and at least one rainfall station measures at least 50 mm within the NCEP rain area. During the study period, a total of 447 MREs occurred with an average 12 per year.

The uncertainty in the forecasting of CTLs up to 3-days ahead is much less than in COLs. In the westerly systems standard deviations of up to 40 m are observed as the ensemble members struggle to pinpoint the location and depth of 500hPa lows. The errors are particularly large for eastward movement systems. The position and depth of CTLs are dealt with more adequately by the ensemble members with standard deviation values generally being less than 10 m. There is also not a trend for errors to increase off-stream in CTLs. However, even though CTLs are dealt with much better than COLs slight differences in position and depth of the CTL can have a significant influence on the rainfall associated with it.

There is predicted to be a general increase in warm cored mid-tropospheric lows over South Africa towards the end of the century. The ensemble average of five CCAM climate projections shows that the number of warm lows over Zambia and Angola is expected to decrease with a slight increase in lows over Namibia. Botswana and north-eastern South Africa. Over the central coast of Namibia there is predicted to be a 40% increase in the number of lows towards the end of the century. The increase in the number lows at this grid point could lead to an increase in the number of heavy rainfall events over northern Limpopo an especially the escarpment.

Streamflow simulations from 10 ECHAM4.5-MOM3 model ensemble members were evaluated to assess the impact of precipitation uncertainty in streamflow forecasting. The results depict a potential 1:1 influence of mean annual precipitation changes to the changes in mean annual streamflow across the model ensemble members. There exists a substantial variation in streamflow simulations across the model ensemble members and across the drainage regions of LRB, with the majority of the model ensemble members overestimating the simulated streamflow. The observed variations in streamflow simulations can be attributed to the differences in model ensemble members' structures. In addition, 14-days and 28-days lead time streamflow forecasts during January 2017 show apparent contrasting uncertainties among the ensemble members, with the longer lead time forecasts depicting more pronounced uncertainty. Overall, the results have important scientific and practical applications. From the scientific perspective, this study points to the need for a holistic consideration of hydrometeorological model parameterization, catchment initial conditions, meteorological inputs, as well as coupling of both climatic and non-climatic drivers. For practical purposes, this study could be seen as a precursor to the development of multi-model rainfall-runoff streamflow forecasting applications or services in an operationally realistic scenario. If such a system is tested and calibrated, then it could be useful to water resources managers in the LRB, for aiding policy planning for future practices, as well as to the South African water management agencies in general.

Four students participated in this project. Elizabeth Webster was awarded an MSc (Meteorology) while Matshidiso Mogale, Lehlohonolo Thobela and Sibongile Mabaso all completed Hons research projects on tropical weather. A workshop demonstrating the importance and widespread impact of CTLs was held and attended by young weather forecasters from all over Pretoria. Initial indications are that the information is now being used in the operational forecasting offices.

Acknowledgements

The project team express their appreciation to the WRC for funding the research and especially to Dr Brilliant Petja for his support and encouragement during the project. We are also indebted to the project Reference Group, who has actively participated in project meetings and have made useful suggestions to improve the research. We would like to single out Dr Eugene Poolman who passed away during the course of this research project. Many ideas used in this research in one way or another originated from him. We also acknowledge the South African Weather Service for providing rainfall data.

The reference group consisted of

Dr N Davis	University of Pretoria
Dr C Lennard	University of Cape Town
Dr C Engelbrecht	Agricultural Research Council
Dr J Malherbe	Council for Scientific and Industrial Research
Dr T Ndarana	University of Pretoria
Dr H Chikoore	University of Venda
Dr E Poolman	South African Weather Service
Ms S Landman	South African Weather Service
Mr M Geldenhuys	South African Weather Service

Table of Contents

List of Figures

List of Tables

This page was intentionally left blank

Chapter 1: Introduction

1.1 Background

Tropical weather systems invade the northern parts of South Africa during the late summer months and are often associated with heavy rainfall and flooding (Dyson and Van Heerden, 2002). Tropical disturbances hardly ever occur between April and October, but rather have a peak between December and February (Preston-Whyte and Tyson, 1993). Dyson and Van Heerden (2002) stated that due to the high frequency of heavy rainfall events that occur in summer over the eastern and north-eastern parts of South Africa, it is important to develop better forecasting techniques that can identify and predict tropical weather systems.

Dyson and Van Heerden (2002) also stated that due to tropical weather systems only affecting South Africa three or four times a year, forecasters often do not have the necessary experience to identify these systems ahead of time. Nevertheless, Poolman, contributing to Dyson et al. (2002) found that the contribution of heavy rainfall days that occur during the summer months and the weather systems that are responsible for them are far more important for the South African hydrology than the heavy rainfall days that occur in the winter months and their associated weather systems. Tropical weather systems play an important role in southern Africa's weather and there is therefore a need to accurately identify tropical weather systems and with a fair amount of lead-time in order for weather alerts to be sent out in a timeous manner and to be acted upon. It is also important to understand how well numerical weather prediction (NWP) deals with predicting the depth and position of these systems and how the forecast uncertainty impacts on hydrological modelling. As tropical weather systems are major rain producers for southern Africa it is imperative to understand what will happen to these systems in a future climate.

In January 2017, a well-developed Continental Tropical Low (CTL) developed over southern Africa, causing flooding of houses and roads. However, even though this synoptic scale weather system was clearly identifiable on satellite imagery (Fig. 1.2), forecasters failed to classify this system as a CTL (SAWS, 2017). It is clear that there is a need to enhance the understanding and identification of these synoptic scale weather systems over southern Africa.

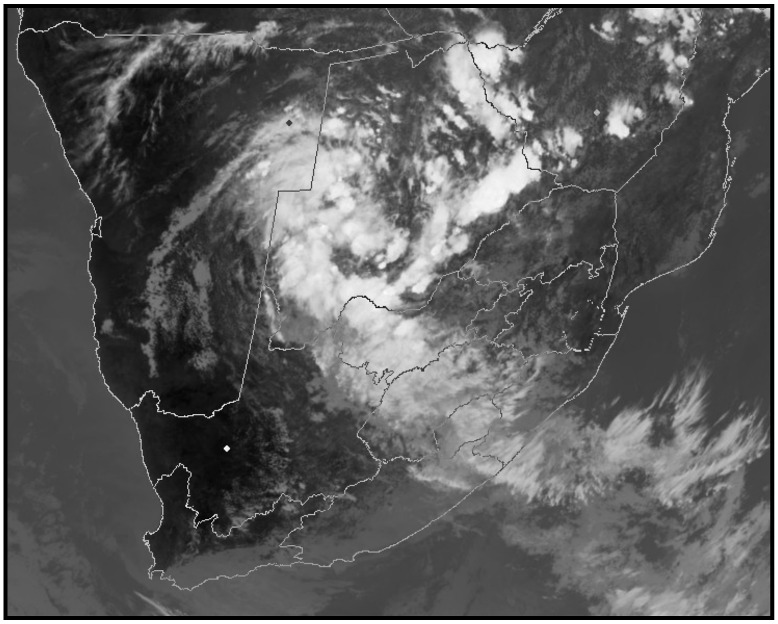

1.2 Aims and objectives of the research

The overall aim of this report is to investigate the character of CTLs over southern Africa in the current and future climate. Specific objectives are to

a. Develop an objective identification methods to identify CTLs.
b. Describe the synoptic climatology of CTLs over southern Africa
c. Identify the rainfall contribution of CTLs to South Africa
d. Investigate the forecast uncertainty of CTLs.
e. Investigate the impact of forecast uncertainty of CTLs of stream flow in the Limpopo Province.

1.3 Report Outline

This report consists of ten chapters. This first chapter introduces the rationale of the study and gives a synopsis of the project aims and objectives. Additional background to the research is provided in the next chapter, along with its contextualisation within the existing literature. Chapter 3 describes the objective identification method used to identify CTLs while Chapters 4 and 5 provides the synoptic and rainfall climatologies associated with CTLs. A CTL case examples is provided in Chapter 6. Chapters 7 and 8 provides information on the forecasting uncertainty of CTLs and details the change in frequency of CTLs in a future climate. Chapter 9 discuss the impact of uncertainty on hydrological modelling over the Limpopo Province. Chapter 10 is a list of main findings of this study and recommendations for future research.

Chapter 2: Literature review and background on tropical weather systems over South Africa

2.1 Introduction

The tropical region can generally be defined as the area demarcated between the Tropic of Cancer (23.5°N) and the Tropic of Capricorn (23.5°S) (Asnani, 2005) and is the source of most of the heat and momentum in the atmosphere (Riehl, 1979). Tropical weather systems, however, are not fixed by these boundaries, but rather follow the position of the sun (Asnani, 2005).

The tropics are generally dominated by rising air while over the subtropics there is sinking air, this causes the formation of the Hadley cell (Laing and Evans, 2016). The Hadley cell causes the meridional circulation in the tropics, which in turn transports heat and momentum to higher latitudes (Asnani, 2005). The equatorial zone is dominated by a low pressure belt, called the equatorial trough, with an area of high pressure found over the subtropics, known as the subtropical high pressure belt (Riehl, 1979). In the area between these two belts, lies a region that is dominated by easterly winds, which have become known as the trade winds (Riehl, 1979).

The weather that occurs in tropical areas ranges from cloudless skies during the dry season to intense rain and winds associated with tropical cyclones (Ramage, 1995). Worldwide, tropical weather systems are known to result in devastating floods, but are also responsible for providing critical rainfall to many regions (Anthes, 1982) which often determines the success of crops (Riehl, 1979).

South Africa is positioned such that the Tropic of Capricorn tracks through the extreme north-eastern parts of the country. Tropical weather systems therefore extend into the northern parts of the republic during the summer months and many be associated with heavy rainfall and flooding (Dyson and Van Heerden, 2002). Over southern Africa, January to March is generally the season with the highest rainfall and is also the period that is mainly linked to tropical circulation (Richard *et al.,* 2001). Southern Africa, broadly defined here as the African countries south of approximately 10°S and represented in Fig. 1.1, is generally regarded as a semi-arid region that has greater variability in rainfall (Blamely and Reason, 2012).

Tropical weather systems occur infrequently over South Africa but nevertheless play a major role in the weather of southern Africa. These systems invade the northern parts of South Africa during the late summer months and are often associated with heavy rainfall and flooding (Dyson and Van Heerden, 2002). Preston-Whyte and Tyson (1993) stated that tropical disturbances have a peak between December and February and are typically late summer weather systems.

2.2 Tropical dynamics

Holton (1992) defines a barotropic atmosphere as one in which the density is a function of pressure alone. This means that isobaric surfaces are also surfaces of constant temperature so that the there is no temperature gradient on a pressure level. In the absence of a temperature gradient the thermal wind will also be zero. The thermal wind is the vector difference between the geostrophic wind on two pressure levels. When the thermal wind is equal to zero the geostrophic wind will not change with height. Therefore in such a theoretical barotropic atmosphere the gradient of geopotential energy remains constant with height and synoptic scale high and low pressure systems will in this ideal situation "stand upright" with height.

Holton (1992) further states that barotrophy provides very strong constraints on the motions in a rotating fluid and is in fact never achieved in the atmosphere. Nevertheless in a tropical atmosphere the circulation will tend towards this situation and low pressure systems will stand upright with height. In the real tropical atmosphere strong surface and middle tropospheric convergence occurs in association with the "upright" low-pressure system. This convergence in turn results in upward motion and if adequate water vapour is available convective cloud or so-called "hot towers" will develop. Riehl (1979) explains the process by which the hot towers act as energy tubes through which energy from the lower troposphere is transported to the upper troposphere where it is distributed horizontally by the upper air divergence. The condensation releases a large amount of latent heat, which is in turn responsible for above normal upper tropospheric temperatures (Triegaardt et at., 1991). The latent heat release therefore, quickly results in a warm core developing above the lower level low (Taljaard, 1985) and tropical lows are characterised by a warm core of temperatures in the middle and upper troposphere. Holton (1992) shows that the geopotential thickness of a layer is directly proportional to the average column temperature with the result that an upper tropospheric high-pressure system forms above the surface low. Furthermore this diverging upper tropospheric high is associated with moist conditions and strong convergence at higher pressure levels.

2.3 Tropical weather systems of South Africa

The main tropical weather systems that affect southern Africa all have some of the tropical dynamical characteristics. The most prevalent being tropical cyclones but the inter-tropical convergence zone, tropical temperate troughs also play a dominate role. CTLs the focus of this research also have very distinct tropical characteristics.

Tropical cyclones are warm-cored cyclonic vortices (Kepert, contributing to Chan and Kepert, 2010), that develop over warm tropical oceans (Anthes, 1982). In the south-west Indian Ocean, a tropical disturbance is classified as a tropical depression once the maximum wind speed reaches between 34-63 knots (Ramage, 1995). There is an average of eleven tropical disturbances that reach tropical depression intensity in the south-west Indian Ocean each summer season (Jury and Pathack, 1991). These systems do not make landfall every year (Malherbe *et al.,* 2012) in fact, less than 5% of tropical cyclones that occur in the south-west Indian Ocean make landfall over southern Africa (Reason and Keibel, 2004, Chikoore *et al.,* 2015). Nevertheless, when these systems do make landfall over southern Africa, they tend to move over areas where large river basins are situated, resulting in enormous impacts downstream due to flooding (Malherbe *et al.,* 2012). . Tropical systems that develop over the ocean and make landfall are responsible for about 50% of the widespread heavy rainfall events over the north-eastern parts of South Africa (Malherbe *et al.,* 2011).

One of the key climatological components of the global atmosphere is the Inter-Tropical Convergence Zone (ITCZ) (Zagar *et al.,* 2011) and is said to be one of the most vital mechanisms of the climate system (Berry and Reeder, 2013). The ITCZ is an area of low pressure that extends around the globe in close proximity to the equator (Taljaard, 1994). The positioning of the ITCZ has a major effect on the annual rainfall over southern Africa (Harrison, 1986) and the overall weather conditions in South Africa (Taljaard, 1994). The position of the ITCZ and the inter-ocean convergence zone troughs during summer are the average locations of zones of convergence as well as zones of active weather (Van Heerden and Taljaard, contributing to Karoly and Vincent, 1998). In the northern hemisphere summer, the ITCZ reaches 20°N and in the southern hemisphere summer, it extends to 17°S (Taljaard, 1994).

During these summer months in southern Africa, when the ITCZ is furthest south, there is generally a low-level tropical/subtropical low pressure that extends a trough southwards across the continent reaching South Africa (Williams *et al*., 1984). Reason *et al.* (2006) defined this low as the Angola Low pressure, which is a shallow heat low that starts to develop over northern Namibia and southern

Angola around October, strengthening in January and February. The Angola Low pressure has been recognised as a cyclonic moisture convergence area that is one of the governing features of rainfall of southern Africa (Mulenga, 1998).

In some instances, the tropical low pressure will interact with a temperate westerly trough and form a cloud band across the subcontinent (Washington and Todd, 1999). These long bands of clouds are one of the major distinguishing features of the southern hemisphere circulation that can be seen on satellite imagery (Harrison, 1986) and represent tropical temperate troughs (TTTs) (Crimp *et al.,* 1997). Tropical temperate troughs can be described as areas of increased convergence that connect tropical and temperate systems (Crimp *et al.,* 1997), which transport energy, moisture and momentum from the tropical to the temperate regions (Harrison, 1986; Van den Heever *et al.,* 1997). TTTs are not unique to southern Africa, but can be found in many regions, including Australia and South America (Hart *et al.,* 2010; Van den Heever *et al.,* 1997). Crimp *et al.* (1997) found that tropical-temperate troughs contribute to approximately 30% of the total rainfall for October and December, 60% of the total rainfall for January and 39% of the mean annual total for southern Africa.

This report focuses on continental tropical low pressure systems (CTL) over the interior of southern Africa. Van Heerden and Taljaard, contributing to Karoly and Vincent (1998) stated that tropical low pressures are one of the three low pressure systems that prevail at low latitudes with the other two being tropical cyclones and heat lows. CTLs are generally defined as having a cool core in the lowest 3-4 km of the low pressure with a warm core aloft (Van Heerden and Taljaard, contributing to Karoly and Vincent, 1998). These weather systems have a typical scale of 500-1000 km (Engelbrecht *et al.*, 2013) with convergence to the east of the low pressure that is accompanied by divergence in the upper air (Preston-Whyte and Tyson, 1993 and Triegaardt *et al.*, 1991). Van Heerden and Taljaard, contributing to Karoly and Vincent (1998) also stated that tropical low pressures can be identified on satellite imagery with the low level circulation being cyclonic and anti-cyclonic in the upper troposphere. More recently Dyson and Van Heerden (2002) developed the Model for the Identification of Tropical Weather Systems (MITS) which assists forecasters in identifying tropical weather systems as well as detecting areas where tropical convection can occur. There are five components of MITS which are focused on the atmospheric dynamics that are necessary for the development of convective rainfall caused by tropical systems. Further details on CTL and MITS will be provided in Chapter 3.

Most heavy rainfall events over Southern Africa have been found to occur over the eastern and north-eastern parts of the country during the summer months (Poolman contributing to Dyson *et al.*, 2002). Dyson and Van Heerden (2002) stated that due to the high frequency of heavy rainfall events that occur in summer over the eastern and north-eastern parts of South Africa, it is important to develop better forecasting techniques that can identify and predict tropical weather systems. These low pressure systems are responsible for widespread heavy rainfall and are often associated with floods as they are particularly slow moving.

Despite the high impact of these weather systems very little is known about the variability, climatological characteristics and rainfall contribution of these systems. Operational meteorologist have until recently struggled to recognise CTLs (SAWS, 2017) and by creating a climatology of these systems, it can be seen how often CTLs occur over southern Africa and how regularly they extend into South Africa. There is also a need to understand the rainfall associated with CTLs on daily rainfall over South Africa as well as the contribution of rainfall CTLs have to the annual rainfall over South Africa. Creating a synoptic climatology and investigating the impact on rainfall over South Africa the significance of these weather systems can be established.

Chapter 3: Objective identification method for CTLs

3.1 Objective identification of synoptic scale weather systems

Objective identification methods have been used to identify synoptic scale weather systems over South Africa (Engelbrecht et al., 2015; Malherbe et al., 2011) and in other parts of the world (Knaff et al., 2008). The objective identification of weather systems makes researching these weather systems more probable for instance by creating climatologies (Malherbe et al., 2011) and understanding processes and movement of these systems better (Engelbrecht et al., 2015). Over southern Africa objective methods have been developed for the ITCZ, TTT, Cut-off lows (COLs) and tropical cyclones.

In order to identify the ITCZ layer- and time-averaged winds in the lower troposphere were utilised (Berry and Reeder, 2013). This automated method that was then used to create a climatology of the ITCZ for the period 1979-2009. It was found that the ITCZ most commonly occurs over the eastern Pacific Ocean, where it is limited to a narrow latitudinal band throughout the year (Berry and Reeder, 2013). Hart et al. (2012) developed an automated objective method to identify TTT events over southern Africa. In their study, they created a climatology of cloud band positions and found that TTTs have two preferred areas of location.

In the past decade methods were developed and refined to objectively identify lows over South Africa (see for example Singleton and Reason, 2006; Favre et al., 2013; Engelbrecht et al., 2015). Engelbrecht et al., 2013 identified closed mid-tropospheric lows by detecting geopotential minima at 500hPa and by stipulating that the lows should be present for at least 24-hrs. In a Cut-off low (COL) study Engelbrecht et al. (2014/5) identified the COL objectively by isolating a geopotential minimum at 500hPa with a cold core of temperatures in close proximity. These lows also had to exist for at least 24 hrs. In order to identify eastward moving tropical lows over the Mozambique Channel Malherbe et al. (2011) located closed lows (minimum geopotential) at 500 and 700hPa with either a high or the absence of a low at 250hPa. They noted that their identification method captured tropical lows over the ocean adequately but the criteria did not necessarily hold as the low moved over the continent of Africa.

Recently, Crétat et al. (2018) objectively identified the Angola low pressure over Angola and the surrounding countries. In their study, they found that there are three low pressures over southern Africa. In order to identify the Angola low and to distinguish it from the other two low pressures, daily anomalies of vorticity at 700hPa were used.

In this report an objective identification method is also be used to identify CTLs. These weather systems are objectively classified and their contribution to rainfall over South Africa determined. A comprehensive discussion on the methodology used to develop an objective identification of CTLs will be provided in Chapter 3.

3.2 Model for the identification of tropical weather systems

Using the atmospheric dynamics that are vital for the development of convective rainfall as a result of tropical weather systems, Dyson and Van Heerden (2002) developed the model for the identification of tropical weather systems (MITS). MITS is used to identify tropical weather systems as well as to detect areas of tropical convection. It was therefore decided that this is an excellent starting point from which to build on further. MITS has five components based on the atmospheric mechanisms of a tropical atmosphere which is illustrated in figure 3.1.

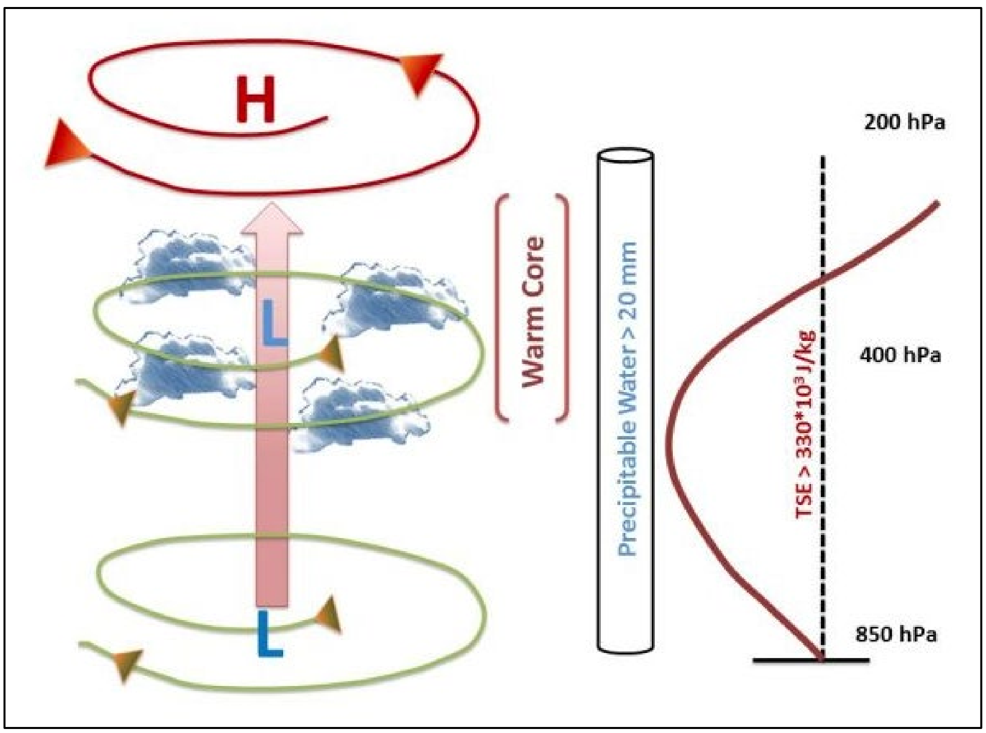

Figure 3.1: Graphical representation of MITS, displaying the components MITS uses to identify a tropical weather systems and areas of tropical convection (After VLAB, 2015).

The first component of MITS states that a low pressure must stand upright from 850 to 400hPa with a ridge of high pressure at 200hPa. This is demonstrated in figure 3.1 by displaying a low pressure at the lower levels (850hPa) in the atmosphere through to the mid-levels (400hPa) with cyclonic circulation. A high pressure is present in the upper air with anti-cyclonic rotation. This illustrates the upright low pressure with a ridge in the upper levels.

The second component is that in the 500 to 300hPa layer, a core of high average column temperatures should be above or in close proximity to the low pressure. Dyson and Van Heerden (2002) found that in order to identify a warm cored tropical system, no specific temperature threshold is used, instead the temperatures are required to be warmer than the surrounding areas.

The third component is that the precipitable water values should be more than 20 mm in the 850 to 300hPa layer and this should be in the same area as the ridge of high pressure at 200hPa, which all needs to exist with upper tropospheric wind divergence. In figure 3.1, a column is used to illustrate that precipitable water values within such a column need to exceed 20 mm. Precipitable water is defined as the amount of water vapour available within a given column of the atmosphere such that if all the water vapour in that column were condensed (Huschke, 1959).

The fourth component states that in the 850 to 300hPa layer, the average total static energy should be greater than $330x10^3 Jkg^{-1}$. This is graphically represented in figure 3.1 on the far right side in the image which displays a vertical profile of TSE showing deep convection. TSE is given by:

$$TSE = C_p T + gz + Lq$$

Where, Cp = the specific heat of dry air, T = temperature, g = gravity constant, 9.8 $m.s^{-2}$, z = the geopotential height in meter (gpm), L = the latent heat of condensation, q = the water vapour mixing ratio. The terms on the right of the equation represent enthalpy, geopotential and latent heat (Triegaardt *et al.,* 1991). In a tropical airmass, the upper tropospheric temperatures are higher than normal, therefore the enthalpy will increase which will in turn increase the TSE. Furthermore the high in the upper troposphere will increase the geopotential. The high moisture content in a tropical low will increase the latent heat term and TSE values. (Dyson and Van Heerden, 2002).

The final component which helps identify rainfall from tropical lows is that the atmosphere should be conditionally unstable up to 400hPa, upward motion should be present from 700 to 400hPa and that precipitable water values should exceed 20 mm. A vertical profile of TSE can be used to identify unstable tropical atmosphere by indicating convective instability (Riehl, 1979). In Fig. 3.1 the atmosphere is convectively unstable to close to 200hPa.

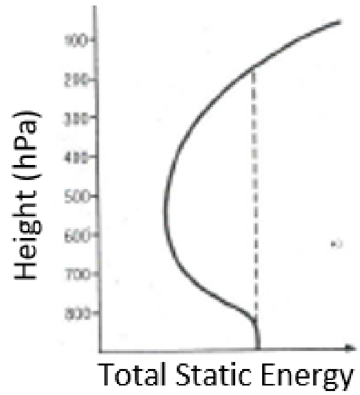

3.3 Objectively identifying CTLs

In order to accurately create a climatology of CTLs over southern Africa as well as to quantify the rainfall contribution of CTLs to South Africa, an objective identification method is created. The objective identification method is broadly based on MITS but some additional criteria were required.

The first criteria of MITS required an upright standing low pressure system. Traditionally a minimum value of geopotential heights will be used to identify the low. However, it was found that the Angola Low often meets this requirement during late summer. The Angola low pressure is a shallow heat low that develops over southern Angola and northern Namibia during the summer months (Reason *et al.,* 2006). The CTL as defined in this report is a deeper low which should have significant cyclonic circulation throughout the troposphere. Therefore to identify upright standing low pressures, it was decided to use minimum (maximum) values of relative vorticity (ζ) to identify a low (high). The first objective method set was that there should be minimum negative values at 850 and 500hPa with maximum positive values at 200hPa.

In a further attempt to distinguish CTLs from the semi-permanent Angola low pressure, deviations of instantaneous values of certain parameters from the long term mean for the individual months are applied. A similar approach was used by Engelbrecht and Landman (2015) who used standardized anomalies to identify rare and thus severe events over South Africa. In this study, the deviations from the norm were applied to vorticity, TSE, column temperature and precipitable water, where each of these components are required to be stronger/higher than the norm for the specific month.

While identifying tropical environments, Dyson (2000) established that in order to sustain a tropical thermal high pressure in the upper atmosphere, precipitable water values of at least 20 mm are required. Therefore this is also a requirement in this study.

The subject method to identify the existence of a CTL has *four* criteria that need to be met. A graphical illustration of this process through the use of a flow chart is provided in figure 3.3. The *first* criteria is to detect **a favourable tropical environment (FTE)**. A grid point is positively identified as an FTE if the following conditions are met:

- Negative relative vorticity values are present at 850 and 500hPa, and are replaced by positive values at 300hPa;
- The cyclonic circulation at the surface and in the mid-troposphere is stronger than normal while the high pressure dominates near the tropopause. Therefore it is required that the deviation from the normal vorticity values for the month under investigation show this anomalous circulation;
- Average tropospheric total static energy (TSE) values should be higher than the long term average for that month;
- The average 500-300hPa temperatures should be higher than the long term average value for that month;
- The precipitable water from 850-300hPa should be greater than 20 mm;
- The precipitable water values should also be higher than the long term average value for that month.

The second criteria is that a closed 500hPa geopotential low with a warm core of 500-300hPa temperatures are present. This is seen in figure 3.3 as a two-fold requirement which leads to the next requirement of the 500hPa low being within a two grid points from the warm core. This is then referred to as a warm low (first orange block in figure 3.3). A closed low pressure (warm core) is identified when the surrounding eight grid points have higher geopotential heights (lower temperatures) than the grid point under investigation. Figure 3.4 illustrates this process, with X representing the grid point that has lower geopotential heights (warmer temperatures) than the 8 grid points surrounding it.

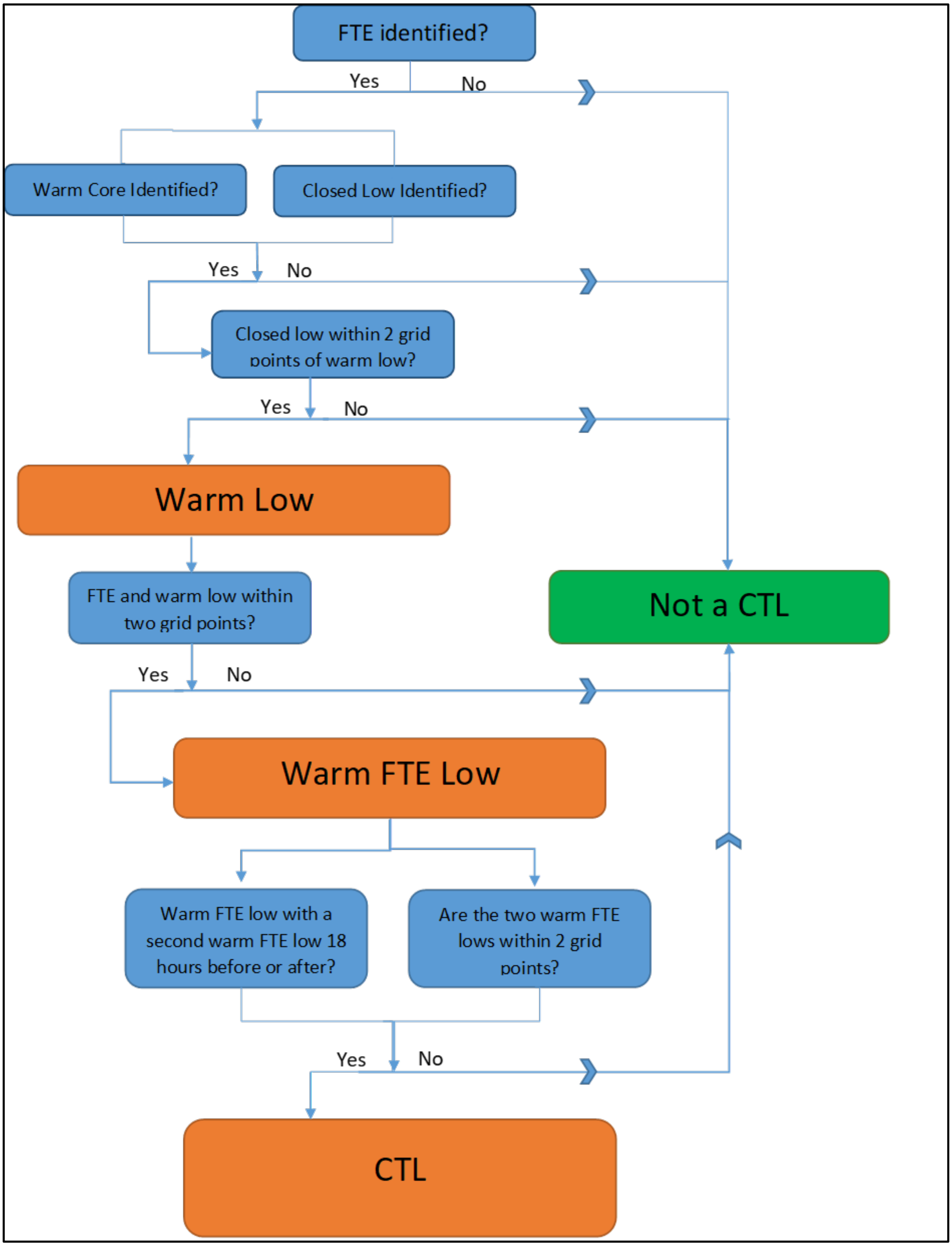

Figure 3.3: Flow diagram illustrating the procedure used to identify a CTL over southern Africa.

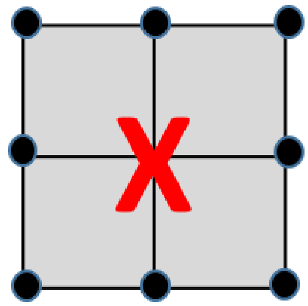

The *second* criteria is that **a closed 500hPa geopotential low with a warm core of 500-300hPa temperatures are present.** This is seen in figure 3.3 as a two-fold requirement which leads to the next requirement of the 500hPa low being within a two grid points from the warm core. This is then referred to as a warm low (first orange block in figure 3.3)**.** A closed low pressure (warm core) is identified when the surrounding eight grid points have higher geopotential heights (lower temperatures) than the grid point under investigation. Figure 3.4 illustrates this process, with X representing the grid point that has lower geopotential heights (warmer temperatures) than the 8 grid points surrounding it.

The *third* criteria is that the **FTE and warm low are within two grid points of each other**. If this requirement is met, the low pressure is then termed a warm FTE low pressure (second orange block in figure 3.3). The *fourth* criteria is two-fold and is related to time. It is required that **the current warm FTE low has another warm FTE low either 18 hours before or after *and* lies within two grid points of the current warm FTE low**. The time requirement is illustrated by using the following example; if the current warm FTE low is at time step t=4, with each time step six hours apart, then another warm FTE low is required to be present at one of the following time steps t=1, t=2, t=3, t=5, t=6 or t=7. In addition, the second part of the fourth criteria, which states that the current warm FTE low pressure is required to be within two grid points of another warm FTE low.

If all of these four criteria are met, then the warm FTE low is now classified as a CTL. The position of the closed low pressure, identified in the second criteria is used as the position of the CTL.

For this research a landmask is used to identify CTLs over land within the domain 17.5 to 32.5°S and 12.5 to 35°E. This domain is illustrated using the grey block in figure 3.5, and only CTLs within this region are considered in the study.

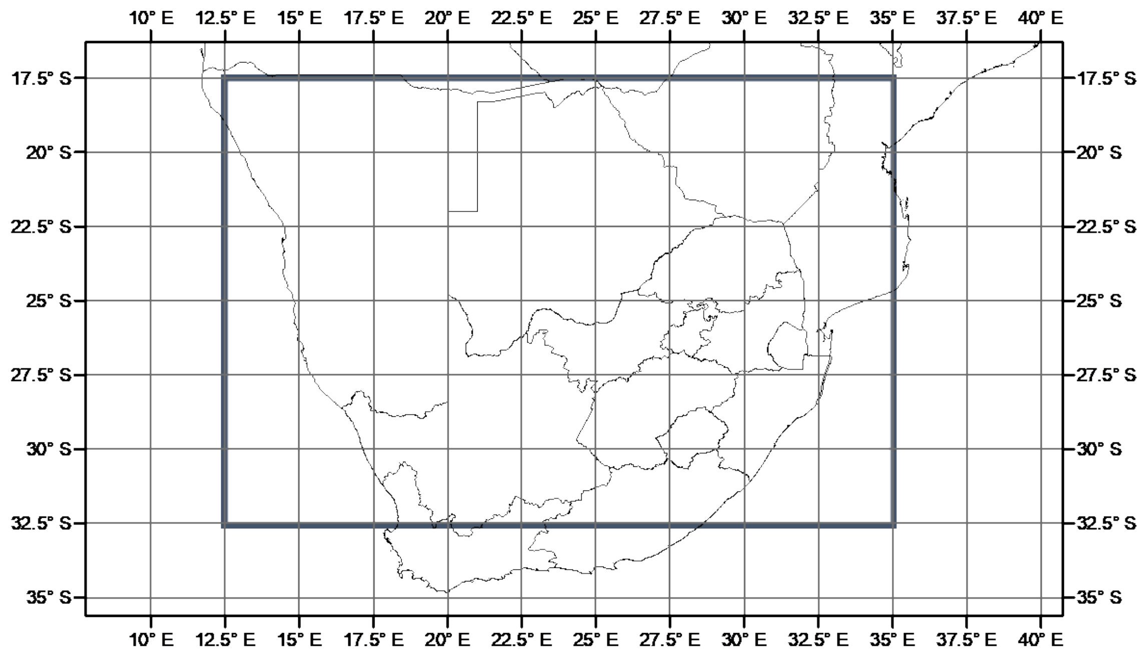
10° E
12.5° E
15° E
17.5° E
20° E
22.5° E
25° E
27.5° E
30° E
32.5° E
35° E
37.5° E
40° E
17.5° S
20° S
22.5° S
25° S
27.5° S
30° S
32.5° S
35° S

Chapter 4: Synoptic climatology of CTLs over southern Africa

4.1 Atmospheric Circulation Data

CTLs generally have a scale of 500-1000 km (Engelbrecht *et al*., 2013) and NCEP reanalysis data (Kalnay *et* al., 1996), which has a horizontal grid resolution of 2.5° (approximately 250 km) and a vertical resolution of 17 levels, adequately resolves these synoptic weather systems. NCEP reanalysis data has previously been used to describe synoptic scale weather systems over South Africa. Engelbrecht *et al*. (2015) used this data to identify synoptic weather patterns that affect the Cape South coast while Malherbe *et al*. (2011) identified landfalling tropical cyclones over southern Africa.

In this research, daily, six-hourly NCEP data for the period December 1979 to March 2018 (only December to March months) was used in order to objectively identify CTLs. The variables used were zonal and meridional wind, temperature and geopotential and specific humidity was used to calculate precipitable water. Other variables calculated were relative vorticity, average column temperature and TSE.

4.2 Geographical distribution of Continental Tropical Low pressures

The objective identification method identified a CTL at a total number of 2929 time steps for the 40-year period from December 1979 to March 2018 over the research area. CTLs occur most frequently over southern Angola and Zambia, where more than 300 events were identified in the at two NCEP grid point. This is on average more than 7 CTLs a season. The number of CTL events steadily decreases further southwards with less than 60 events observed over the South Africa region (south of 22.5°S indicated with a blue block in Fig. 4.1). The total number of CTL events over the SA region is 342, with the highest number recorded at a single grid point (55), over south-western Mozambique/north-eastern Limpopo. This high number is probably influenced by landfalling tropical cyclones. The other hotspot over the South African region (Fig. 4.1) is on the border between Namibia and Botswana. The furthest south a CTL ever occurred was 32.5°S, this only took place only once on 23 January 2011.

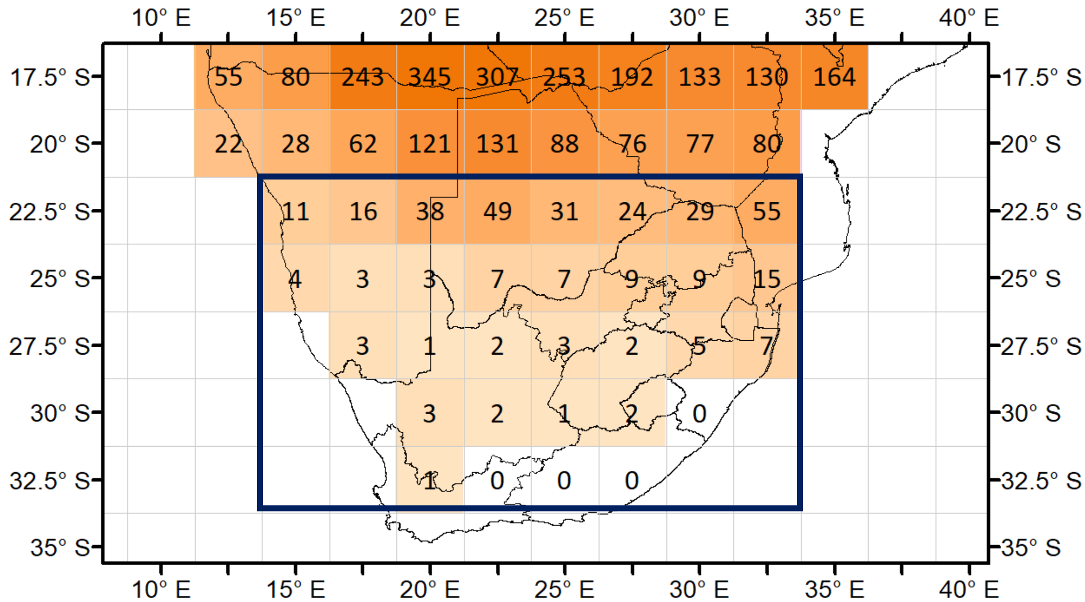

Figure 4.1: Geographical distribution of the total number of CTL events identified over southern Africa with the block illustrating the area defined as the South Africa region, south of 22.5°S.

Considering the entire domain in Figure 4.1 and the complete period, a total number of 2929 events were identified. This is an average of approximately 732 CTL days (see Section 5.1 for an explanation of a CTL day) which translates to 19 CTL days per year (Table 4.1). For the South Africa region, the area south of 22.5°S, a total number of 342 time steps satisfied the criteria, which represents two CTL days per year. This is considerably less than the contribution further north. There are 19 CTL days per year over the entire region but only 2 over the South African region (Table 4.1)

Table 4.1: CTL events per year for the entire region as well as for the South African region4:2

	Entire Region	South Africa (south of 22.5°S)
Total events	2929	342
CTL days	732	85
CTL days per year	19	2

From these results, it is clear that CTLs are rare over the Republic of South Africa and are even less likely to reach the central interior of the country. Instead, these weather systems seem to favour the north-eastern parts of the country. The average return period of CTLs over the central interior of the country is 78 years, whereas over the northern parts of Limpopo province the return period is a lot lower at five years.

The geographical distribution of CTL events vary slightly per month (Fig. 4.2). Dyson *et al.* (2015) stated that during the late summer months (January to March) the atmospheric circulation over Gauteng takes on tropical characteristics. Those results are echoed in this research, where CTL events occur a lot higher frequently over Gauteng from January, while during December months there are very few CTL events and they are confined to the eastern parts of South Africa. It is uncommon for CTLs to extend south of 22.5°S during December months (Fig. 4.2a), while from January (Fig. 4.2b), there is a clear increase in events reaching the southern and western interior of South Africa.

In February, CTLs occur further westwards into the northern parts of the Northern Cape in South Africa. A few CTLs still occur over northern KwaZulu-Natal and into southern Mozambique, but the number of events decrease from January months. By March, (Fig. 4.2c), the number of CTL events decrease further in the north-eastern parts of southern Africa, while there is an additional increase in events over the western interior of South Africa. This coincides with Taljaard (1996) who indicated how the 50 mm isohyet moved westward over South Africa during the summer rainfall season from the western parts of the Free State in December to the Northern Cape Province by March.

January has the highest number of CTL events (Fig. 4.3), with 36% of CTL events occurring during this month, followed very closely by February with 34%. CTL events seldom occur in December (only 15%), and are even less frequent in March with only 14% of the CTL events occurring during this month.

4.3 Temporal characteristics of CTLs

Further analysis on the temporal characteristics of CTLs were investigated by calculating the number of CTL events per time step (Fig. 4.4). If there was more than one CTL at a certain time step (for instance over Mozambique and western Botswana), that time step was only counted once. The highest frequency of CTLs occurs at 18Z, followed closely by 00Z. However, unlike mesoscale convective complexes (MCCs), that display nocturnal characteristics (Laing and Fritsch, 1993), these results show that CTLs have no noteworthy difference in the time step frequencies.

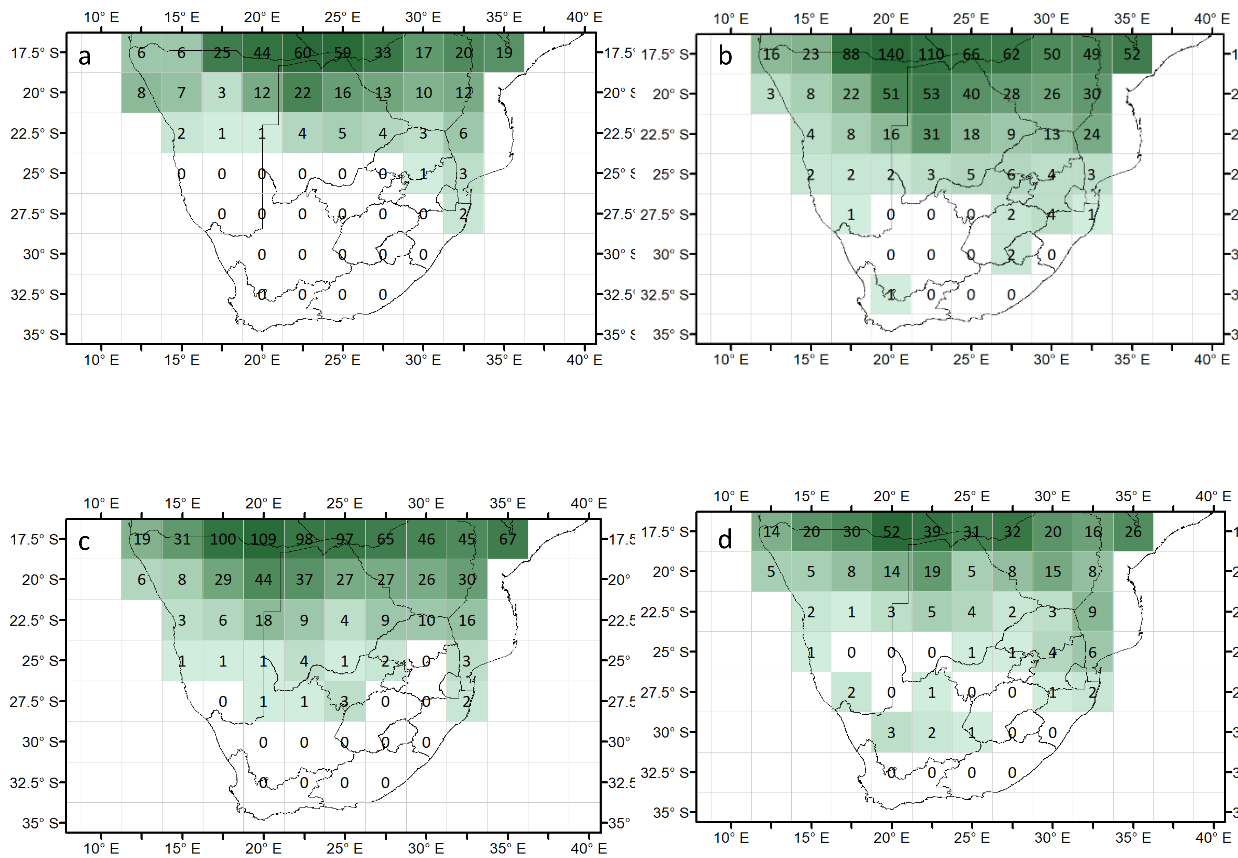

Figure 4.2: Geographical distribution of the total number of CTLs identified over southern Africa during (a) December, (b) January, (c) February and (d) March.

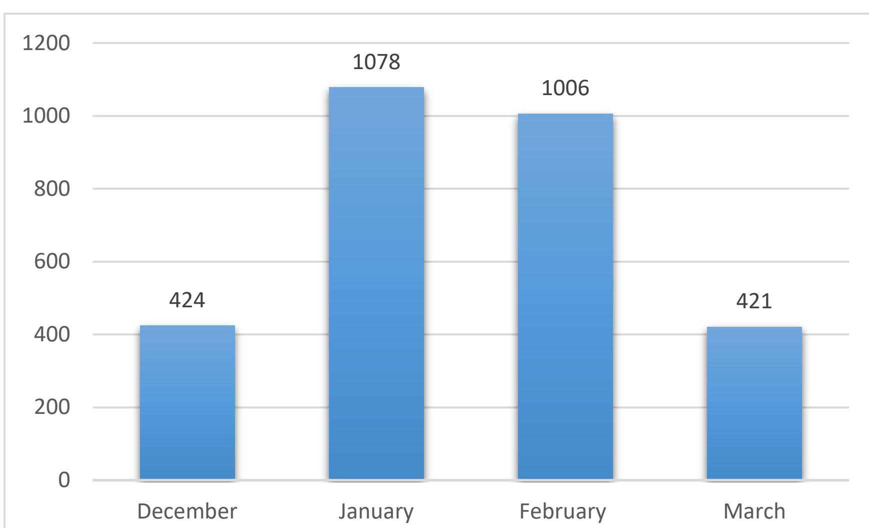

Figure 4.3: Graph displaying the total occurrence of CTLs per month (December, January, February and March).

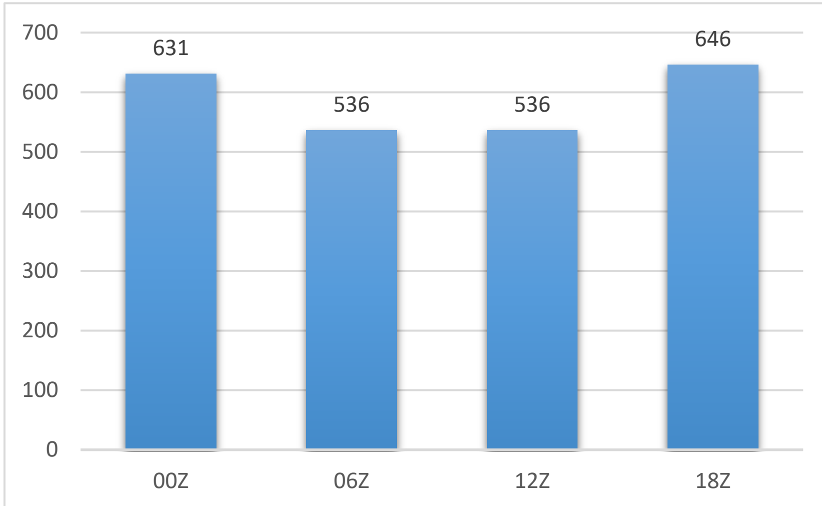

Figure 4.4: Graph showing the frequency of occurrence of CTLs at time steps 00, 06, 12 and 18Z.

The life span of CTLs was calculated using the total number of consecutive days a CTL exists. There were 410 days when CTLs lasted for more than one day and the average life span is 2.8 days. By far, the majority of CTLs exist for less than 3 days (Fig. 4.5), with only three existing for more than 13 consecutive days. The highest number of days a CTL existed for was 19, this was a recent event that occurred between 3 and 21 January 2017. The other two cases where a CTL existed for more than 13 days were February 2000 and January/February 2014 where each of these CTL cases lasted for 16 days.

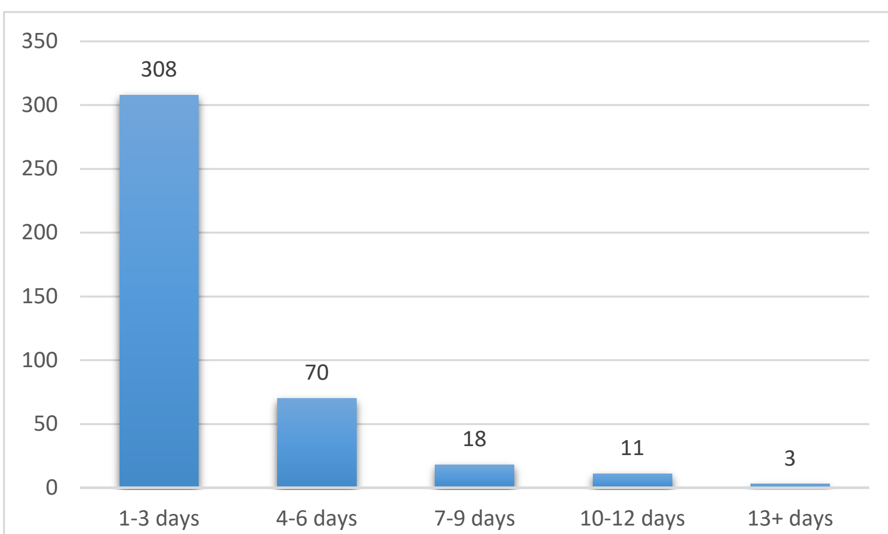

Figure 4.5: Graph showing the number of consecutive days a CTLs existed per threshold of 1 to 3 days, 4 to 6 days, 7 to 9 days, 10 to 12 days and more than 13 days.

4.4 Seasonal Distribution of Continental Tropical Low pressures

Table 4.2 shows the monthly distribution of CTL events for the entire period. On average, 75 CTL events occur each season. The majority of these events transpire during January with an average of 28 CTL events, followed very closely by February with 26 events. December and March have the same average number of events of 11.

The 1999/2000 season had the highest number of CTL events with 197 and every month except December had an above average number of CTL events most of which occurred in February (100). In February 2000 floods occurred over north-eastern South Africa, when tropical weather systems moved over Mozambique and into the north-eastern parts of South Africa, causing devasting floods on two separate occasions during the month (Dyson and Van Heerden, 2002). The previous season 1998/99 had the 2nd highest number of CTL events and in this instance all the months had an above normal number of events but the number of events more evenly distributed through the season. Another season with an exceptionally high number of CTL events were 2016/17 when 145 events occurred. This season followed the exeptionally dry 2014/15 and 2015/16 seasons over the summer rainfall areas of South Africa (Botai et al., 2016). During 2016/17 only March had a below normal number of events with January month receiving 87 CTLs.

The lowest number of CTL events in a season occurred during the 1985/1986 season with only 4 events and according to Richard *et al.* (2001) rainfall over the summer rainfall areas of South Africa was well below normal during this season. During the drought of 2014/15 and 2015/16 (Botai *et al.,* 2016) the number of CTL events were far below normal with all the months in these seasons receiving below normal number of events. From the 1983/1984 season to the 1986/1987 season, three of the lowest CTL event seasons occurred. These seasons coincided with below normal rainfall over southern Africa (Richard *et al.,* 2001).

The 2002/2003 season started off with both December and January experiencing far below the average CTL events, however from February, the average CTL events were far above the monthly average for the respective months. During the recent very dry 2015/2016 season, there were only a total 25 CTL events with no events occuring during January. Even more recently, the 2017/2018 season mainly had below normal number of CTL events, however during February, there were almost double the number of average CTL events for that specific month which resulted in the seasonal CTL events only being slightly below the seasonal average.

Table 4.2: The number of CTL events from the 1979/1980 season to the 2017/2018 season. The totals and averages for each month are provided as well as the total for the season. Yellow blocks indicate the lowest three CTL seasons with the green blocks indicating the highest

Season	December	January	February	March	Seasonal Total
1979/1980	7	2	9	10	28
1980/1981	6	19	31	3	59
1981/1982	8	15	19	0	42
1982/1983	6	17	21	0	44
1983/1984	8	9	0	3	20
1984/1985	20	25	4	8	57
1985/1986	0	3	1	0	4
1986/1987	4	10	0	1	15
1987/1988	19	6	36	7	68
1988/1989	0	25	62	19	106
1989/1990	7	28	4	4	43
1990/1991	2	47	36	11	96
1991/1992	30	5	0	13	48
1992/1993	32	14	43	14	103
1993/1994	3	51	8	2	64
1994/1995	14	9	39	7	69
1995/1996	7	63	31	12	113
1996/1997	10	59	39	13	121
1997/1998	10	50	39	14	113
1998/1999	32	51	50	20	153
1999/2000	9	44	100	44	197
2000/2001	13	8	35	18	74
2001/2002	7	7	11	10	35
2002/2003	6	17	50	35	108
2003/2004	3	29	44	38	114
2004/2005	13	21	8	3	45
2005/2006	19	47	55	23	144
2006/2007	6	14	29	10	59
2007/2008	35	59	1	6	101
2008/2009	23	30	11	9	73
2009/2010	0	28	29	6	63
2010/2011	2	32	0	4	38
2011/2012	7	43	7	10	67
2012/2013	9	50	16	3	78
2013/2014	14	35	43	10	102
2014/2015	1	19	9	4	33
2015/2016	5	0	12	8	25

Season	December	January	February	March	Seasonal Total
2016/2017	19	87	29	10	145
2017/2018	8	0	45	9	62
Average	11	28	26	11	75

After further analysis (Table 4.2), it has been found that February is the month with the highest number of times when zero events occurred in a season and that overall, February is also the month that had the highest occurrence of CTL events, which was 100 events in a single month. Overall, February also has the highest variation with a standard devation of 21.6. December and March also have the lowest variability with a standard deviation of less than 10 for both months.

Further analysis on the CTL events per season were conducted where the data was standardized using the long term average and standard deviation. These results are depicted in Fig. 4.6 for the total CTLs per season and in Fig. 4.7 for the individual months. From Table 4.2 and Figure 4.6 it is seen that during the 1980s there was generally a below normal occurance of CTL events. During the late 1990s there was an above normal occurrence of CTL events with their occurences becoming quite variable after that. During the early part of the period, before the 1988/1989 season, there were nine below normal CTL seasons identified (Fig. 4.6). However, from the 1995/1996 season, there were five consecutive seasons of above normal CTL events which included the 1999/2000 extreme rainfall season. There is nevertheless a clear increase in the number of CTL events during the period 1979 to 2018, as shown by the trend line in Fig. 4.6, Man-Kendell test for trends shows this to be significant to the 90% confidence level. The individual months also show an increasing trend overall (trend lines in Fig. 4.7), but with only the January trend being significant (Fig. 4.7b). The Mann-Kendall Test for Significance (Wilks, 2011) was used, with a significance level of 90%. However, the tau correlation coefficient in the Kendall Test for Significance (Wilks, 2011) does not support the significance in the upward trend.

In Fig. 4.6, the colour of the bars describe the El Niño-Southern Oscillation (ENSO) phase during the December-January-Febraury period, with the red bar colours indicating warm periods (El Niño) and blue indicating cold periods (La Niña) (Climate Prediction Centre Internet Team, 2018). The black coloured bars indicate the neutral phases. During the entire period, there were a total of 13 El Niño seasons, with 11 of these coinciding with below normal CTL event seasons and only two seasons where El Niño was assocaited with above normal CTL event seasons (1997/98 and 2002/03). There were a total of 13 La Niña seasons, of which 6 corresponded with above normal CTL events.

The effect ENSO has on southern Africa is that usually during El Niño events, below normal rainfall amounts occur while during La Niña events, above normal rainfall is received (Lyon and Mason, 2007 and Crétat *et al.,* 2018). This is not always true as is the case of the 1997/1998 season which was a strong El Niño event that landed up being a season where near or even above normal rainfall occurred (Lyon and Mason, 2007). From the graph below, it is shown that during this strong El Niño, an above normal amount of CTL events also occurred during that season. There is a stronger correlation between warm ENSO seasons and below normal CTL events that there are with cold ENSO seasons and above normal CTL events.

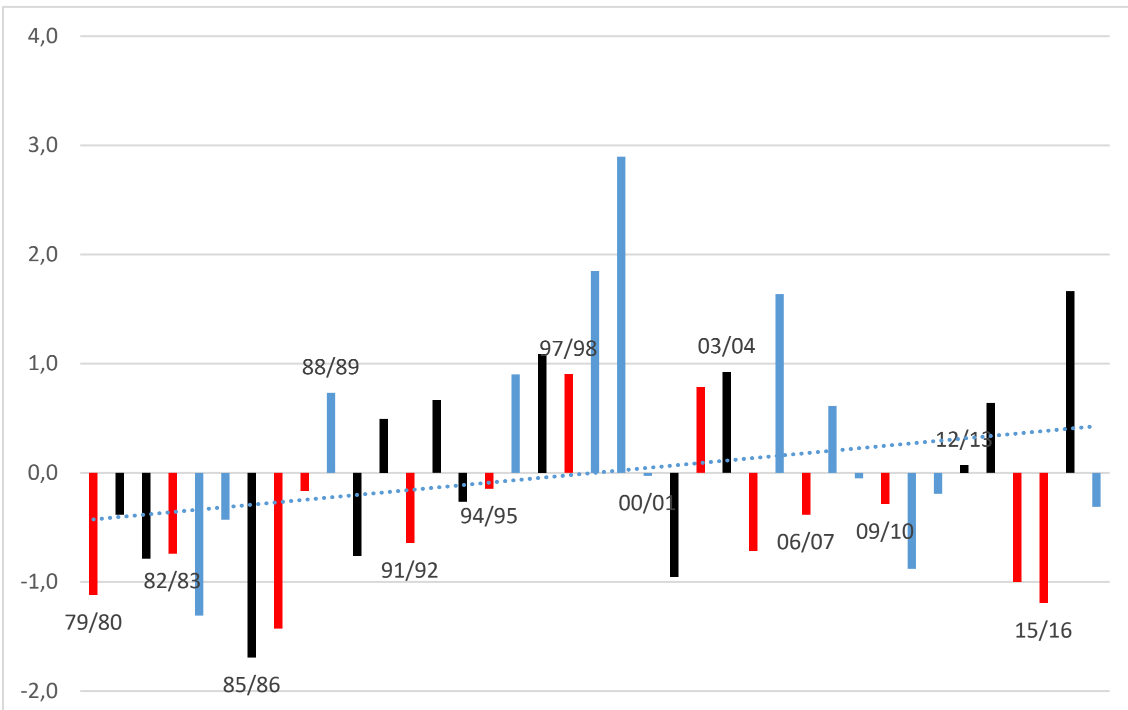

Figure 4.6: Standardized CTL event anomalies per season, with the dotted line indicating a trend line. Red bars indicate a warm ENSO period while a blue bar indicates a cold periods.

4.5 Summary

From the results presented above, it can be stated that overall, the highest occurrence of CTL events is found over southern Zambia and Angola. There is a rapid decrease in CTL events further south towards South Africa with a return period of 75 years over the central interior of the country. CTLs occur most frequently during January months and extend over the central interior of South Africa in March. There is an increasing trend of CTL events over southern Africa, with the highest trend being in January and a medium negative correlation with ENSO, signifying that a warm Enso event is associated with below normal CTL events.

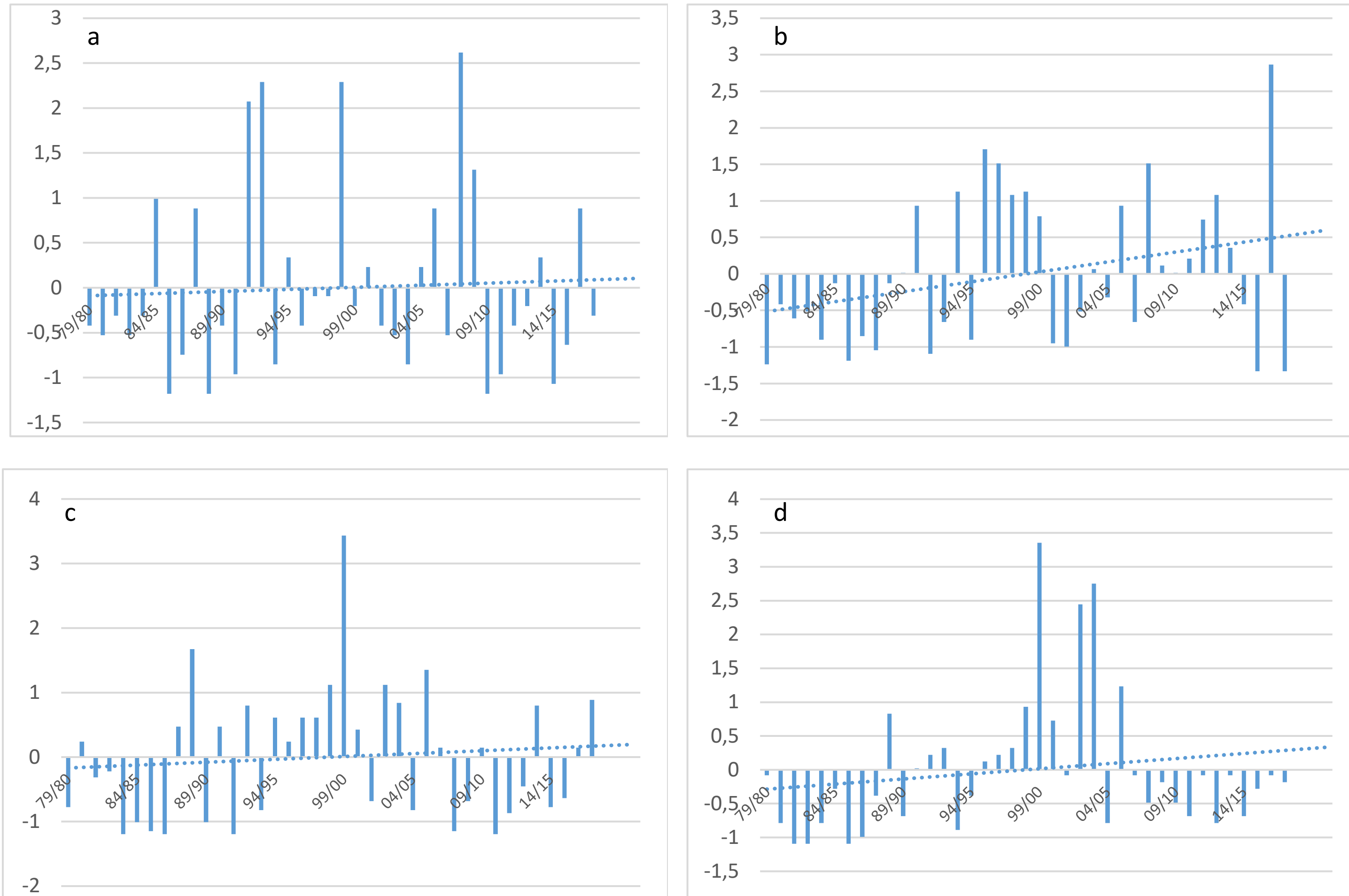

Figure 4.7: Standardized anomalies of the CTL events for each season for (a) December, (b) January, (c) February and (d) March.

Chapter 5: Rainfall associated with CTLs over South Africa

In the following section, the rainfall contribution CTLs have to South Africa will be presented. This is a continuation of the results given in Chapter 4, as the climatology of CTLs are used to quantify the rainfall contribution using daily rainfall station data supplied by SAWS for the period 1979-2017. Some CTL rainfall features are discussed in this chapter as well as comparisons made with the long term mean rainfall over the area. In addition, the general rainfall distribution around a CTL is also provided.

5.1 Gridded Rainfall

Daily observed rainfall station data supplied by SAWS was used to determine the rainfall contribution of CTLs to South Africa. This rainfall was converted to 0.5° grids so that a relative homogeneous density network can be obtained and to find a rainfall figure representative of synoptic scale rainfall. This is a similar method employed by Engelbrecht *et al*. (2013) when investigating the contribution of closed upper tropospheric lows to rainfall.

A 21 by 21 point, 0.5° grid is assigned to every NCEP grid point (Fig. 5.1). This results in a 10° area representing the rainfall in every NCEP grid point which is located in the centre. In figure 5.1, "a" represents each 0.5° area and "B" the centre of the NCEP grid point. The maximum rainfall amount measured by any of the rainfall stations in each area "a" are used as the representative value for that specific grid. Figure 5.2 shows the NCEP grid points where the 5° radius around the grid point falls into the borders of South Africa and rainfall data is available. For some of the grid points (red stars in Fig. 5.2) only the southern extremes of the 10° area falls into the borders of South Africa and a limited number of rainfall stations are available for analysis.

The NCEP data used to identify CTLs are available in 6-hr intervals and 4 possible CTLs could have been identified at every grid point in a 24-hr period (referred to as a CTL event in Chapter 4). Rainfall data is only available once a day at 08:00 SAST and the temporal resolution of the two data sets had to be consolidated. The CTL events were grouped per day with each day starting at 08:00 SAST (day 1) and continuing until 08:00 SAST on the following day (day 2). The CTL events that occur in a 24-hr period prior to 08:00 SAST on day 2 are grouped together and termed a CTL day. There could be a number of CTL events that form part of one CTL day. The location of the CTL is assigned to the relevant NCEP grid point and the rainfall value for each area "a" (Fig. 5.1) is then obtained for each CTL day.

	0.5°	1°	1.5°	2°	2.5°	3°	3.5°	4°	4.5°	5°	5.5°	6°	6.5°	7°	7.5°	8°	8.5°	9°	9.5°	10°
0.5°	a	a	a	a	a	a	a	a	a	a	a	a	a	a	a	a	a	a	a	a
1°	a	a	a	a	a	a	a	a	a	a	a	a	a	a	a	a	a	a	a	a
1.5°	a	a	a	a	a	a	a	a	a	a	a	a	a	a	a	a	a	a	a	a
2°	a	a	a	a	a	a	a	a	a	a	a	a	a	a	a	a	a	a	a	a
2.5°	a	a	a	a	a	a	a	a	a	a	a	a	a	a	a	a	a	a	a	a
3°	a	a	a	a	a	a	a	a	a	a	a	a	a	a	a	a	a	a	a	a
3.5°	a	a	a	a	a	a	a	a	a	a	a	a	a	a	a	a	a	a	a	a
4°	a	a	a	a	a	a	a	a	a	a	a	a	a	a	a	a	a	a	a	a
4.5°	a	a	a	a	a	a	a	a	a	a	a	a	a	a	a	a	a	a	a	a
5°	a	a	a	a	a	a	a	a	a	a	a	a	a	a	a	a	a	a	a	a
5.5°	a	a	a	a	a	a	a	a	a	a	a	a	a	a	a	a	a	a	a	a
6°	a	a	a	a	a	a	a	a	a	a	a	a	a	a	a	a	a	a	a	a
6.5°	a	a	a	a	a	a	a	a	a	a	a	a	a	a	a	a	a	a	a	a
7°	a	a	a	a	a	a	a	a	a	a	a	a	a	a	a	a	a	a	a	a
7.5°	a	a	a	a	a	a	a	a	a	a	a	a	a	a	a	a	a	a	a	a
8°	a	a	a	a	a	a	a	a	a	a	a	a	a	a	a	a	a	a	a	a
8.5°	a	a	a	a	a	a	a	a	a	a	a	a	a	a	a	a	a	a	a	a
9°	a	a	a	a	a	a	a	a	a	a	a	a	a	a	a	a	a	a	a	a
9.5°	a	a	a	a	a	a	a	a	a	a	a	a	a	a	a	a	a	a	a	a
10°	a	a	a	a	a	a	a	a	a	a	a	a	a	a	a	a	a	a	a	a

Figure 5.1: A 21 by 21 point grid illustrating the rainfall data distribution around each NCEP grid point (represented by the orange block B). The 5° area surrounding the NCEP was divided into smaller grids of 0.5° each (a). The maximum rainfall of all rainfall stations in each of the grids (a) were identified and represents the daily rainfall in that particular grid point.

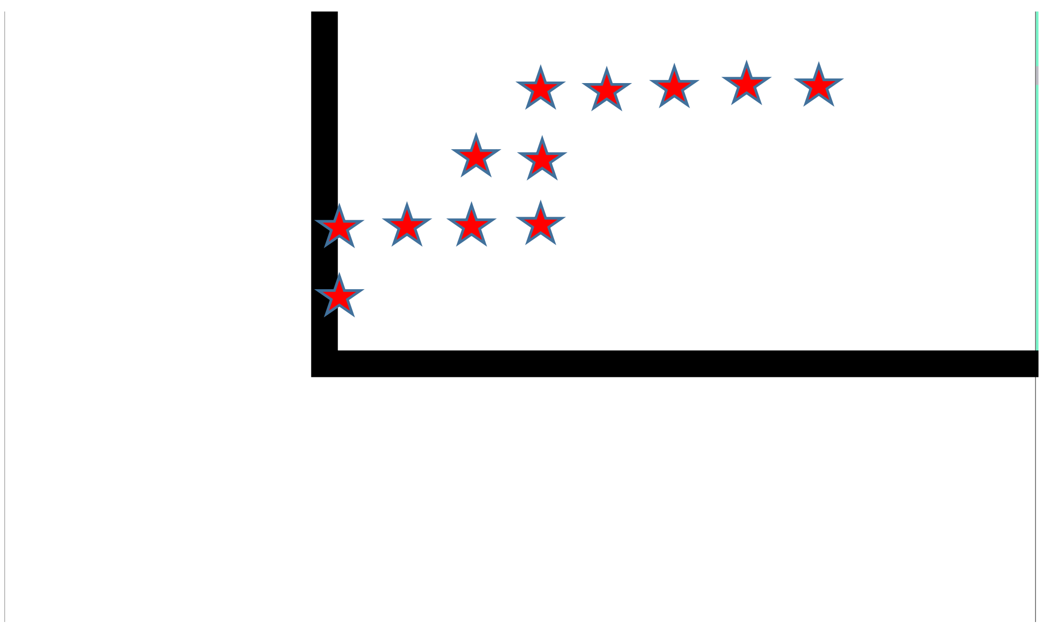

Figure 5.2: NCEP grid points for which rainfall data from the South African Weather Service is available. Blue circles indicate the NCEP grid points where there is an adequate amount of rainfall data available, while the red stars indicate the NCEP grid points where the rainfall data availability is limited and these grid point were not used the analysis.

The rainfall for each CTL day is calculated. The average rainfall per NCEP grid point for all CTL days was calculated as well as the maximum rainfall recorded at each grid point for any CTL day. Rainfall extremes are calculated and compared to the long term rainfall extremes.

5.2 Defining daily rainfall values

A total of 2929 CTL events were recognized objectively between 1997 and 2018. Using the method described above a total of 1553 CTL days were identified in the domain where rainfall data is available (Fig. 5.2).

The rainfall per CTL day is calculated for a 10° region (rainfall area) with the central NCEP grid point being the position of the CTL (Fig. 5.1). This will be referred to as the NCEP rain area. One should consider that there is limited availability of rainfall data, especially towards the north of the study area. In Fig. 5.3, the green dots represent the NCEP grid points where some rainfall data is available in the 10° area representing the NCEP rain area. Each NCEP rain area (red block) surrounding a NCEP grid point is divided into a 21 by 21 grid of 0.5° resolution. The ideal circumstance is that a rainfall value should be available in all of the 441, 0.5° grid points in the NCEP rain area. However, this is not the case. The CTLs that are positioned further south, as in figure 5.3, will have more 0.5 grid points with rainfall than the CTL days positioned further north (Fig. 5.3b). Even though rainfall values in some of the NCEP grid points outside of South Africa are quite limited, it was decided to include these grids in order to investigate the influence of CTLs on South Africa's rainfall when the CTL is located outside of the borders of the republic. In Fig. 5.3b for instance a CTL located over Botswana could influence the rainfall over a vulnerable South African rainfall area bordering Botswana. There is also an overlap of NCEP rain areas for different NCEP grid points as displayed in figure 5.3a, where the NCEP rain area with the centre at X_1 overlaps with NCEP rain area with the centre at X_2.

The issues which arise with the inadequate rainfall distribution will be illustrated later in section 5.3.3. CTL rainfall in the north of the area may be unrepresented.

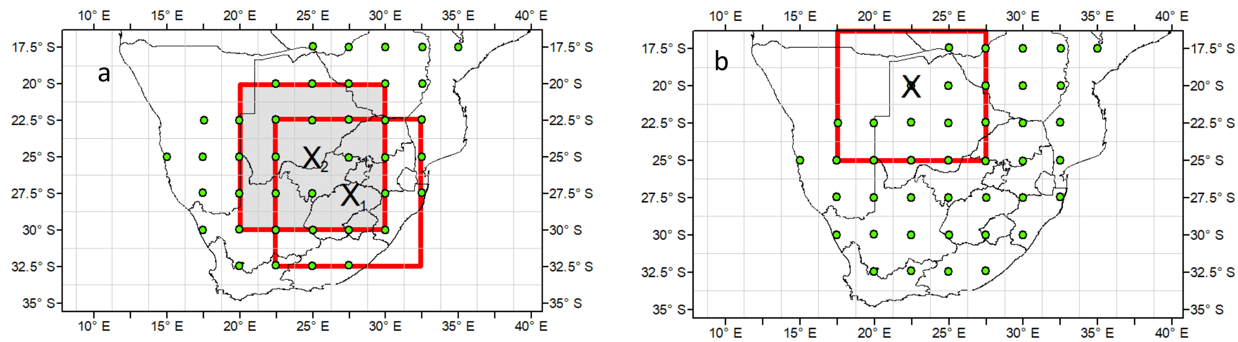

Figure 5.3: Red blocks indicate the 10° NCEP rain area for 3 different NCEP grid points. The green dots are NCEP grid points where some rainfall is available over South Africa in the NCEP rain area. NCEP grid points outside the borders of South Africa have rainfall values available only in a fraction of the NCEP rain area while grid points over South Africa have rainfall over the entire rainfall area (a). As an example in (b) only the extreme northern parts of North West Province and western Limpopo will have rainfall values for the particular NCEP grid point. There is an overlap of NCEP rain areas as X_1 represents the centre of a NCEP rain area that overlaps with that of X_2

5.3 Rainfall contribution of CTLs to South Africa

5.3.1 Seasonal CTL rainfall

The total CTL rainfall for each season (December to March) is provided in Fig: 5.4. The highest CTL rainfall seasons were 1987/1988, 1995/1996, 1999/2000, 2003/2004 and 2016/2017 seasons.

The 1999/2000 season was a very active CTL season with the highest number of CTL events ever recorded occurring during this season (Table 4.2). During February 2000, tropical cyclone Eline made landfall over Mozambique and moved westwards over the interior of the subcontinent. A CTL was first recognised on 4 February and continued until 19 February 2000. This CTL was the second longest lasting CTL which existed for a total of 16 days but was mainly situated around 17.5°S. The long term average number of CTL events for the month of February is 26, however during February 2000 an exceptional number of 100 CTL events occurring during this month (Table 4.2). Earlier that year, in January, another long-lasting CTL (12 days) was present and also mainly persisted around the 17.5°S latitude. Even though these events were situated quite far north, they have contributed to the high CTL seasonal rainfall. One can only imagine the true influence these CTLs had to the rainfall contribution over the areas further north of the study area.

In the 2003/2004 season ENSO was neutral, however the CTL rainfall during this neutral phase was particularly high (Fig. 5.4). This season had a very slow start in terms of the number of CTL events with December only having 3 events, which is far below the long term average of 11 (Table 4.2). January had 29 which is very much in line with the norm, however, from February, the CTL events increased rapidly and into March with more than three times the long term average CTL events for March.

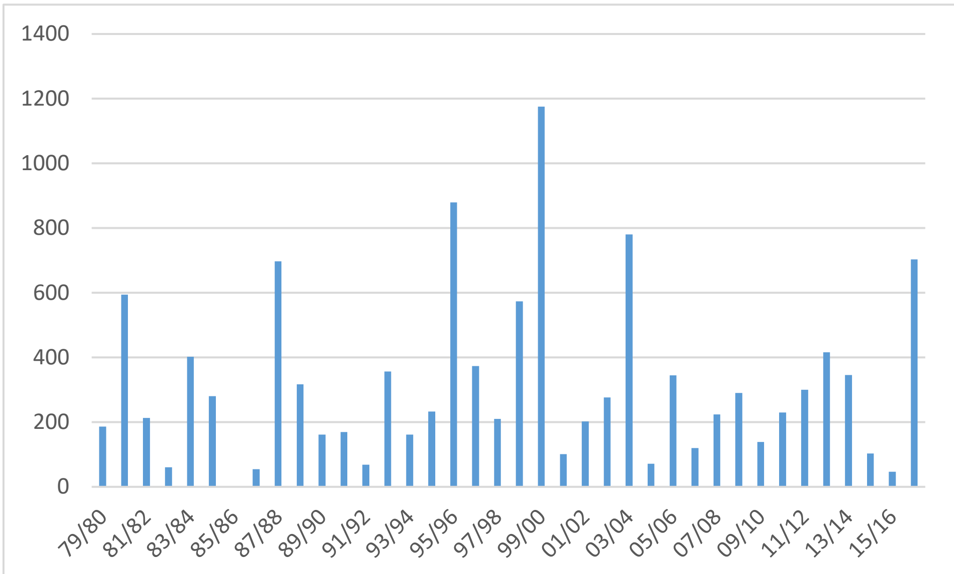

Figure 5.4: Total seasonal CTL rainfall totals (mm) for all NCEP rain areas.

The 2016/2017 season started off with above normal number of CTL events for December, however, January 2017 was an exceptional month with more than triple the average number of CTL events for that month recorded. During this month the longest consecutive day CTL also existed, which lasted for 19 days.

Extremely high rainfall amounts occurred during February 1988 (Triegaardt *et al.,* 1991). This was as a result of a CTL which was first identified on 7 February using the objective identification method presented in Chapter 4 but continued to be observed intermittently until 29 February 1988. At that time, the floods caused by this CTL were considered to be the worst experienced in living memory (Quinn, 1988) with some areas over the central interior of southern Africa receiving between 400 and 600% of the monthly mean rainfall (Triegaardt *et al.,* 1991). The objective identification method for CTLs did not identify a CTL on each day throughout this period.

5.3.2 Monthly CTL rainfall

The rainfall for each CTL day was used to calculate the monthly CTL rainfall in order to determine in which month the highest CTL rainfall occurs. The percentage contribution of each month towards the total CTL rainfall is shown in Fig. 5.5. The bulk of the CTL rainfall occur in January, with 42% of the total CTL rainfall taking place during this month. This result is very much in line with the monthly climatology results (Fig. 4.3), which show that January has the highest number of CTL events. Also, similar to the climatology results, December and March have the fewest CTL events, these months also have the lowest frequency of CTL day rainfall.

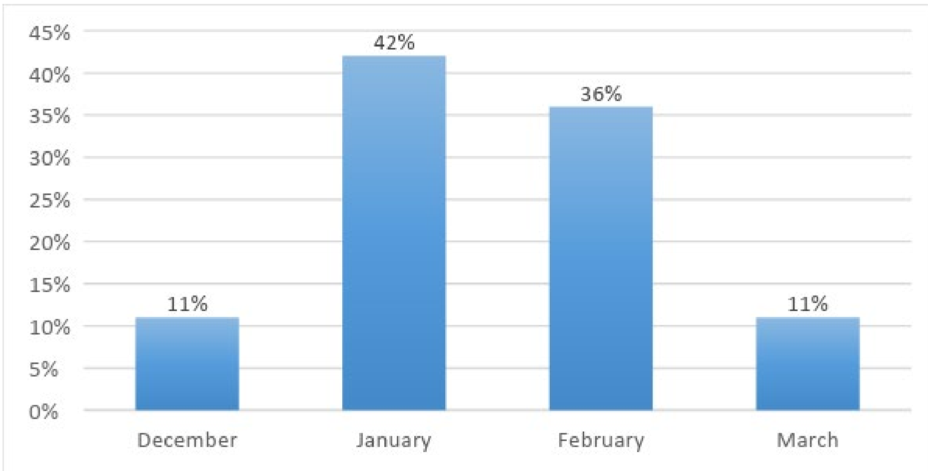

Figure 5.5: Frequency (%) of total CTL rainfall for each month.

The average monthly CTL day rainfall was used to determine the variation in the geographical distribution of CTL rainfall for each of the months (Fig. 5.6). Over South Africa, (south of 22.5°S), the CTL rainfall during December (Fig. 5.6a) is very much restricted to the extreme north-eastern parts of the country. The highest average CTL rainfall in a NCEP rainfall area over South Africa is 10 mm over northern KwaZulu-Natal. The NCEP rain area for this grid point includes a large part of the eastern half of South Africa.

There is a clear change in the rainfall distribution from December to January (Fig. 5.6b), where the rainfall extends further south and westwards, however the highest rainfall is still associated with the NCEP grid point centred over northern KwaZulu-Natal. The CTL which was identified to occur the furthest south was during a January and an average of 4 mm across the NCEP rain area. Geographically CTLs have a higher frequency over the eastern parts of South Africa (Fig. 4.2) and the rainfall values also show higher rainfall in the east than the west of South Africa. Another possible reason for the higher rainfall values in the east is the presence of the escarpment and warm Mozambique current which contributes to enhanced rainfall.

In February (Fig. 5.6c), the highest rainfall values occur further westwards and are centred over the northern parts of the Northern Cape. CTLs occur furthest south during March (Fig. 4.2d) and therefore the average rainfall associated with CTLs during March is also far south. The rainfall as a result of CTLs during March stretches across most of South Africa covering the western and most of the eastern parts of the country. The westward shift of the monthly CTL rainfall pattern coincides with the westward advance of the 50 mm isohyet from December to March over South Africa (Taljaard, 1996).

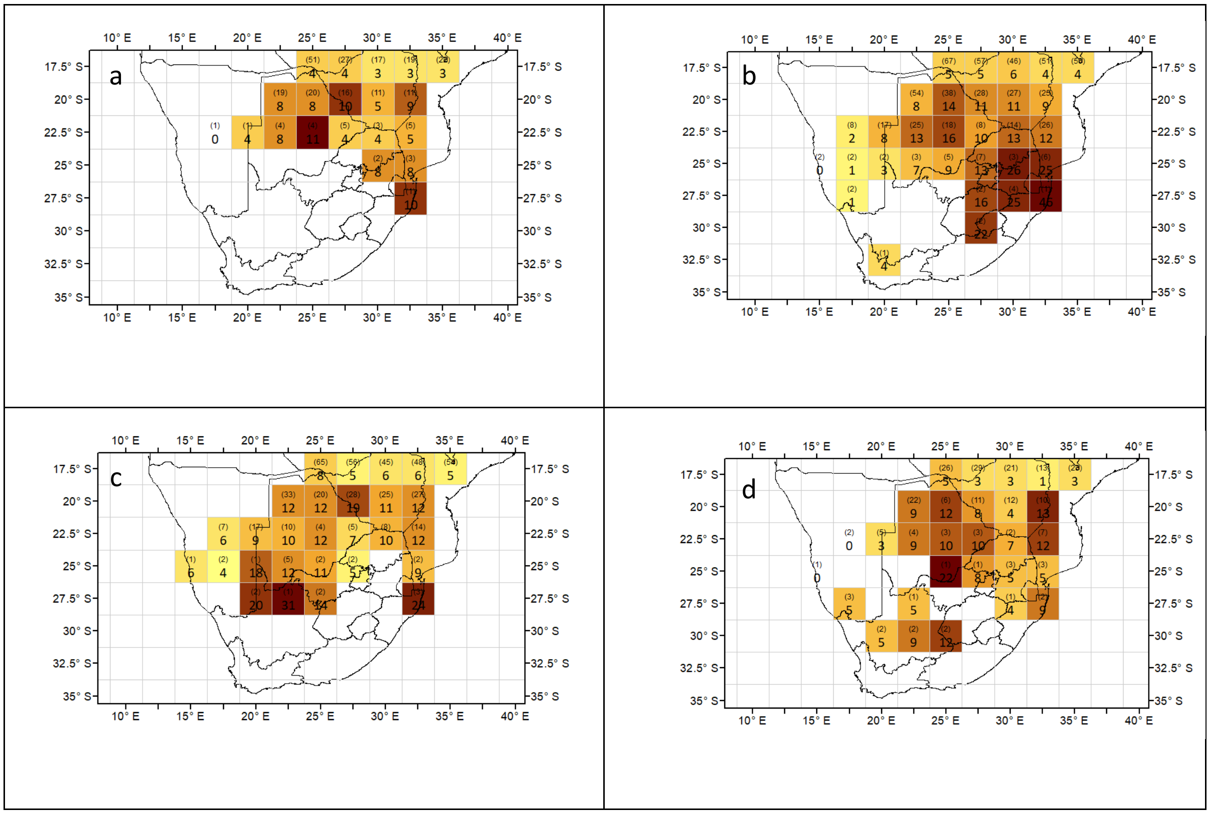

Figure 5.6: Geographical distribution of the average rainfall per CTL day with the number of CTL days in brackets above each value for (a) December, (b) January, (c) February and (d) March.

5.3.3 Average daily Continental Tropical Low pressure rainfall

The average daily CTL rainfall across per NCEP rain area is generally between 10 and 13 mm (Fig. 5.7a). There is a rapid decrease in CTL rainfall from east to west. The region indicated by the block in Fig. 5.7a, only had two CTL days in total. The rainfall figures in this area may not be totally representative, however it is clear that on these 2 days widespread and heavy rainfall occurred. The highest average rainfall amounts are in the northern and eastern parts of the block. This shows that the rainfall as a result of CTLs has a greater influence on the northern and eastern areas of South Africa and less of an effect further south-west, into the Western Cape.

Over southern Africa (area south of 22.5°), the number of CTL days (amounts in brackets in Fig. 5.7a) decrease south and westwards while the average CTL rainfall increases southwards. A possible reason for this is the limited rainfall availability in the northern areas which will influence the daily rainfall. However, as the CTL moves further south and eastwards in encounters more moisture and rainfall values will increase.

In order to fully appreciate the significance of these results and understand the contribution CTLs have to the rainfall over South Africa, a comparison of CTL rainfall is made with long term mean rainfall per NCEP grid point (Fig. 5.7b). The long term mean rainfall is calculated in each NCEP rain area for every day during December, January, February and March from 1979 to 2017.

From visual inspection of figure 5.7b, it can be seen that the average rainfall during CTL days (a) is far higher than the long term mean rainfall (b). Over the entire study area, the average CTL day rainfall is 10 mm per grid point while the mean value is only 5 mm overall. This shows that the rainfall as a result of a CTL clearly contributes significantly to the rainfall over the area.

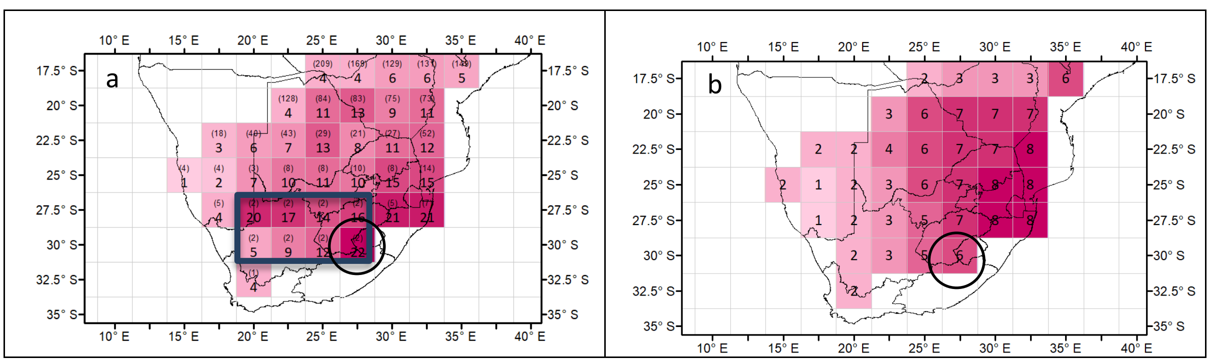

Figure 5.7: Geographical distribution of the (a) average rainfall per CTL day with the number of CTL days in brackets and (b) the long term mean rainfall across the region. The highest average CTL rainfall value of 22 mm is circled in (a) with the corresponding grid point also indicated in b

The highest average CTL rainfall in an NCEP rain area is 22 mm (circled), this value is more than 3.5 times higher than the long term mean value (circled in Fig. 5.7a and b) for the same position. The average NCEP rain for this specific point includes most of the eastern parts of South Africa. However, one should consider than the average daily CTL rainfall at this grid point was calculated for 2 days only.

In Fig. 5.8 the rainfall distribution for selected NCEP rainfall areas are shown. If the NCEP grid point is located over Namibia or Botswana only a fraction of the 144 grid boxes have rainfall values (Fig.5.8a).

This limits robust interpretation of rainfall in these grid boxes. However, it is noteworthy to see how far from the position of the CTL heavy rainfall occurs (Fig. 5.8 a-c). As the CTL moves east and southwards, closer to South Africa, the availability of rainfall increases and a more representative rainfall distribution becomes available. A common trend in the CTL rainfall for all NCEP rainfall areas is that the heaviest rainfall (shaded values) occur east of the CTL with significant less rainfall to the west Fig. 5.8 (h-l). When the NCEP rainfall area includes the escarpment very heavy rainfall follows (Fig. 5.8 e, k and l).

Heavy rainfall can already be experienced over Limpopo province when the CTL is still some 500 km away over Botswana. As the CTLs moves eastward, heavy rainfall continues over the province but now with extreme values over the eastern escarpment.

The value of the information captured in figure 5.8 is potentially of enormous significance to any operational forecaster. This demonstrates that an area positioned more than 600 km away from the central point of a CTL, can still be affected by the rainfall as a result of that CTL.

5.4 Composite CTL rainfall.

A composite CTL rainfall filed is created in order to investigate the rainfall distribution associated with a CTL, irrespective of the geographical position of the CTL. In order to visualise the rainfall distribution, this grid is divided into four quadrants, Q1, Q2, Q3 and Q4. The central point (white block) is excluded from the calculations so that the number of grid points in each quadrant is equal. The quadrant, Q4, has less data due to the north-western parts of the study area mainly falling outside of the South African borders with less rainfall data being available for this study. The purpose of creating an arbitrary grid is to assist forecasters in identifying the quadrant where the highest rainfall generally occurs during CTL events. This information can be used by forecasters as a first guess as to where to expect the significant rainfall associated with a CTL.

The average rainfall (Fig. 5.10) for each 0.5° grid is calculated in this composite. Upon visual inspection the highest average rainfall amounts during CTL days is mainly towards the east (Q1 and Q2) of the CTL. This is also shown in Table 5.1 where the average rainfall values per quadrant is shown. Quadrants 1 and 2 have the highest average rainfall with 19 mm and 16 mm respectively. This indicates that the area to the east of the CTL is in fact, the area where the bulk of the rainfall occurs during CTL days. It is very important to remember that local topography needs to be taken into account. For example, over KwaZulu-Natal, in South Africa, when a CTL is positioned over Richards Bay, very heavy rainfall will occur to the west of the low as the warm moist air rise against the southern escarpment.

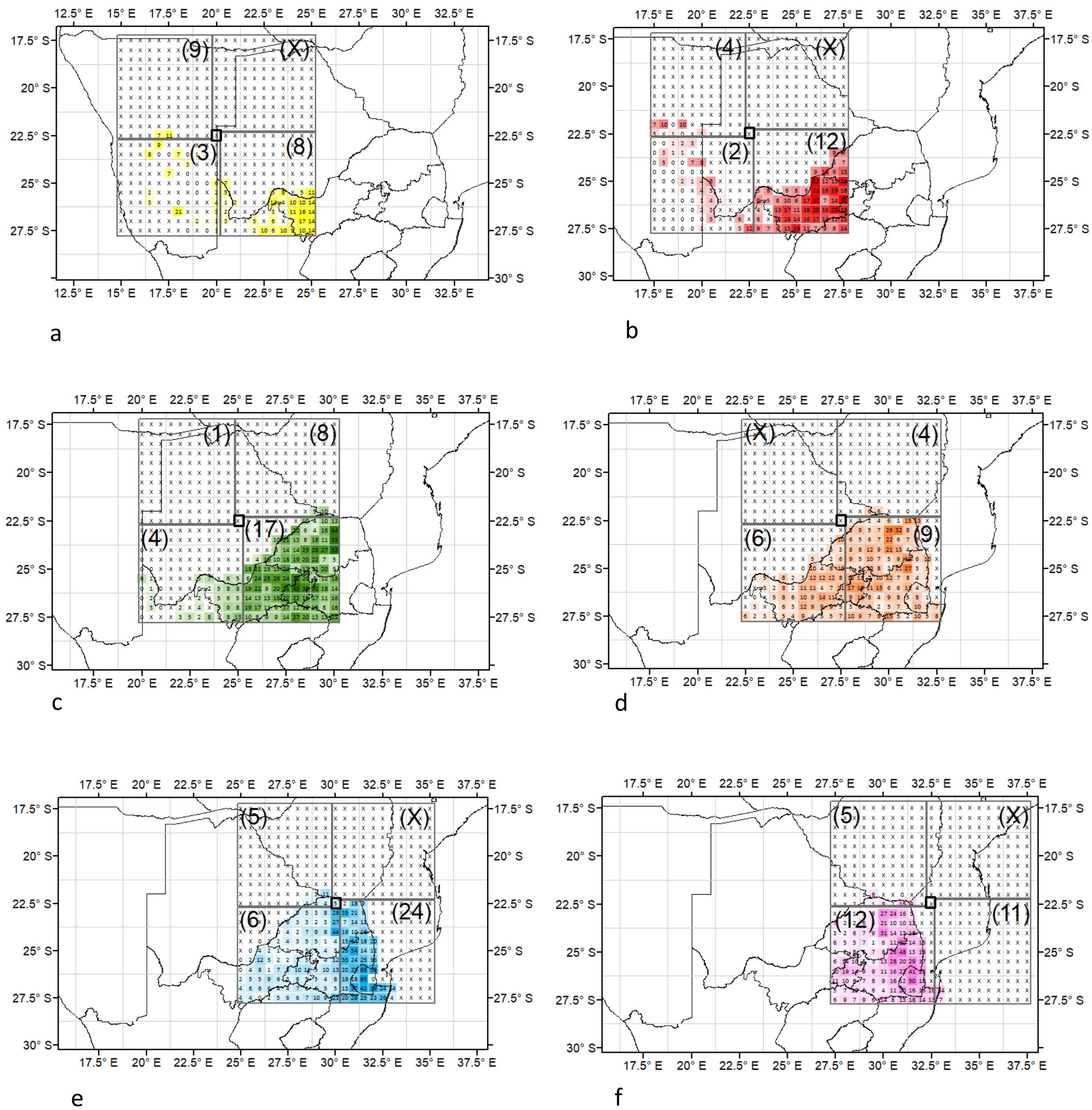

a
b
c
d
e
f

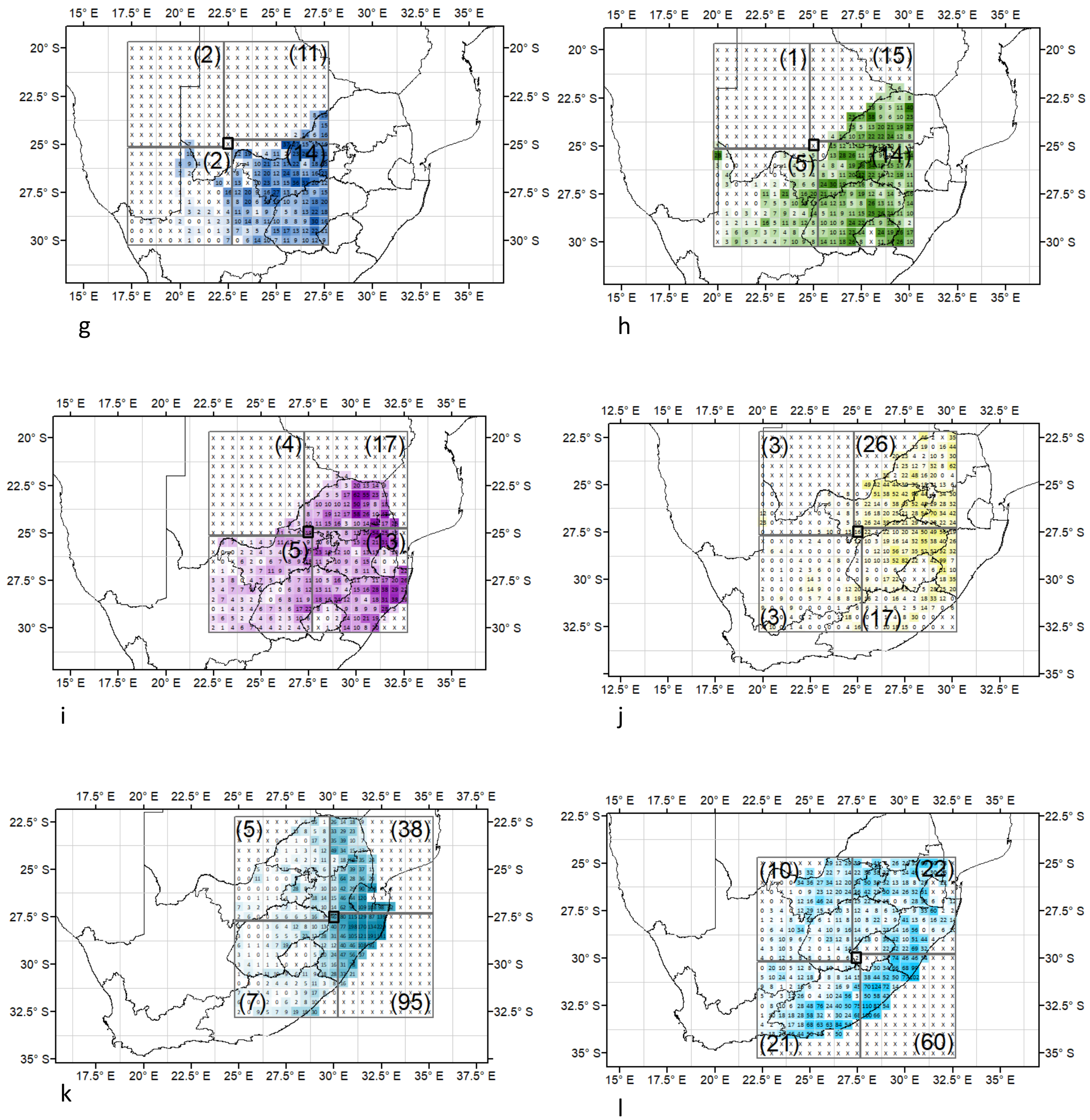

Figure 5.8: Average CTL rainfall distribution for selected NCEP rainfall. The position of the CTL is in centre point in the small circled box. The value in brackets represents the average rainfall per quadrant.

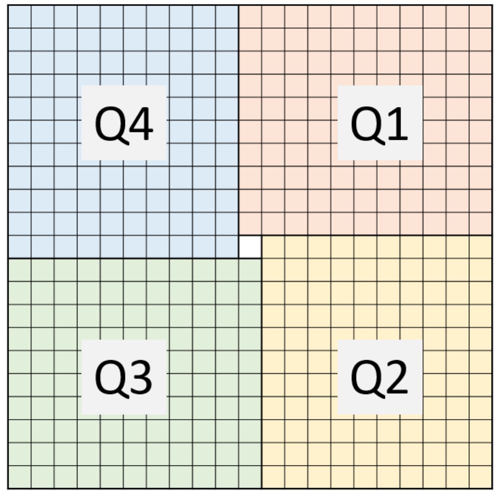

Figure 5.9: Arbitrary grid distribution with each quadrant divided into Q1, Q2, Q3 and Q4

							14	17		21			9				35	22		
	10					40	15	11			24	24	13			30	25	14		
			7	8	28	19	13	11	12	19	25	11	11	18	24	16	19	20	15	
2	3			8	31	14	9	12	12	29	23	15	20	15	24	19	19	39	9	27
5	5		3	4	4	18	18	10	10	11	19	34	14	13	12	18	20	14	14	10
1		3	6	8	10	10	22	14	12	14	14	17	15	13	17	14	16	16	11	9
1	5	4	3	11	26	24	14	9	11	21	20	16	18	22	39	28	20	14	23	27
12	5	4	3	7	14	13	9	14	14	16	17	13	17	26	25	24	15	15	13	17
3	1	4	4	5	24	14	13	14	10	19	18	16	23	21	26	20	22	29	15	20
6	3	6	3	3	8	14	15	10	14	16	20	26	19	20	29	25	24	14	15	19
3	2	4	2	5	8	10	17	11	11	20	16	20	15	20	26	16	21	14	22	17
5	4	3	2	5	20	17	14	13	12	31	24	24	24	23	37	24	17	15	24	32
6	5	5	6	6	14	9	12	12	17	24	14	17	19	25	25	19	15	17	15	19
4	4	5	6	6	15	9	11	18	12	17	14	13	22	16	15	15	17	21	19	22
4	4	4	4	4	5	9	19	8	10	9	13	23	13	13	15	13	18	12	12	13
5	3	5	3	4	7	13	16	8	9	9	13	17	12	11	17	9	14	10	14	16
4	6	6	4	6	18	15	11	12	10	17	17	15	14	13	26	22	13	11	15	27
4	7	7	5	6	10	8	9	7	10	13	11	11	11	12	19	16	13	13	11	19
4	5	6	8	7	11	8	8	9	7	13	9	11	14	11	22	12	13	15	13	23
4	6	6	4	4	4	7	13	7	7	8	10	13	8	8	11	11	14	9	10	11
4	3	5	4	5	6	8	11	7	7	9	9	11	7	8	11	10	13	8	9	11

Figure 5.10: Composite CTL rainfall distribution during CTL days.

As can be seen in the results displayed in Table 5.1, Q1 had the highest percentage of rainfall grids that met the thresholds of at least 20 mm, 50 mm and 100 mm. In Q1, 42% of rainfall points measured at least 20 mm, 13% measured at least 50 mm and 3% measuring 100 mm. The rainfall extremes measured in Q3 and Q4 are very similar, with the same percentage of extremes measured in each of these quadrants. Overall, it is quite rare for any station to measure at least 100 mm during a CTL day as an average of only

2% of CTL days measured at least 100 mm. It is a lot more common for at least 20 mm to be measured, with 26% of grids measuring at least 20 mm during CTL days.

Table 5.1: Average rainfall of each grid point for all quadrants (Q1, Q2, Q3 and Q4) for all CTL days and frequency of different rainfall thresholds

	Average rain per quad (mm)	% of grids ≥20 mm during all CTL days	% of stations ≥50 mm during all CTL days	% of stations ≥100 mm during all CTL days
Q1	19	42	13	3
Q2	16	27	9	2
Q3	9	17	5	1
Q4	10	17	5	1
Average	14	26	8	2

5.5 Extreme rainfall

A Major Rain Event (MRE), was defined by Dyson (2009) for Gauteng when the average daily rainfall exceeds 10 mm and at least one station measuring at least 50 mm. Adapting the definition for this report, a MRE is defined as an event where the average rainfall over a NCEP rain area exceeds 10 mm and one rainfall station measures at least 50 mm within the NCEP rain area.

During this study period, 447 MREs occurred during CTL days (Table 5.2). January had the highest number of MREs with 195, followed closely by February with 166. December had the least number of MREs with only 36. There is an average of 12.1 MREs per year that occur during CTL days across the study area, with 5.3 MREs during January and 4.5 during February. When comparing these results to those found by Dyson (2009) for rainfall over Gauteng, she found that January had 3.1 MREs and February 2.3. These results echo those of Dyson (2009) even though the study area and period are different.

Table 5.2: Total number of MREs per month with the average MREs per year for each of the months that occurred during CTL events.

	Major Rain Event (Average rain ≥10 mm and station rain ≥50 mm)	
	Total	Average MRE days per year
December	36	0.9
January	195	5.3
February	166	4.5
March	50	1.3
Total	447	12.1

5.6 Summary

CTLs contribute significantly to the rainfall over South Africa. The average rainfall as a result of CTLs is far higher than the overall average rainfall, with the average rainfall per grid point during CTL days being double the overall average rainfall. January has the highest CTL day rainfall as well as the highest number of extreme rainfall events and MREs. Overall, February has very similar results to January with the results just being slightly less for all criteria. The highest average CTL day rainfall occurs over the eastern parts of South Africa. From December to January, the average rainfall is confined to the north-eastern parts of the country and by March, the rainfall distribution extends across most parts of South Africa. The general distribution of rainfall around a CTL is found to occur to the east of the CTL, however, the extreme rainfall amounts generally occur towards the south. This information should be of substantial value to an operational forecaster as once a CTL is expected to develop over an area, the forecaster will then be able to delineate the area that is most likely to be affected by rain and therefore possible flooding as a result of a CTL. When a CTL exists, 26% of the time a forecaster can expect at least 20 mm of rain to be recorded at any given station, with more than 40% certainty that this rain will occur in Q1.

Chapter 6: CTL Case study

From 14 to 20 January 2013, devastating floods swept across Limpopo and Mpumalanga provinces resulting in the deaths of 12 people in South Africa and 9 in Mozambique (SAWS, 2017). This devastation was as a result of a CTL that developed over south-eastern Zimbabwe and advanced westwards. This chapter uses the CTL of January 2013 as a case study to demonstrate how the objective identification method can be utilized in identifying a CTL and to illustrate where rainfall occurs relative to the CTL.

6.1 Objective Identification of the CTL on 14 January 2013

Following the methodology presented in Chapter 3, CTLs were identified at 49 time steps during January 2013. To demonstrate the process that is followed when identifying a CTL, the event of 14 January 2013 at 12Z is used. In an operational environment, the long term mean would not be known, therefore using the variables presented in this report that are readily available in a forecasting environment, will be used to identify the CTL.

On 14 January 2013, a low pressure is seen at 850 and at 500hPa (black lines in Fig. 6.1a and b) with a high pressure aloft (300hPa) (Fig. 6.1c). Coinciding with the surface low and upper high pressures, are areas of negative relative vorticity at 850 and 500hPa and positive vorticity at 300hPa (green lines in Fig. 6.1). Negative values of relative vorticity display areas of cyclonic rotation, while positive values show anti-cyclonic rotation in the southern hemisphere. This indicates that there is an upright low pressure in the lower and mid-levels of the atmosphere with a high pressure aloft.

There is a clear warm core in the 500-300hPa column (shaded blue area in Fig. 6.1c) that is positioned over western Zimbabwe and north-eastern Botswana. The warm core is in very close proximity to the 500hPa low pressure (black lines in Fig. 6.1c).

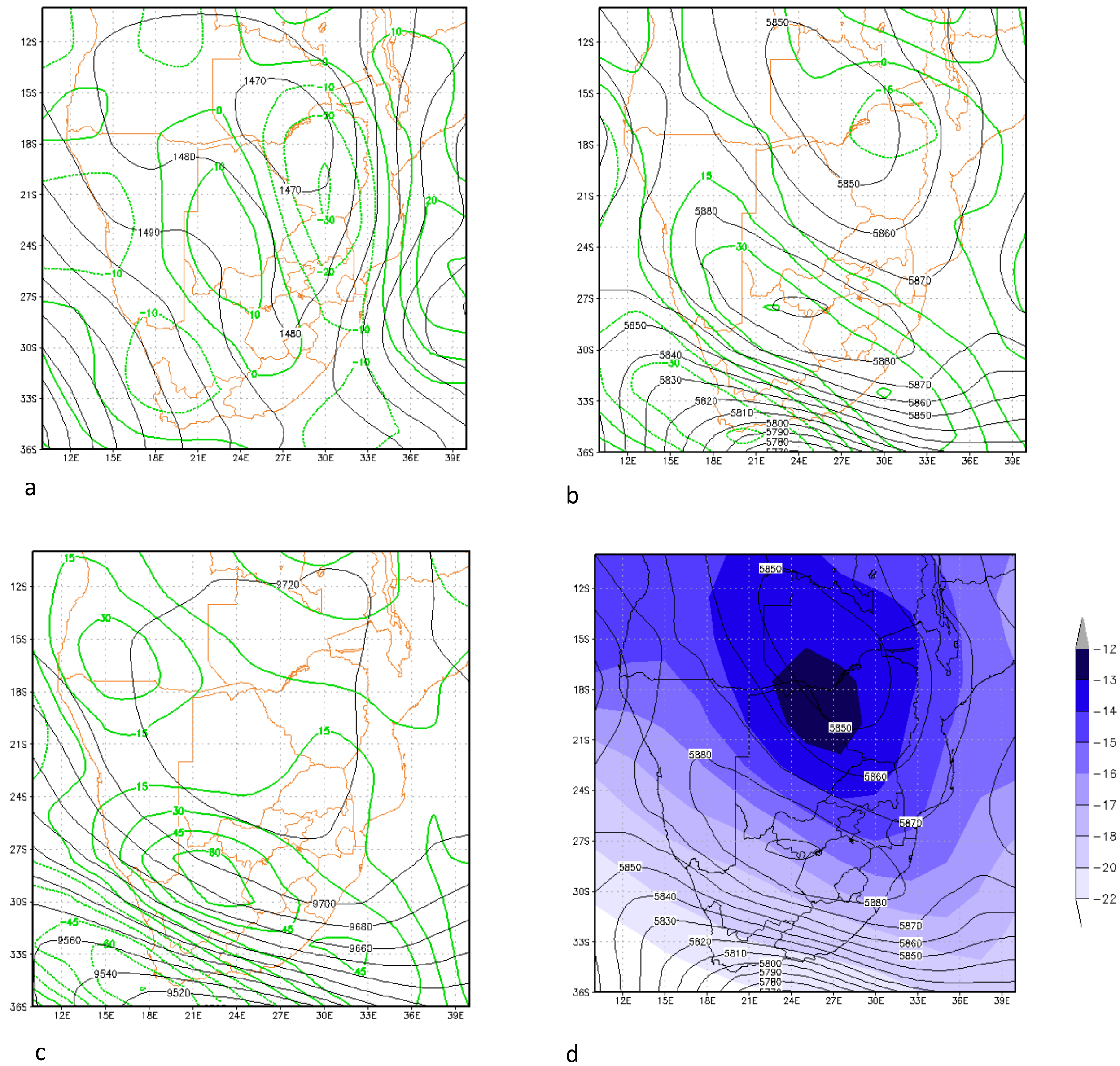

Figure 6.1: Relative vorticity (green lines in units of 10^{-5} s^{-1}) and geopotential heights (black lines) at (a) 850hPa, (b) 500hPa and (c) 300hPa on 14 January 2013.The average 500-300hPa temperatures are shown in d

There are two regions that stand out in Fig. 6.2a where very high TSE values occur. These regions are positioned over southern Zimbabwe where the CTL is located and eastern Namibia. A very broad area of TSE values higher than 330×10^3J.kg^{-1} covers most of the region, except for the small area in the extreme south-west, which have lower values.

The atmosphere is very moist on 14 January 2013 as seen in Fig. 6.2b. The distribution of the precipitable water is strikingly similar to the TSE values (Fig. 6.2a). There are also two areas of very high precipitable water values which correspond to the high TSE cores. Precipitable values exceeding 20 mm cover most of the region, extending into the northern parts of South Africa. Values in the vicinity of the CTL is above 35 mm and above 25 mm over Limpopo and Mpumalanga Provinces where heavy rainfall occurred (see figure 6.5).

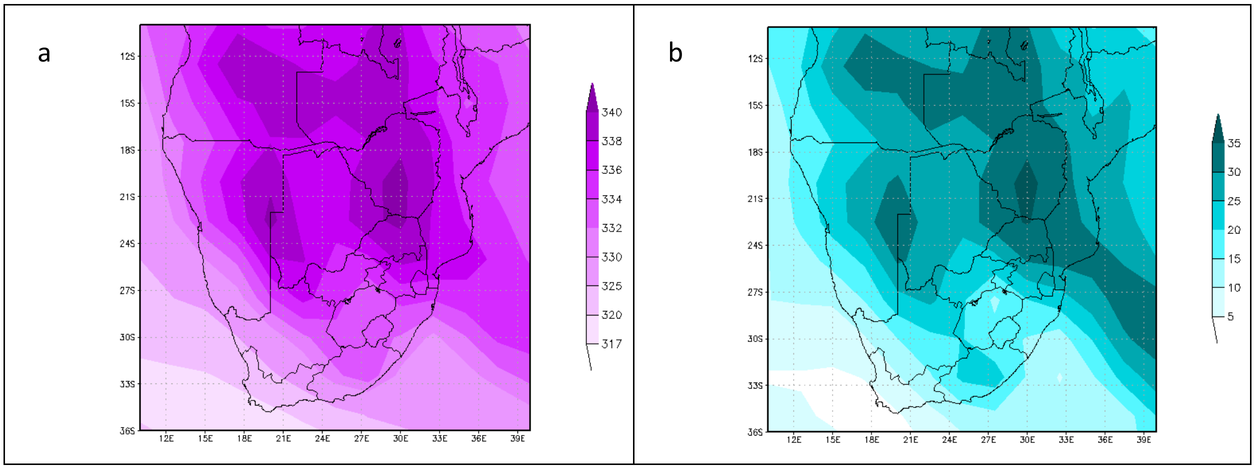

Figure 6.2: Average Total Static Energy in the 850-300hPa column on 14 January 2013. Units in 103J.kg-1 (a) and precipitable water values in the 850-300hPa column in units of mm (b)

After examining the atmospheric conditions on 14 January 2013, it is clear that the dominant weather system is a CTL. The position of this low pressure is given by the location of the lowest pressure at 500hPa (Fig. 6.1b), which is found at 17.5°S and 27.5°E.

6.2 Lifespan and movement of the Continental Tropical Low pressure

During January 2013, 49 events were identified (6-hrly time intervals). This case study focuses on the CTL that existed over the eastern parts of the study area. The CTL was first identified on 10 January 2013 at 06Z and continued to exist until the 18th at 12Z. This is a total of nine days which is quite a long duration considering the average lifespan of a CTL is 3 days or less (Fig. 4.5). The CTL initially developed over south-eastern Zimbabwe and followed a general westwards track (Fig. 6.3). The CTL remained stationary from the 10th 060 to the 13th at 00Z (3-days) at 20°S and 32.5°E (south-eastern Zimbabwe). It then headed north-westwards into northern Zimbabwe by the 14th at 00Z. The furthest south the CTL existed was at 25°S and 27.5°E on the 14th at 06Z (southern Limpopo). At 12Z on the 14th, the CTL was positioned at 17.5°S and 27.5°E (circled in Fig. 6.3).

The CTL progressed further westwards, through the extreme southern parts of Zambia and into south-eastern Angola. On the 15th, the CTL moved to south-western Zimbabwe, but by the 16th at 18Z, it made its way back to the extreme south-eastern parts of Angola. The CTL headed southwards on the 17th, into western Botswana and eventually progressed north-eastwards on the 18th at 12Z which was the final CTL event identified for this system.

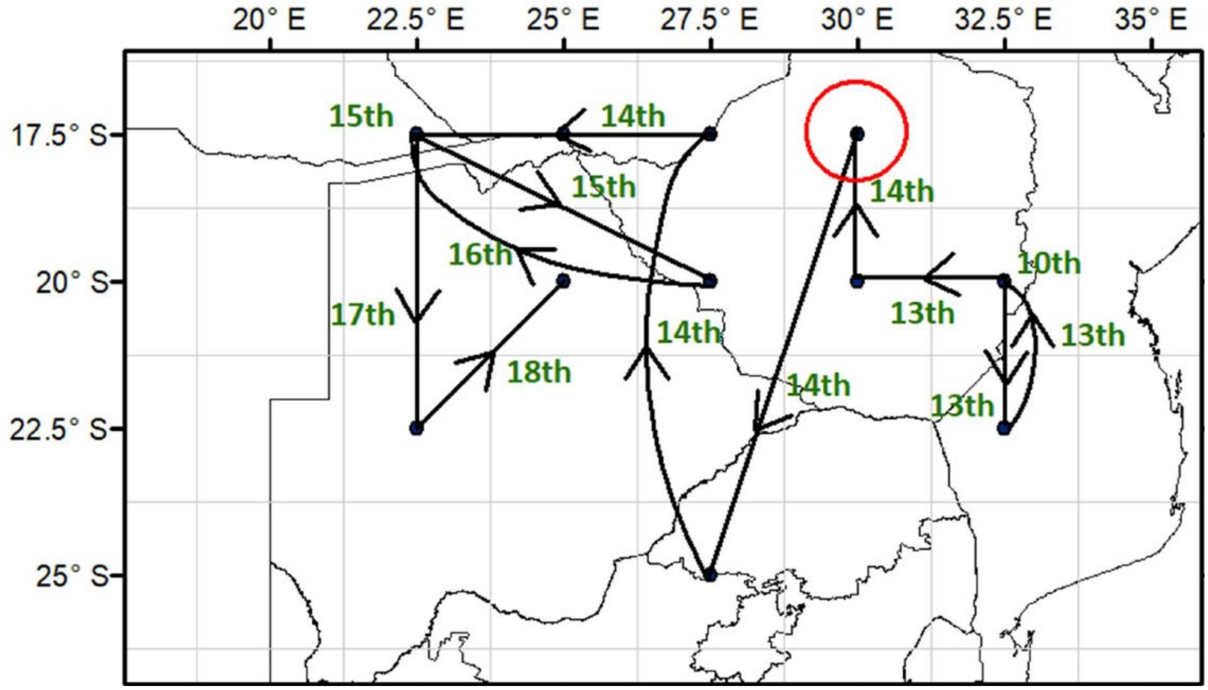

Figure 6.3: The path followed by the CTL from 10-18 January 2013.The arrows indicate the direction of movement with a general westwards motion during the lifespan of the CTL. The red circle indicates the position of the low pressure identified on 14 January 2013 at 1200Z.

6.3 Rainfall associated with the CTL on 14 January 2013

Green colours on the airmass Red-Blue-Green (RGB) satellite image indicate a warm airmass with a high tropopause, blue show a cold airmass and red represents an advection jet (Kerkmann, 2005). On 14 January 2013, a warm airmass is clearly present over Zimbabwe, Botswana and Mozambique (green colour in Fig. 6.4). The objective identification method identified a CTL at the position indicated in figure 6.4, this is the centre of the 500hPa low pressure.

On 14 January at 12Z, the main cloud masses were positioned over southern Mozambique (Fig. 6.4a), by 18Z on the same day, the clouds started shifting to the west and were positioned over Zimbabwe (Fig. 6.4b). The CTL also progressed westwards, positioned over the extreme southern parts of Zambia (Fig. 6.4b). NCEP reanalysis appears to have identified the low approximately 2.5 ° west of the actual position as indicated by the satellite image. Very high daily rainfall amounts were observed on the 14th of

January 2013 with 100-200 mm recorded in northern and central Limpopo (Fig. 6.5). High rainfall amounts (≥50 mm) are also observed along the Mpumalanga escarpment. This result reiterates what was presented in section 5.2 where the influence the escarpment has on the average CTL rainfall distribution is discussed. This low was responsible for heavy rainfall over South Africa and especially Limpopo even though it was situated very far north (5 degrees) of the northern most part of South Africa.

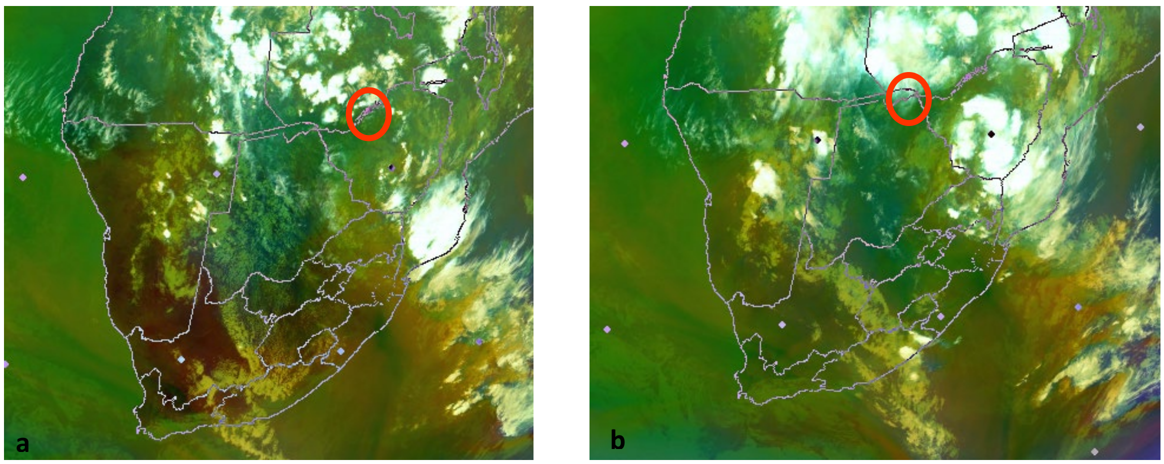

Figure 6.4: Airmass RGB satellite image on 14 January 2013 at 12Z (a) and 18Z (b) with the "L" indicating the central position of the CTL that was identified using the objective identification method (© EUMETSAT, 2018)

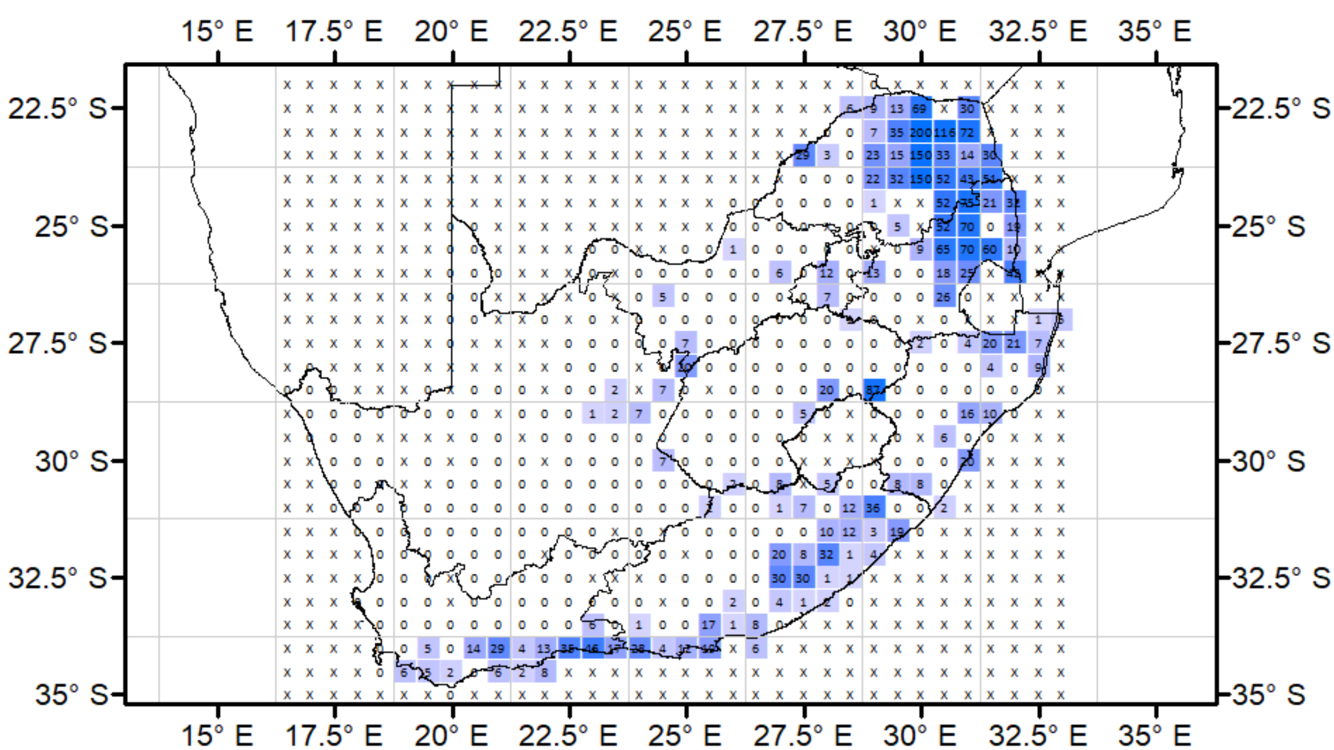

Figure 6.5: Geographical distribution of the rainfall per 0.5° grid over South Africa on 14 January 2013.

The CTL then followed an anti-cyclonic motion with the final CTL location over north-eastern Botswana on the 18th of January at 1200Z (Fig. 6.6). The cloud bands associated with this CTL extended all the way into the eastern interior of South Africa where rainfall amounts of more than 50 mm were recorded over KwaZulu-Natal (Fig. 6.7). Once again the influence the topography has on the rainfall is clearly seen in Fig. 6.7 with higher rainfall amounts observed along the escarpment.

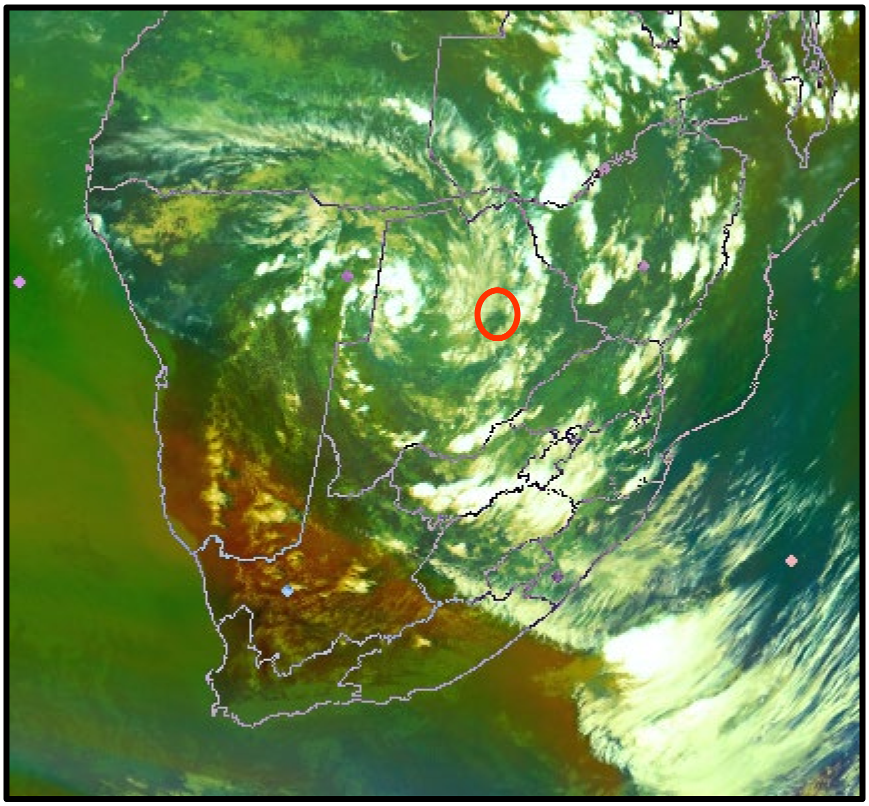

Figure 6.6: Same as Fig. 6.4 but for 18 January at 12Z (© EUMETSAT, 2018).

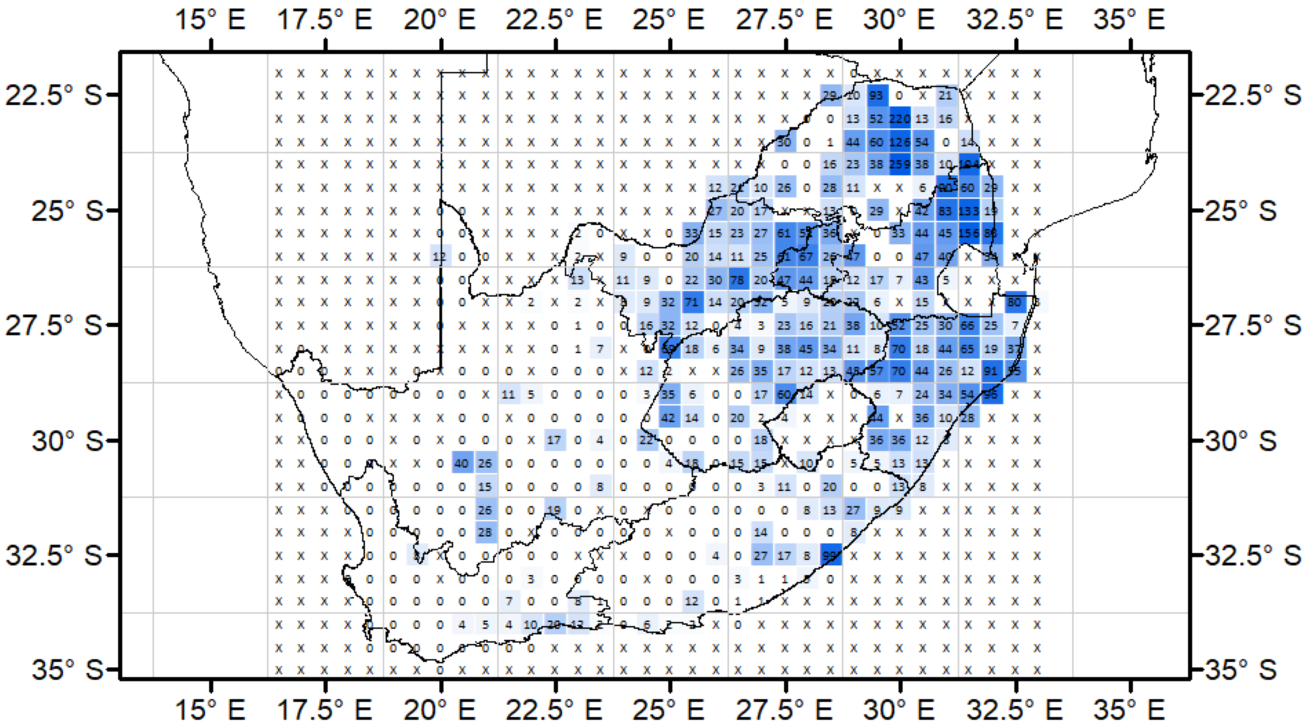

Figure 6.7: Geographical distribution of the CTL rainfall per 0.5° grid across South Africa on 18 January 2013.

6.4 Summary

The objective identification method presented in this report accurately identified the CTL that occurred from 10-18 January 2013 although the location differs slightly from the main cloud bands. The impact this CTL had on Limpopo and Mpumalanga Provinces was enormous (SAWS, 2017). Lives were lost and many homes were completely washed away. Flooding resulted in several thousand crocodiles escaping from a crocodile farm in Limpopo. The tourism industry was severely affected with many parks closed for two weeks. Three border posts between South Africa and Botswana were also closed as a result of the widespread flooding.

Even though the daily rainfall amounts as a result of a CTL are not as high as it could be from a tropical cyclone, it is the continual rainfall amounts in the order of 50-100 mm per day that result in the widespread adverse impacts. This case study demonstrates that due to the slow movement, long-lived lifespan of the CTL and the broad extent of the rain bands, these weather systems are capable of devastating effects causing prolonged disruptions to daily life.

Chapter 7: Forecast uncertainty of CTLs

7.1 Introduction

In Chapter 5 and 6 it was shown that due to the general slow movement and tropical nature of CTLs, they often cause heavy rain, resulting in flooding. In general, weather forecasters would benefit greatly from gaining insight into the frequency of occurrence of tropical weather systems due to the heavy rainfall events which have been documented to occur in association with them. In this chapter we aim to quantify the uncertainty in the prediction of CTLs over southern Africa. The question is asked: How accurate are the location and depth of CTLs predicted over southern Africa? Two CTLs are investigated, one moved considerably over southern Africa, and the other was semi stationary. The CTL results are also compared to a heavy rainfall producing Cut-off Low (COL) over South Africa in order to place the results in context with other synoptic scale weather systems over South Africa.

7.2 Data and Method

Interactive Grand Global Ensemble (TIGGE) (Bougeault et al., 2010) data were obtained from the European Centre for Medium Range Weather Forecasts (ECMWF) from the web at apps.ecmwf.int/datasets/data/tigge/. ECMWF and National Centre for Environmental Prediction (NCEP) ensemble forecast (5 ensemble members each) were downloaded for the 1200 UT model run initiation times. The analysis as well daily forecasts for up to 6-days ahead were acquired for NCEP and ECMWF. The data are available in 2.5° horizontal resolution for December2010, February 2014 and January 2017. The geopotential heights at 500hPa are used in the analysis.

The predictability of CTLs are explored by calculating the standard deviation between the 10 ensemble members. Studies have found an increase in uncertainty with progression of time (Anwender et al., 2008, and Harr et al., 2008) and especially as tropical lows transitions to extratropical.

7.3 Results

Three case studies are conducted. December 2010 were chosen as this was a heavy rainfall producing COL which occurred in late summer months and including this COL provides good insight into the difference in predictability between CTLs and weather systems of the extra-tropics. In February 2014 a CTL was semi-stationary over southern Africa while in January 2017 the CTL moved considerably. Both the February 2014 and January 2017 CTLs had life spans of more than 11-days.

7.3.1 The COL of December 2010

A weak upper air low developed west of South Africa on the 11th of December 2010. Although this low was semi-stationary west of the country it continued to deepen into a COL on the 14th after which it started to move eastwards over South Africa on the 15th and 16th. The COL redeveloped west of the country on the 17th where it quickly started to weaken. The results are shown for the 14th when the COL developed west of South Africa and for the 16th when the COL moved eastwards.

Fig.7.1 shows the location of the COL west of southern Africa on the 14th (top left) with relatively small standard deviation values in the centre of the low (8 m). The 10 ensemble members were in general agreement on the location and depth of the COL during the analysis time. The 1-day lead time forecast for 20101214 the uncertainty in the position and depth of the low increased with standard deviation values west of Namibia as much as 25 m. The 3-day lead time forecast the uncertainty was similar but with larger standard deviation values in the westerly trough south of the COL. Note how the 3-day ahead forecast the uncertainty was less than the forecast with shorter lead times. In this example the uncertainty with the development of the COL west of southern Africa was largest in the forecast with the shortest lead time (1 and 2 days ahead).

On the 16th (Fig. 7.2) the COL was located over south-western South Africa with a weak low off the west coast (top left). The ensemble average of the 1-day placed the low quite accurately on the south coast although the depth of this low was underestimated. The uncertainty in the forecast was largest over the Southwestern Cape with standard deviation values between 18-20 m. The forecast with 2-day lead time was considerably more uncertain underestimating the depth of the low as well as placing the low too far north over South Africa. The standard deviation on the Western/Eastern Cape border was between 25-35 m. The 10 ensemble members could not agree with the placement of the COL 3-day ahead with standard deviation between 35-45 m over the southwestern part of South Africa. Unlike the forecasts valid for the 14th in this instance the largest uncertainty occurred for the forecasts with the longest lead time. During this period the COL moved eastwards and the ensemble members did not agree with the placement and depth of the COL.

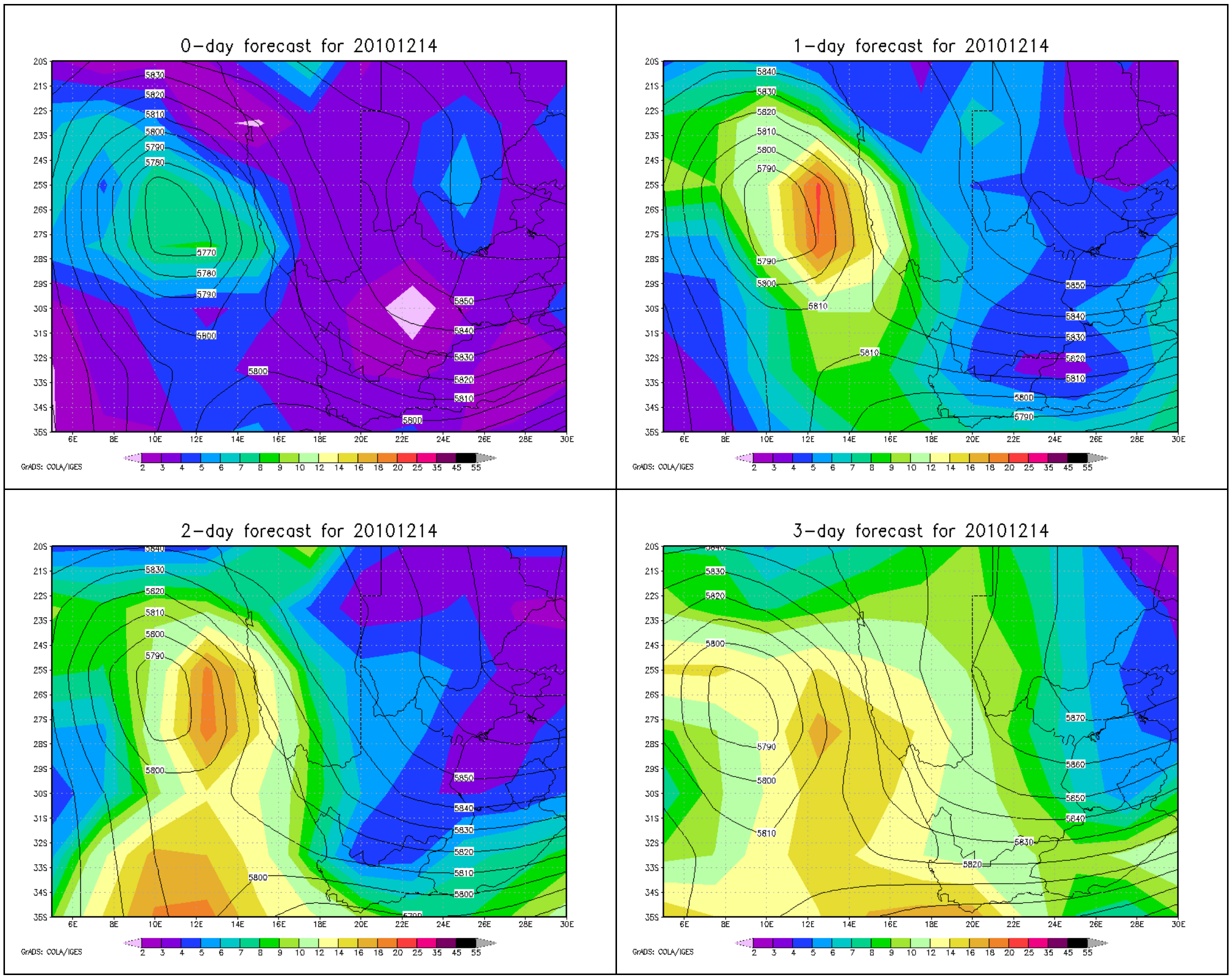

Figure 7.1: The 500hPa geopotential height ensemble average forecast for 12 December 2010 with lead times of 0, 1, 2 and 3-days. The standard deviation (m) of the 10 ensemble members are shaded.

Fig. 7.3 shows the forecasts from the models runs on the 15th for 0-3 days ahead. On the 15th the low was on the coast of southern Africa busy moving towards the south coast. What is quite evident from Fig. 7.3 is how the uncertainty grew with increasing lead time and the uncertainty was translated downstream to southeast of South Africa. Uncertainty increased with increasing lead time west of South Africa where the second low developed.

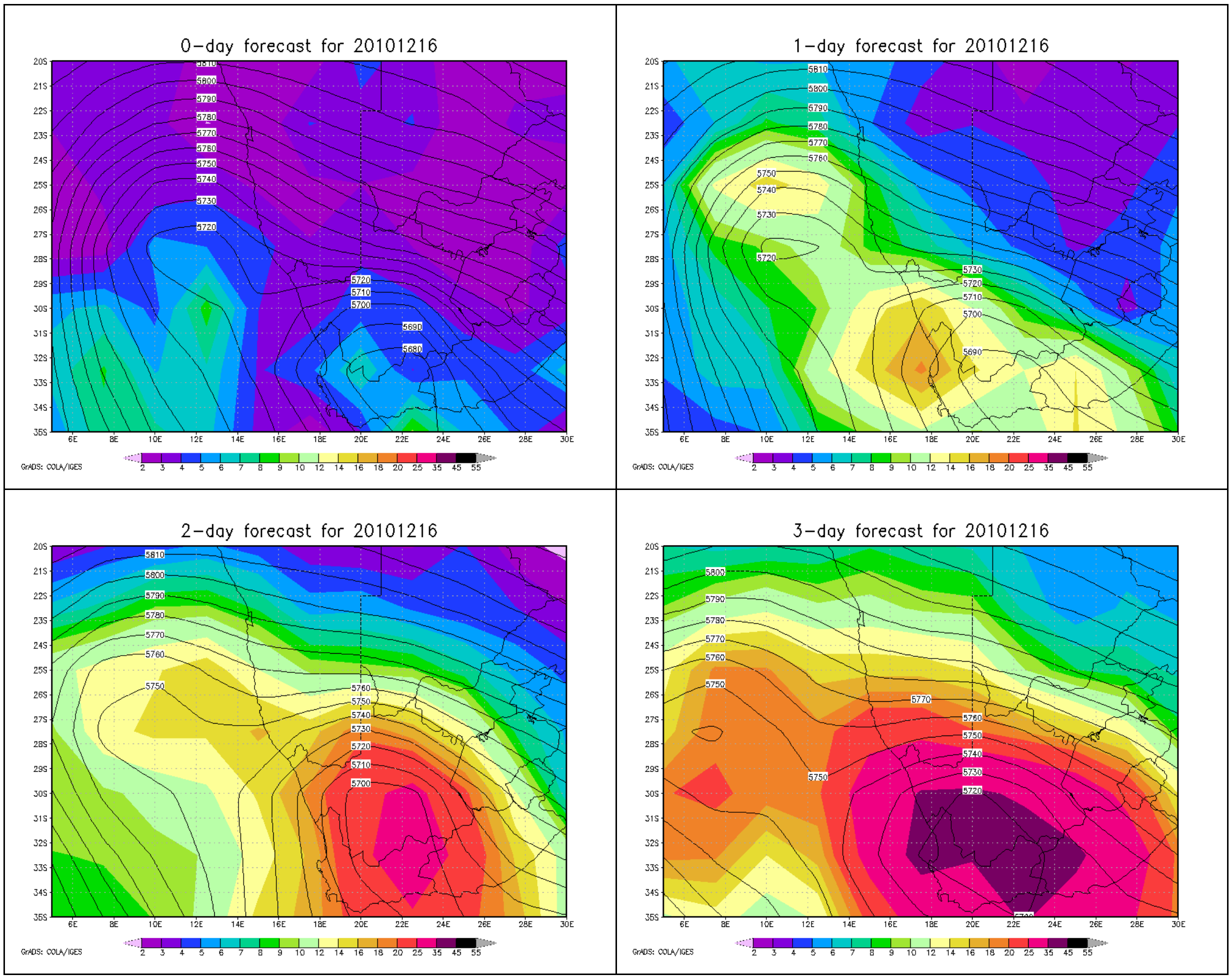

Figure 7.2: The 500hPa geopotential height ensemble average forecast for 16 December 2010 with lead times of 0, 1, 2 and 3-days. The standard deviation (m) of the 10 ensemble members are shaded.

This case study illustrates how the uncertainty in the forecast increases significantly with increasing lead time and how the uncertainty propagates downstream with longer lead times. When the low developed and was semi-stationary west of South Africa the uncertainty was much smaller than for when the COL was moving eastwards and dissipating.

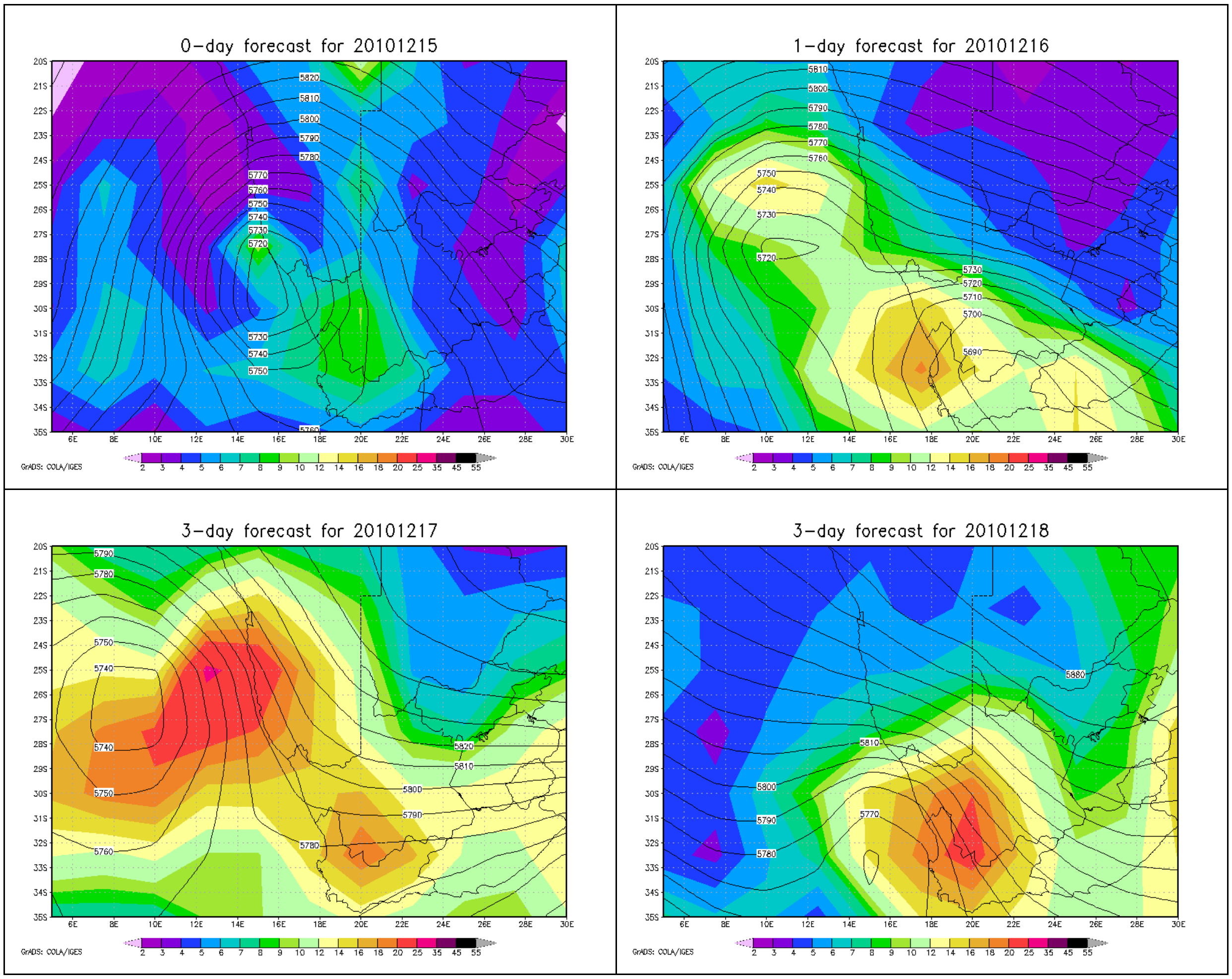

Figure 7.3: The 500hPa geopotential height ensemble average forecast for analysis time 15 December 2010 at 1200Z. Images are shown for lead times of 0, 1, 2 and 3 days. The average standard deviation (m) for all 10 ensemble members are indicated in shaded

7.3.2 The semi-stationary CTL of February 2014.

A CTL was present for 11-days over southern Africa from the 28th of January 2014 to the 8th of February 2014. The latitudinal position of this low remained at approximately 20°S, moving to 22.5°S on only 3 days. The longitudinal position of the low varied between 20°E and 22.5°E and on one single day touching the Namibian coast at 17.5°E. This low was semi-stationary for the entire 11-days. Results are shown for the 4th of February when the low oscillated somewhat eastward and for the 8th of February when the low started to dissipate.

On the 4th of February the analysis show (0-day forecast in Fig. 7.4) that the low was located on the Namibia/Botswana border and at approximately 22.5°S. For the analysis time the standard deviation is quite low with values between 2-4 m. The forecast for 20140204 with 1-day lead time was good with standard deviation less than 5 m. The depth of the low was slightly underestimated but the standard deviation remain relatively low and the different ensemble members therefore placed the low in a similar location. For the 2-day lead time forecast the uncertainty increases slightly with standard deviation values now about 7 m and the location of the CTL too far west over Namibia. For the 3-day lead time the uncertainty increases as the standard deviation is between 7-8 m over Namibia. Larger uncertainty is present over the southern part of South Africa in the westerly wind regime.

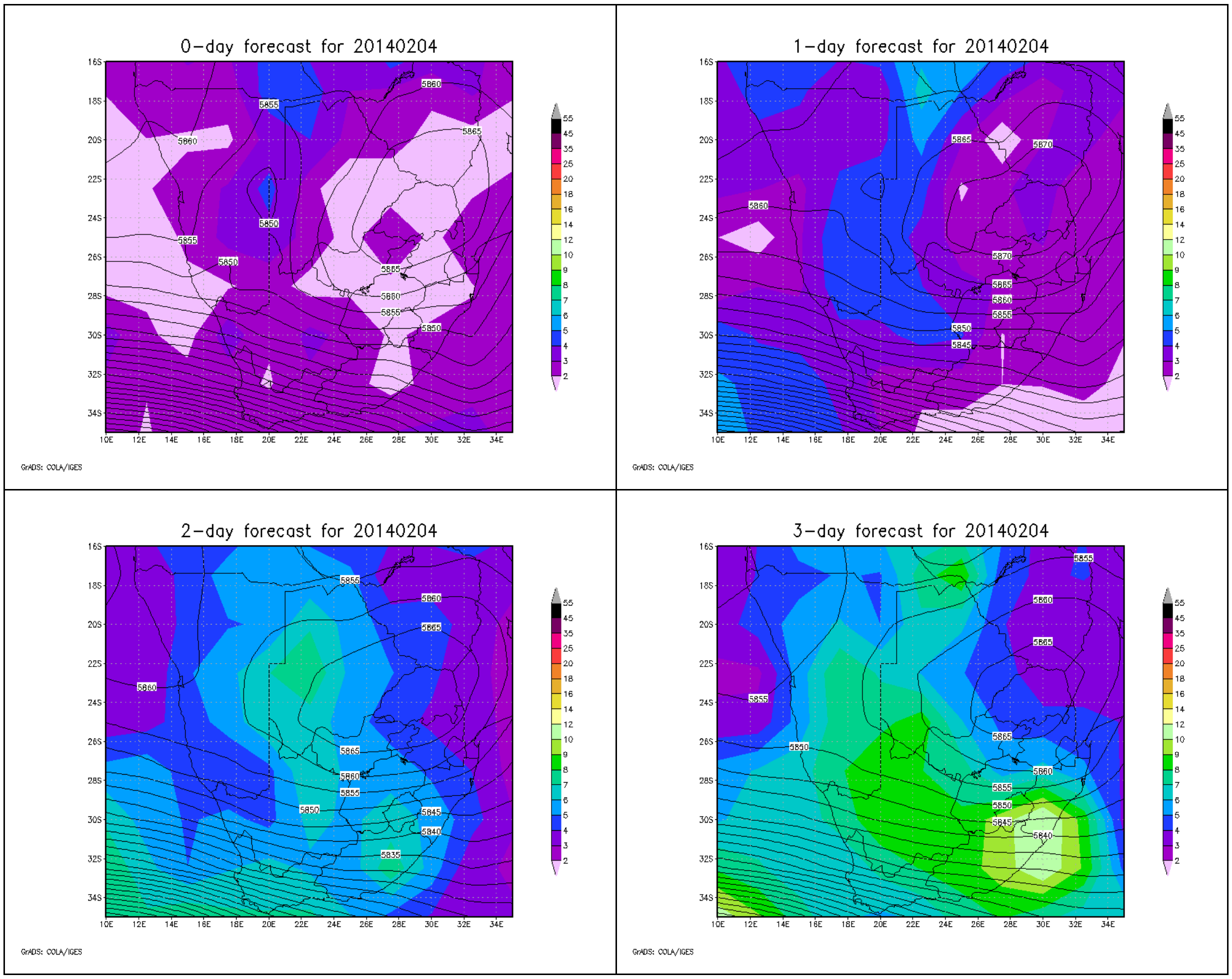

Figure 7.4: The 500hPa geopotential height ensemble average forecast for 4 February 2014 with lead times of 0, 1, 2 and 3-days. The standard deviation (m) of the 10 ensemble members are shaded.

On the 8th of February the low is weak over Namibia and Botswana with only a trough visible (top left in Fig. 7.8). The forecast with 1-day lead time the standard deviation in the location of the low is only 7-8 m increasing slightly for the 2 and 3-day lead time forecasts. The centre of the low is too deep and placed too far north over Botswana. The 3-day lead time forecast the uncertainty is large (25-35 m) in the westerly wind area over the southern extremes of Africa. The westerly trough will cause tropical low to move eastwards and eventually dissipate. The interaction between tropical and extra-tropical is more uncertain that the position of the tropical low.

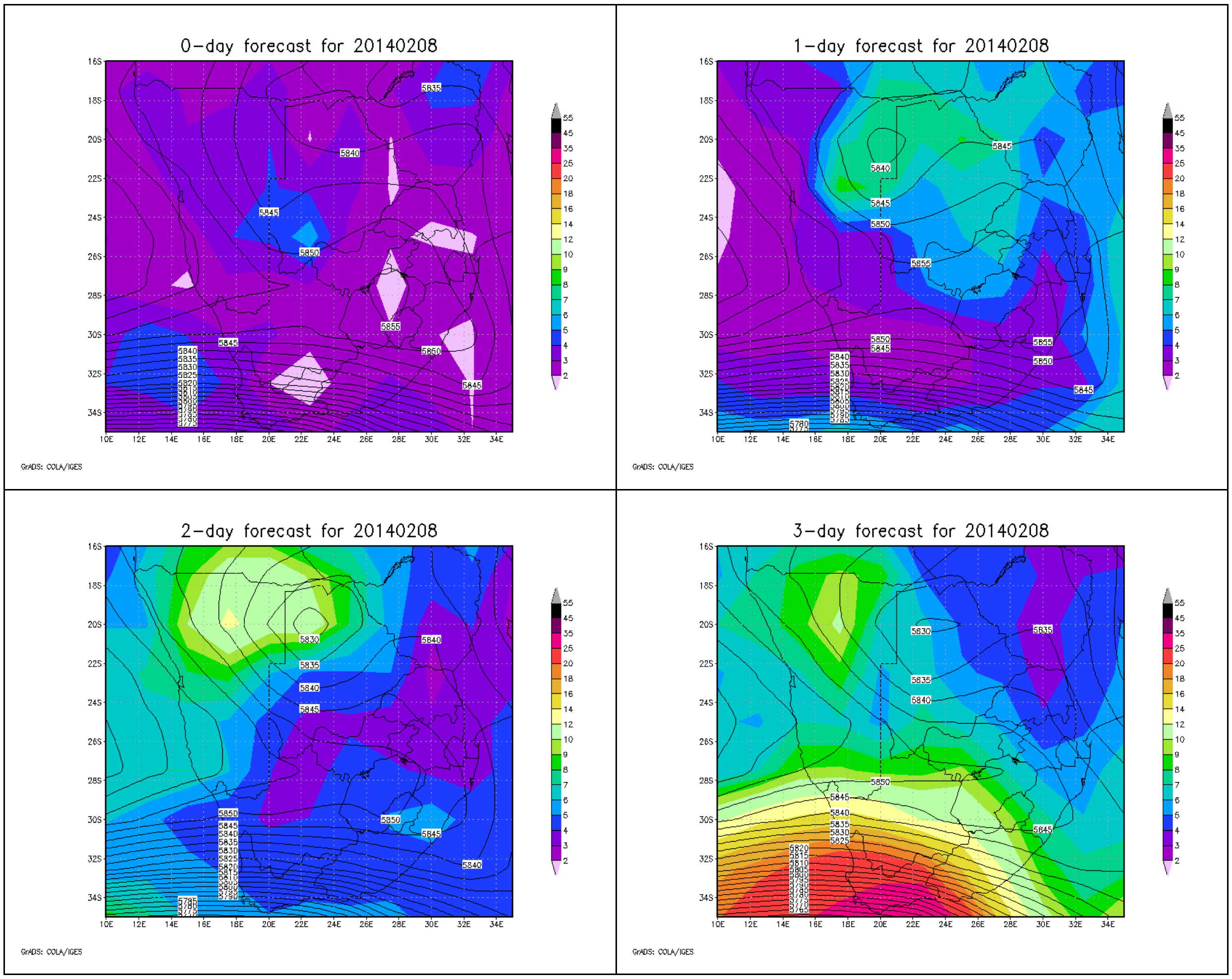

Figure 7.5: The 500hPa geopotential height ensemble average forecast for 4 February 2014 with lead times of 0, 1, 2 and 3-days. The standard deviation (m) of the 10 ensemble members are shaded.

In this case study the forecast with 1-day lead time was very good with little uncertainty. The uncertainty increases with increasing lead time but the largest uncertainty occurs in the westerly wind through in the south and west with the location and depth of the CTL being less uncertain.

7.3.3 The heavy rainfall producing CTL of January 2017

The CTL developed over southern Africa on the 3rd of January 2017 but unlike the February 2014 example this low moved considerably over the southern sub-continent of Africa. By the 7th of February the low was located over south-eastern Botswana causing heavy rainfall over the 4 northern provinces of South Africa. Remarkably the CTL moved westward to central Botswana on the 9th and even further north-westward in the following few days. On the 13th it started to move eastward again eventually moving into the Mozambique Channel on the 17th. Results for the 7th and 15th are presented here in order to show how well the position of low is captured by the ensemble forecast when it moves. In this instance the precipitation forecast available from the ensembles are also discussed in order to demonstrate how slight shifts in the position of the CTL influences the rainfall over South Africa considerably.

On the 7th of January the low was located over south-eastern Botswana with the 10 ensemble members being in good agreement about the position of low as standard deviation values did not exceed 7 m (Fig. 7.6, 0 day forecast). The average ensemble forecast for the 7th with one day lead time placed the low in a similar position over Botswana and with good certainty as the standard deviation was only 8-9 m. For 2-days lead time the location of the low was too far north over Botswana but with the standard deviation remaining rather low, the largest values being over southern Botswana. For 3-days lead time the low was not placed far enough south over Botswana with largest uncertainty on the Botswana/Namibia border.

Fig. 7.7 depicts the location of the CTL over Zimbabwe on the 15th (0 forecast). In this example the ensemble average of the 500 geopotential heights were consistent for all 3 lead times with standard deviation values in the CTL never more than 6 m. The ensemble predicted the position and depth of the CTL very well over Zimbabwe, even with 3-days lead time. The largest errors on the 3-day lead time forecast was the position of the Atlantic Ocean High west of South Africa.

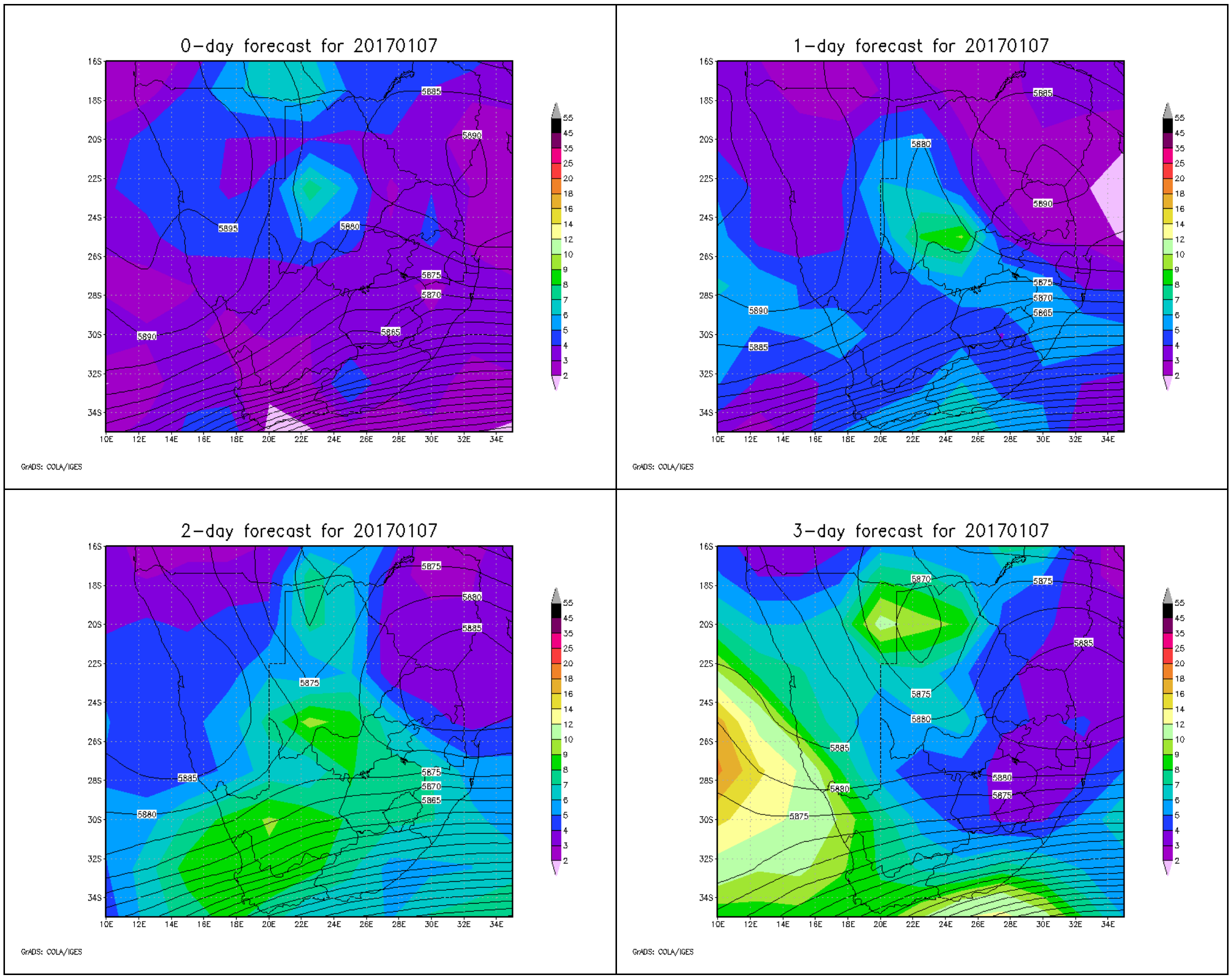

Figure 7.6: The 500hPa geopotential height ensemble average forecast for 7 January 2017 with lead times of 0, 1, 2 and 3-days. The standard deviation (m) of the 10 ensemble members are shaded.

Figure 7.8 shows the 3-day forecast with analysis time on the 11th of January 2017. Note how at the time of the analysis the standard deviation in the position of the low was between 14-16 m. This indicates that at the time of the analysis there was uncertainty in the ensemble members about the location and depth of the low. The uncertainty with 1 and 2 day lead time forecast in fact decreases and for 3-day lead time the standard deviation were small. Unlike the westerly wind systems, uncertainty in the location and depth of low pressure systems in the tropics do not seem to translate downstream.

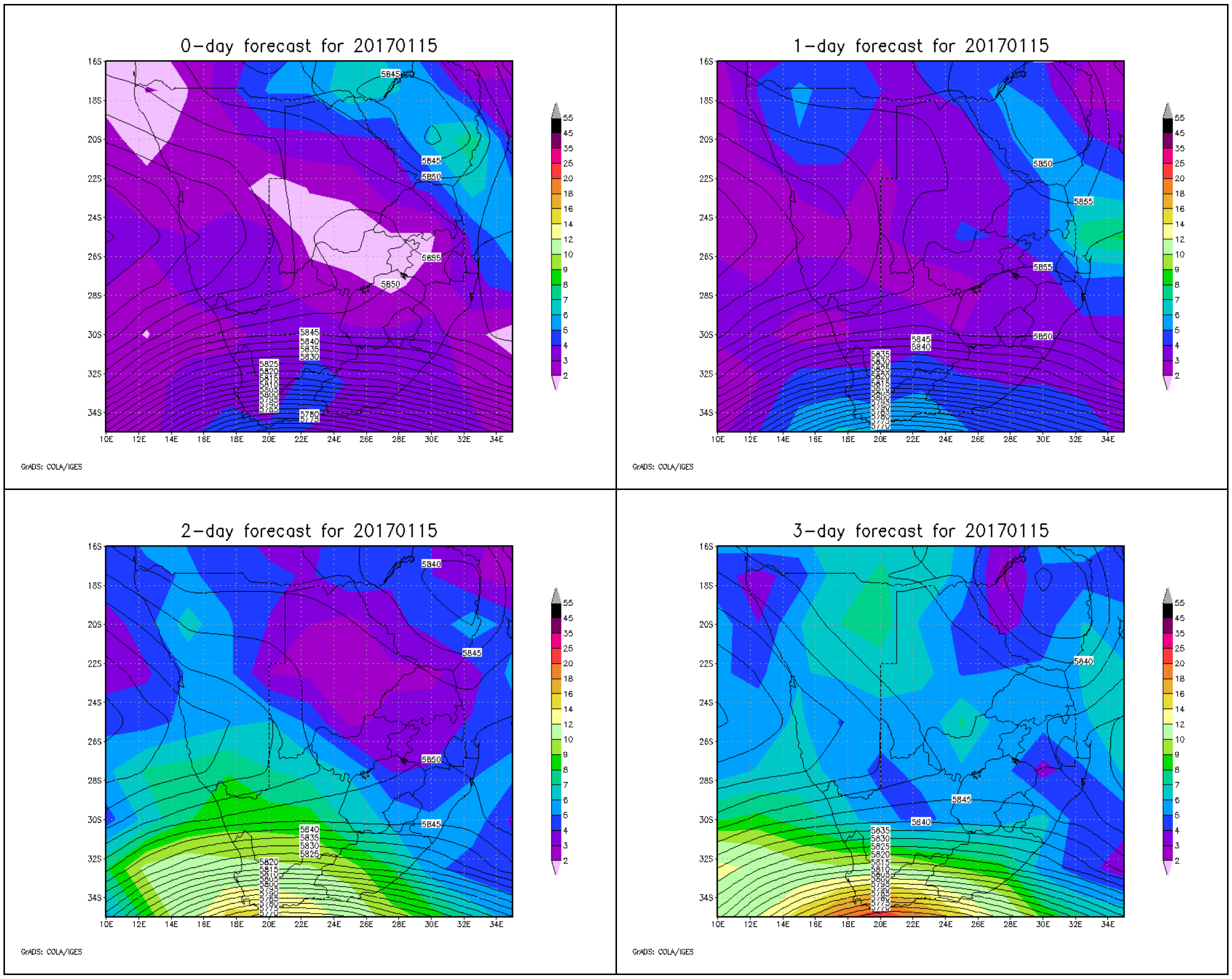

Figure 7.7: The 500hPa geopotential height ensemble average forecast for 15 January 2017 with lead times of 0, 1, 2 and 3-days. The standard deviation (m) of the 10 ensemble members are shaded.

In Fig. 7.6 we saw that the position and depth of the CTL over south-eastern Botswana was forecast with certainty for 1-day lead time. In Fig. 7.9 the positions of the low for 2 ensemble members are shown. In both examples the depth of the low was predicted to be between 5870 and 5875 m. Both ensemble members also placed the low at the approximate same location but with stronger geopotential gradient for ensemble member 4 (right panel on Fig. 7.6). The blue contours depict the 24-hr precipitation as predicted by the ensemble member for 1200 UT on 7 January 2017. For ensemble member 1 the precipitation extends into Limpopo and southwards to KwaZulu-Natal. Ensemble member 4 the rainfall totals are higher (double over south-western Botswana) with absence of rainfall over Limpopo and KwaZulu-Natal. Figure 11 is a cross section of the precipitation forecast of all 10 ensemble members over Limpopo (position of the cross section indicated in Fig. 10). This figure indicates the variability of the rainfall prediction with some members predicting as much as 65 mm in the east with other as little as 1 mm. Even though the ensembles show that the position and depth of the low was predicted with certainty, slight shifts in the location and depth of CTLs can have a significant effect on the precipitation forecast.

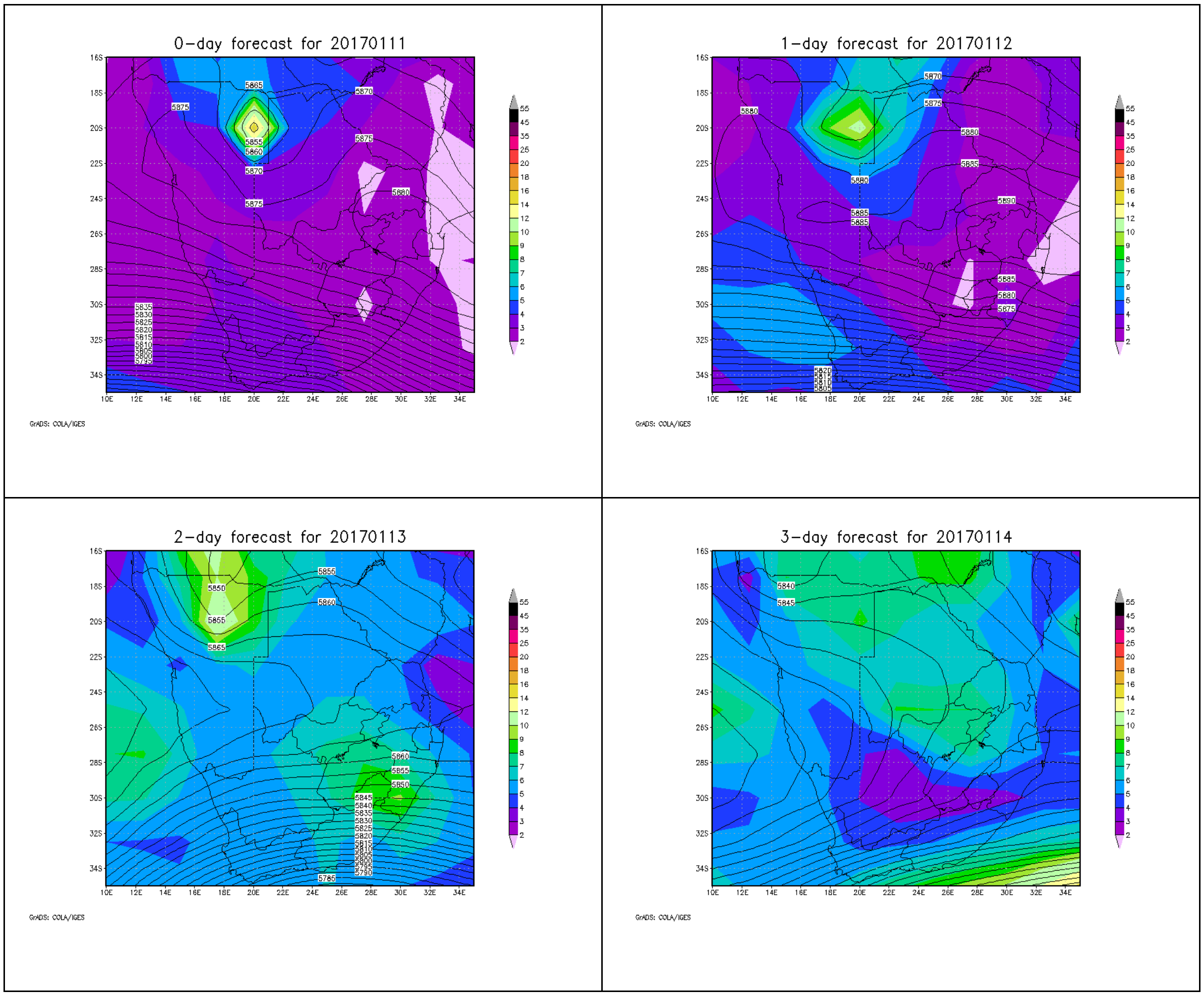

Figure 7.8: The 500hPa geopotential height ensemble average forecast for analysis time 11 January 2017 at 1200Z. Images are shown for lead times of 0, 1, 2 and 3 days. The average standard deviation (m) for all 10 ensemble members are indicated in shaded.

This case study shows how the eastward movement of the low were predicted with certainty for up to days ahead with some uncertainty developing with lead times of 3-days.

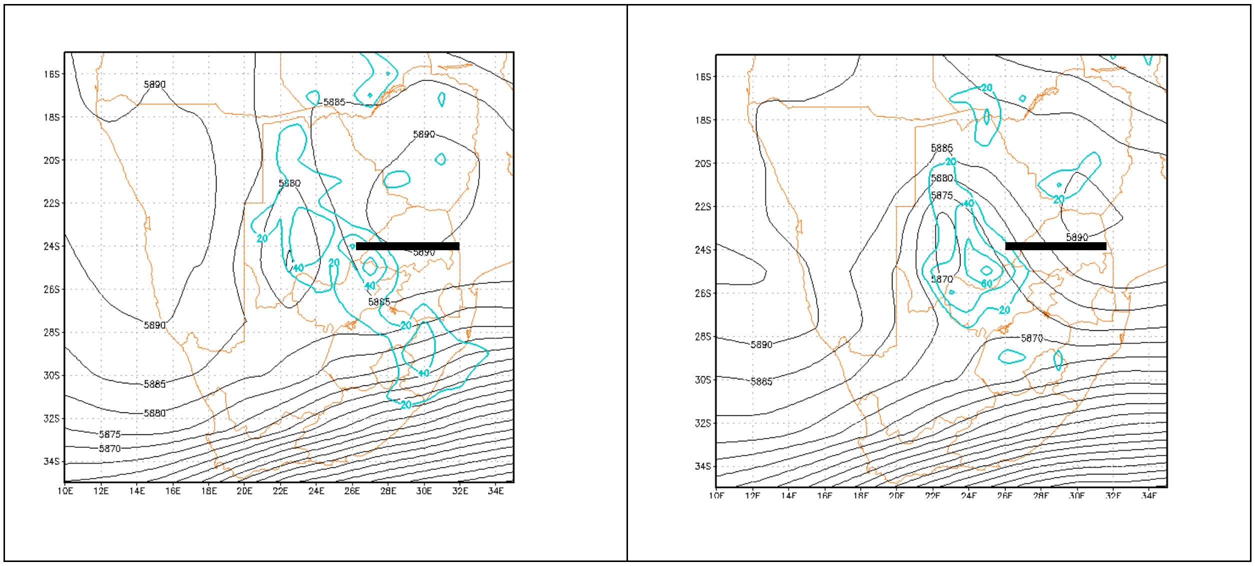

Figure 7.9: The 1-day lead time forecast of 500hPa geopotential heights and precipitation for 7 January 2017 from NCEP ensemble member 1 (left) and ensemble member 4 (right).

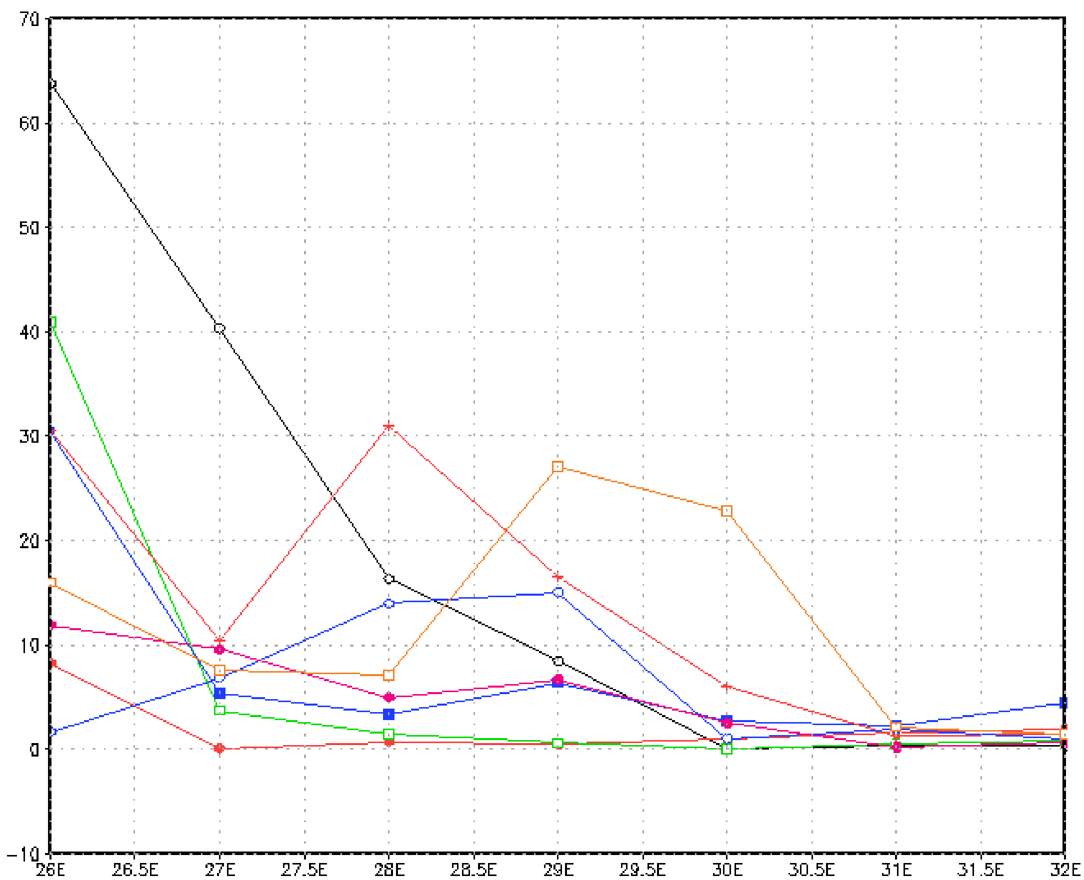

Figure 7.10: A cross section of the 1-day lead time precipitation forecast for 7 January 2017 for all 10 ensemble members over the Limpopo province. Position of the cross section indicated in Fig. 7.9.

7.4 Discussion

The uncertainty associated with weather systems of the subtropics, such as COLs are considerably larger than for CTLs. In the COL the uncertainty translated downstream with increasing lead time especially when the COL start to move eastwards. The December 2010 examples showed that there was less uncertainty when the COL is stationary.

The movement and depth of CTLs are generally predicted with certainty for up to 2-days ahead. The largest uncertainty when CTLs are present tend to happen over the southern extremes of the country where westerly wind systems are present. The CTL investigated here were predicted with certainty whether the low moved or was semi-stationary. Despite the relative certainty in position of the CTL, the rainfall predictions generated from the different ensemble members are highly variable.

Chapter 8: Warm cored tropical lows in a future climate

8.1 Introduction

In this chapter the 1979-2018 climatology of continental tropical lows (CTLs) as prepared with NCEP data will be compared to state of the art regional climate model simulations. Two future periods are considered 2019-2059 and 2060-2099.

8.2 Experimental design of the regional climate model simulations

The regional climate model used in the project is the conformal-cubic atmospheric model (CCAM) developed by the Commonwealth Scientific and Industrial Research Organisation (CSIRO) (McGregor 2005, McGregor and Dix, 2001, 2008). CCAM is a variable-resolution global atmospheric model, which can be applied in at quasi-uniform resolution to function as an atmospheric global circulation model, or alternatively in stretched-grid mode to provide high resolution over an area of interest. It employs a semi-implicit semi-Lagrangian method to solve the hydrostatic primitive equations. The model includes a fairly comprehensive set of physical parameterizations. The GFDL parameterizations for long-wave and short-wave radiation are employed, with interactive cloud distributions determined by the liquid and ice-water scheme of Rotstayn (1997). A stability-dependent boundary layer scheme based on Monin Obukhov similarity theory is employed (McGregor et al., 1993), together with the non-local treatment of Holtslag and Boville (1993). The cumulus convection scheme uses a mass-flux closure, as described by McGregor (2003), and includes downdrafts, entrainment and detrainment. CCAM is coupled to the dynamic land-surface model CABLE (CSIRO Atmosphere-Biosphere Land Exchange). CABLE includes six layers for soil temperatures, six layers for soil moisture (solving Richard's equation) and three layers for snow (Kowalczyk et al., 2006). Fig. shows a quasi-uniform conformal-cubic grid, of C192 (about 50 km) resolution in the horizontal.

An ensemble of high resolution CCAM simulations of present-day climate and projections of future climate change over South Africa has been analysed as part of the project research. Five GCM simulations of the Coupled Model Intercomparison Project Phase Five (CMIP5) and Assessment Report Five (AR5) of the Intergovernmental Panel on Climate Change (IPCC), obtained for the emission scenario described by Representative Concentration Pathway 8.5 (RCP8.5) were downscaled to 2.5 ° resolution globally for direct comparison with NCEP data. The simulations span the period 1960-2100. RCP8.5 is a low mitigation scenario. The GCMs downscaled include the Australian Community Climate and Earth System Simulator (ACCESS1-0); the Geophysical Fluid Dynamics Laboratory Coupled Model (GFDL-CM3); the National Centre for Meteorological Research Coupled Global Climate Model, version 5 (CNRM-CM5); the Max Planck Institute Coupled Earth System Model (MPI-ESM-LR) and the Community Climate System Model (CCSM4). The simulations were performed on supercomputers of the Centre for High Performance Computing (CHPC) of the Meraka Institute of the CSIR in South Africa. In these simulations CCAM was forced with the bias-corrected daily sea-surface temperatures (SSTs) and sea-ice concentrations of each host model, and with CO_2, sulphate and ozone forcing consistent with the RCP8.5 scenario. The model's ability to realistically simulate present-day southern African climate has been extensively demonstrated (e.g. Engelbrecht et al., 2009; Engelbrecht et al., 2011; Engelbrecht et al., 2013; Malherbe et al., 2013; Winsemius et al., 2014; Engelbrecht et al., 2015). Most current coupled GCMs do not employ flux corrections between atmosphere and ocean, which contributes to the existence of biases in their simulations of present-day SSTs – more than 2ºC along the West African coast. An important feature of the downscalings performed here is that the model was forced with the bias-corrected sea-surface temperatures (SSTs) and sea-ice fields of the GCMs. The bias is computed by subtracting for each month the Reynolds (1988) SST climatology (for 1961-2000) from the corresponding CGCM climatology. The bias-correction is applied consistently throughout the simulation. Through this procedure the climatology of the SSTs applied as lower boundary forcing is the same as that of the Reynolds SSTs. However, the intra-annual variability and climate-change signal of the CGCM SSTs are preserved (Katzfey et al., 2009).

8.3 Identification of CTLs in CCAM simulations

The data available from the CCAM simulations mimic the NCEP data to a large extent. The horizontal resolution is 2.5° and data are available from 850 to 300hPa at 6-hr intervals. In order to do a direct comparison between NCEP and the CCAM simulation it was decided to identify only warm lows in this section. The criteria were that a warm core of temperatures should exist within a grid point of a geopotential low at 500hPa. We also constrict the lows to occur over the continent by using a land mask. In this chapter we refer to these lows as warm lows.

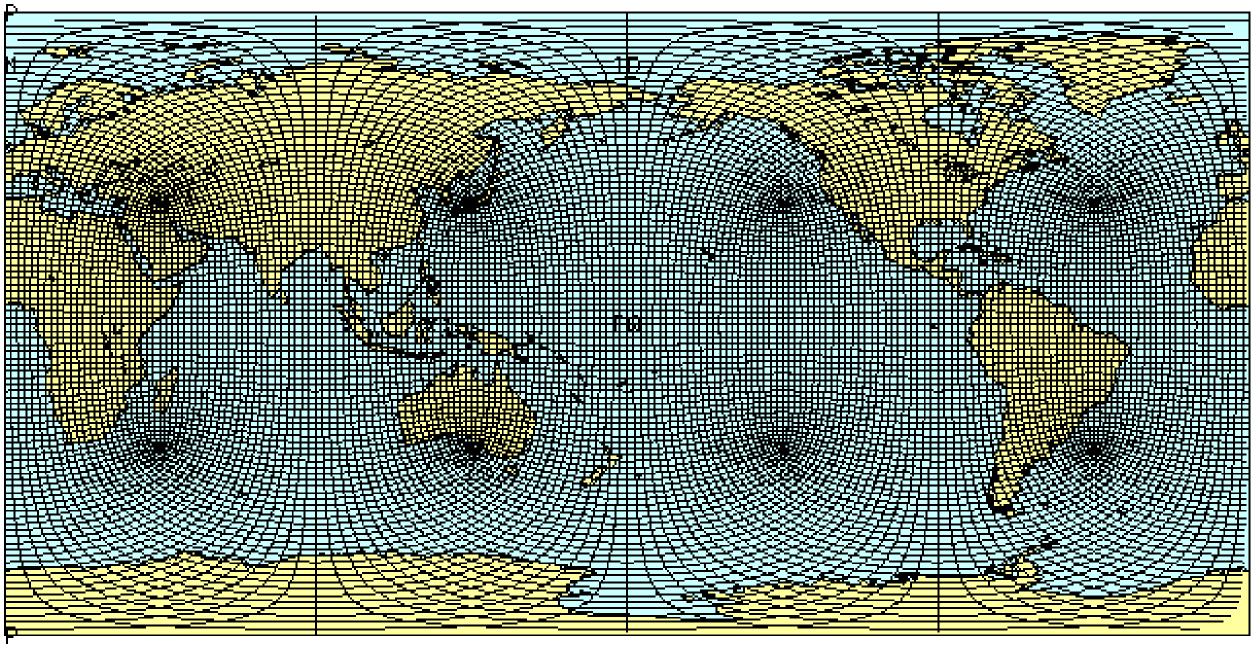

Figure 8.1: C192 quasi-uniform conformal-cubic grid (every 4th grid point is shown), which provides a horizontal resolution of about 200 km globally

8.4 Results

The NCEP data from 1979/80-2017/18 (39-years) identified an average number of 280 warm lows while the ensemble average of the 5 CCAM projections identified an average number of 365 warm lows in the same period (Table 8.1). The five different ensemble members identified the average number of lows very similarly with values varying between 364 and 365. The same holds true for the average number of warm lows identified by the different ensemble members for the two future projections. The ensemble average from 2019/20-2058/59 (40-years) is 379 and from 2059/60 to 2098/99 the average is 379 (Table 8.1). This indicates an increase of close to 15 warm lows per 40 year period until the end of the century.

Table 8.1: The average number of CTLs for the different periods under investigation. The NCEP results are indicated by NCEP while the ensemble average of the CCAM climate projections for the tree different periods are denoted by CCAM.

	Average
NCEP (1979/80-2017/18)	280
CCAM (1979/80-2017/18)	365
CCAM(2019/20-2058/59)	379
CCAM(2059/60-2098/99)	394

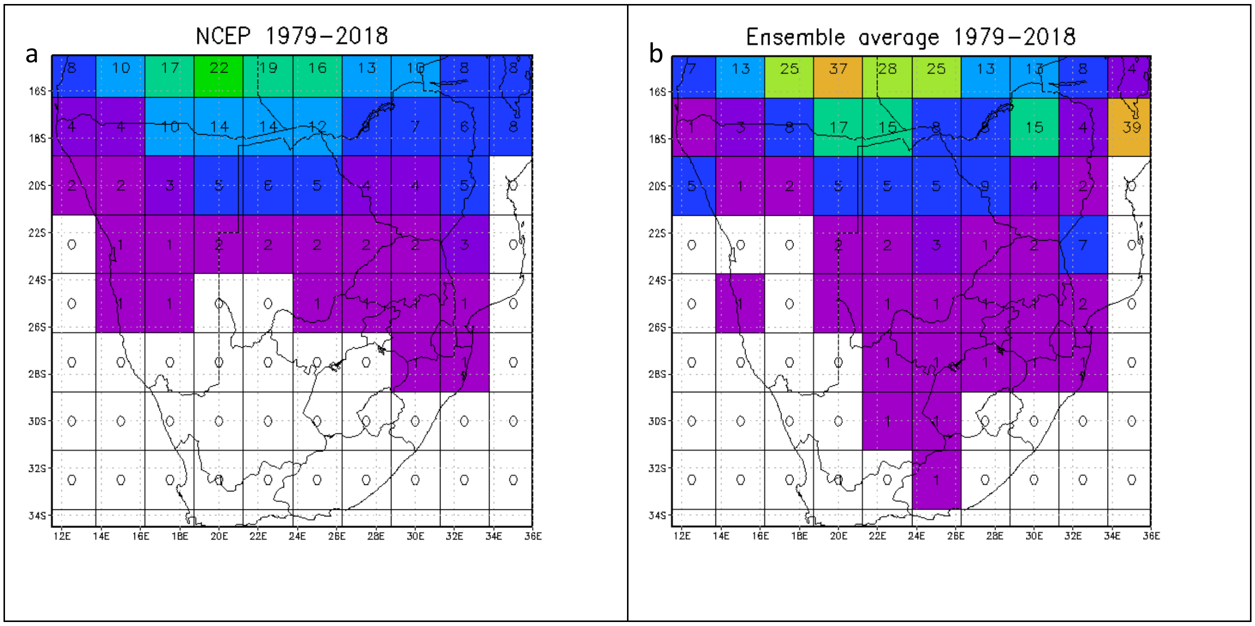

Figure 8.2:The average number of warm lows per grid point from (a) NCEP and (b) CCAM ensemble average between 1979/80 to 2017/18.

The CCAM ensemble average identified a total of 85 more warm lows than NCEP in the current climate (Table 8.1). The number of lows at around 18°-24° S are very similar in both datasets especially over the western parts of the domain (Fig. 8.2). The largest differences appear at around 15.5 ° S on and around the border between Angola and Zambia. The CCAM ensemble average (right in Fig. 8.2) identified around 10 lows more per grid point during this 39 year period over this area. There is also large differences at the grid point over Mozambique at 18 ° S. CCAM identified 31 more lows at this grid point than NCEP. CCAM identifies warm lows much further south over South Africa than NCEP.

For the period 2019-2059 the CCAM ensemble average identified a few less warm lows over the northern extremes of the study area over Zambia/Angola (Fig. 8.3). The average number of warm lows are projected to decrease by between 2 to 4 over this area. Further south and especially over Namibia the 2019-2059 ensemble average identified 2 to 3 more lows than the current climate. Over central northern Namibia this is a 100% increase in the average number of warm lows. In Mozambique the grid point on the eastern edge of the domain is projected to have a 7 more warm lows on average during the 2019-1059 period. Over South Africa the number of warm lows are predicted to be approximately constant with slight increases in the north-east of the Republic.

During the last 40-years of the 21st century (2059-2099) the total number of warm lows are predicted to increase from 365 in the current climate to 394. The number of lows over Zambia/Angola have a downward trend but just further south at 18 ° S the number of lows increase by 2 or 3 but by as much as 15 over the Mozambique grid point. This one grid point account for more than 50% of the increase in the total number of lows between the current climate and 2059-2099. Over north-eastern South Africa the number of warm lows are projected to increase but with a slight decrease over central South Africa.

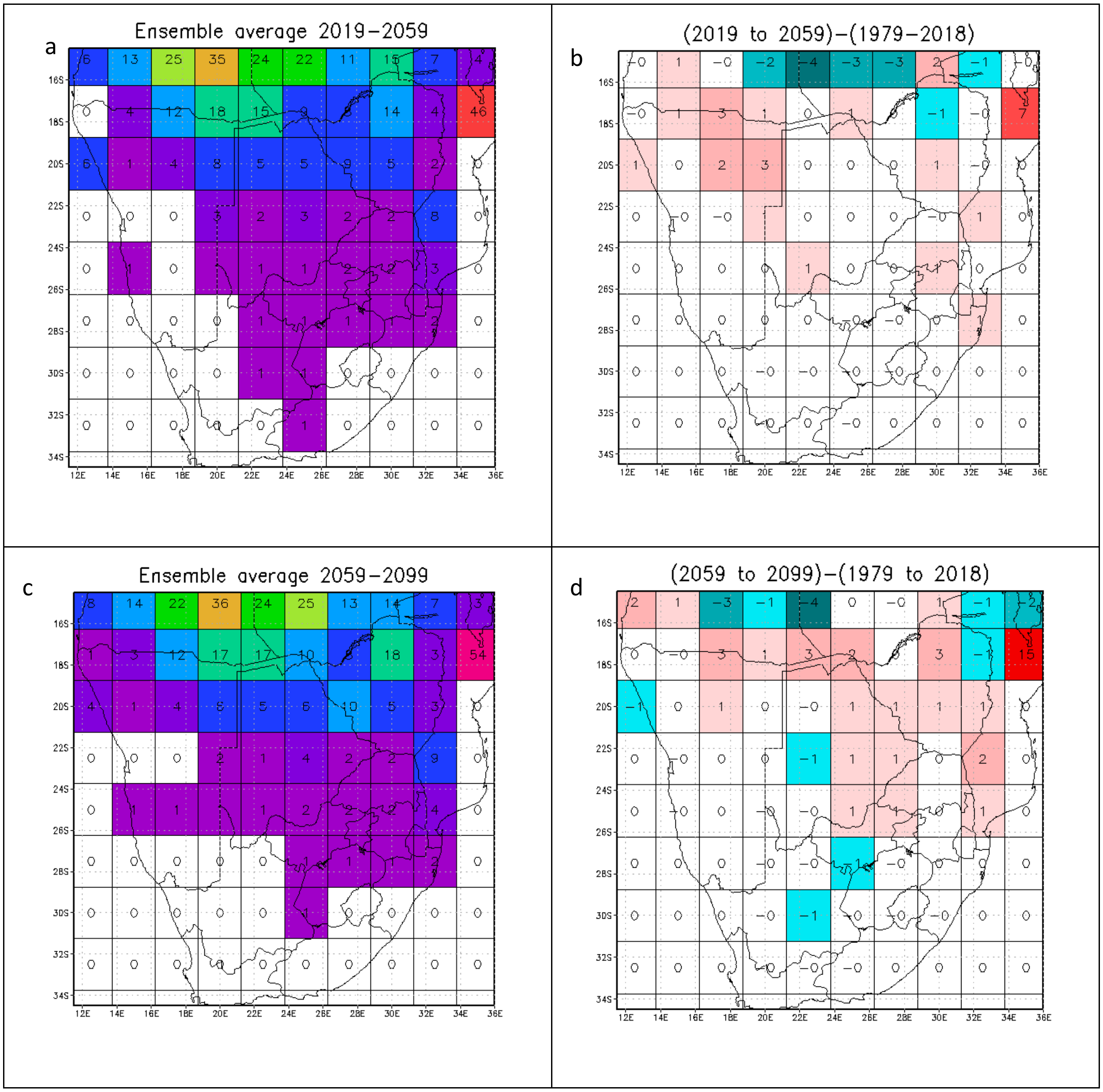

Figure 8.3: The average number of warm lows per grid point from the CCAM ensemble average for 2019/20 to 2058/59 (period 1) (a) and 2059/60 to 2098/99 (period 2) (c). The difference in the average number of lows between period 1 and the current climate is shown in (b) and between period 2 and the current climate in (d)

8.5 Discussion

The ensemble average of the CCAM climate projections mimicked the current climate of warm lows over southern Africa to a large extent even though the CCAM ensemble average identified more lows than NCEP. The general distribution and of lows are similar with the highest number of lows over Zambia and Angola decreasing southwards. CCAM identified more warm lows over South-Africa than NCEP.

Generally the average number of warm lows increase over southern Africa with more lows predicted to occur further south over Namibia and Botswana than the current climate. There is a slight increase in the number of warm lows over north-eastern South Africa towards the end of the century while the number of lows over central South Africa decrease slightly. There is projected to be a decrease in warm lows over Zambia and Angola.

It is worth noting that for the three periods under investigation in this chapter the 5 ensemble members of the CCAM climate projection was in very good agreement with the regards to the average number of warm lows per period but also the geographical distribution of the lows over South Africa.

The difference between NCEP and CCAM projections in the current climate is largely influenced by one grid point over Mozambique. The CCAM ensemble average identified 400% more warm lows than NCEP at this grid point. This grid point also contributes around half the number of low increases from the current climate to period 1 and 2. It is predicted that there will be in total 14 more lows between the current climate and the first period over the study area. At this one grid point alone 7 more lows are predicted to occur. Of the increase in 29 lows between the current climate and the second period 15 occur at the Mozambique grid point. The increase in warm lows over southern Africa for the rest of this century is largely influenced by this one grid point.

This warm lows at this grid point located on the coast of Mozambique may be tropical cyclones or decaying tropical cyclones. The circulation around such an intense low situated at this location will contribute to increased rainfall over the southern parts of Mozambique, Zimbabwe and the Limpopo Province. The escarpment of Zimbabwe and Limpopo will further increase the occurrence of heavy rainfall. The circulation at this grid point and the surrounding oceans should be further investigated.

The decrease in the number of warm lows over Zambia and Angola with the increase in the number of lows further south over Namibia and Botswana will also result in the shift of rainfall further south over these areas

Chapter 9: Hydrological impact of forecast uncertainty associated with CTLs

Christina Botai and Jaco de Wit
South African Weather Service
Christina.botai@weathersa.co.za

9.1 Summary

Streamflow forecasting is essential for flood forecasting, including early flood warning systems. Precipitation is the most important hydrometeorological input parameter required for effective streamflow forecasting. The accuracy of this valuable parameter influences the performance of streamflow forecasting. To assess the impact of precipitation uncertainty in streamflow forecasting, this study evaluated streamflow simulations derived from 10 ECHAM4.5-MOM3 model ensemble members. The Limpopo River Basin was selected for this study, due to its association with widespread and heavy rainfall, which are often attributed to tropical low pressure systems. Sensitivity of streamflow to the changes in precipitation, assessed by using precipitation elasticity estimates depict a potential 1:1 relationship across the majority of the model ensemble members. In addition, the results depict pronounced uncertainty contrasts among the different model ensemble members. Majority of the model ensemble members seem to have overestimated the simulated streamflow, however, application of bias correction leads to reduced uncertainty across all the ensemble members. The quality of streamflow forecasts for January 2017 was assessed by using the differences in three statistical metrics, namely, the mean error, the root mean square error and the mean absolute error. The results depict pronounced uncertainty, particularly in 50% of the model ensemble members. The uncertainty contrasts seem to increase for longer lead time (28 days ahead) forecasting. In addition, bias correction, which works effectively for long term data (over 20 years) did not necessarily reduce the uncertainty of streamflow forecasts. In fact, in some cases the bias correction resulted in more amplified uncertainty contrasts. Overall, this study points to the need for developing a multi-model rainfall-runoff streamflow forecasting application or service vital for operationally realistic scenarios. Future work for this research will involve increasing the ECHAM4.5-MOM3 model ensemble members and consider different time lag forecasts for robust skill assessments. The current research work only considered two sub-basins (out of 27) of the Limpopo River Basin, for future work the research will consider broadening the tests, thus including more sub-basins across the Limpopo River Basin.

9.2 Introduction

Streamflow forecasting plays an essential role in water resources planning and management. Information derived from streamflow forecasting can be utilized in, among others, flood caution, reservoir operations, quantification and assessment of water hydropower generation, domestic and irrigation water scheduling (Irene et al., 2013). In addition, decision-making in water management requires accurate streamflow forecasts information. According to Milly et al. (2005), streamflow can be considered as a spatio-temporal integral that represents runoff (the difference between precipitation and evapotranspiration averaged over many years) over a river basin. From this perspective, streamflow can be seen to exhibit strong nonlinear dependency on hydrometeorological and climatic factors (Sivapalan et al., 2011; Xu et al., 2013) as well as anthropogenic influences (Bawden et al., 2014; Amoo and Dzwairo 2017). In addition, streamflow forecasting can also be affected by physical characteristics of a catchment and drainage basin (Li et al., 2011; Patil and Stieglitz, 2012), such as topographic terrain characteristic, type of drainage network, basin orientation, extent of artificial and indirect drainage, land use, soil type and vegetation cover (Fetter, 1988; Ward and Lynch, 1996).

Precipitation is considered as the key meteorological input parameter required in streamflow forecasting. Thus to achieve accurate streamflow forecasts, precipitation has to be predicted with high precision and sufficient lead time to allow appropriate actions in relation to information applicability (e.g. issuing of flood warning messages). This is however a challenging task due to the existence of large amount of uncertainty in the precipitation information that tend to propagate into streamflow forecasts. Numerous studies have researched on different methods that can be used to reduce uncertainties related to precipitation estimation. The most commonly used approach is based on REAL (Radar Ensemble generator designed for usage in the Alps using LU decomposition) ensemble generation method proposed by Germann et al. (2009). Using this method, the uncertainty of precipitation estimates that propagate into hydrologic models during streamflow forecasting can be evaluated, i.e. feed the model with precipitation ensemble members and observe the output spread (Germann et al., 2009; Villarini et al., 2009). This contribution assessed how ensemble precipitation uncertainties affect streamflow simulations, focusing on the Limpopo River Basin (LRB), an area associated with continental tropical low-pressure systems (CTLs).

9.3 Study Area

The Limpopo River Basin (LRB), depicted in Fig. 9.1, is one of the largest drainage areas in the Southern African Development Community (SADC) region, with catchment area of 408 000 km^2. The LRB catchment area is shared among four SADC countries, namely, South Africa, Botswana, Zimbabwe and Mozambique, see Table 9.1 for the area, percentage of the drainage area of the river basin per country and the major watersheds. The Limpopo River flows north, and joins the Marico and Crocodile Rivers, where it borders between South Africa and Botswana, then the border between South Africa and Zimbabwe, before descending to Mozambique, and eventually flows into the Indian Ocean at Zongoene near Xai-Xai, Mozambique (LBPTC 2010).

Table 9.1: Area and percentage of the LRB for the transboundary countries. (Source: LBPTC 2010)

Country	Area in each country (km^2)	Percentage of the Basin	Major watersheds
Botswana	81 400	20%	4
Mozambique	79 800	20%	3
South Africa	184 150	45%	12
Zimbabwe	62 900	15%	3
Total	408 250		27 (5 are shared between at least two countries

Most of the LRB catchment area is semi-arid with a highly variable climate that is prone to extreme weather and climate events such as floods, droughts and occasionally, tropical cyclones. The river basin is influenced by various climate factors such as dry continental tropical, equatorial convergence zone, moist marine subtropical eastern and marine western Mediterranean air masses (FAO, 2004). In particular, the LRB is highly susceptible to frequent flood events (during wet seasons and years) and droughts (during dry seasons and years), see Table 9.2 for some of the devastating droughts and floods recorded in the past, which had major impacts to the LRB.

Table 9.2: Natural meteorological catastrophes that have affected LRB in the past. (Source: WMO, 2012)

Year	Type of disaster	Influenced by tropical cyclone
2008	flood	Jokwe
2007	flood	Favio
2003	flood	Defina
2002-2003	drought	
2001	flood	Dera

The Limpopo catchment area is characterized by a highly seasonal distribution of rainfall (WMO, 2012) and this has a significant impacts on the hydrology of the LRB. The area receives most of its rain (95%) between October and April. The distribution of rainfall varies from as low as 200 mm/year in the western semi-arid areas of the catchment to over 1 500 mm/year in the south-middle part of the catchment, and 600 mm/year in the eastern part, near the Indian Ocean. The mean annual precipitation of the basin is approximately 530 mm, although much of the rainfall events are intense (resulting in flash floods) and highly sporadic, associated with convective thunderstorms and occasionally, tropical cyclones (WMO, 2012). Mean annual minimum and maximum temperatures range between 8°C in the south to 20°C in the east of the basin, and 23°C in the south to 32°C in the east of the basin, respectively.

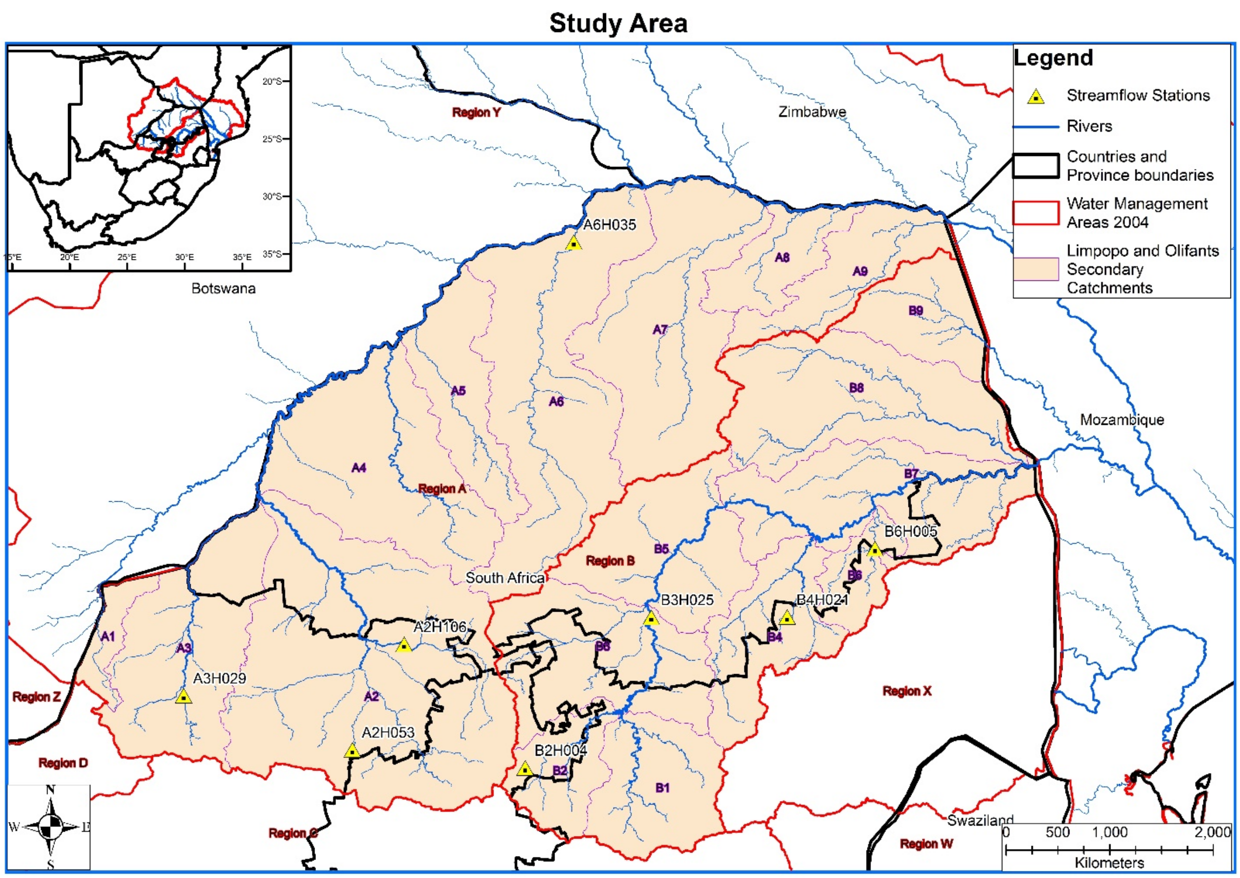

Figure 9.1: Limpopo River Basin map

9.4 Data

Streamflow observational data was obtained from the Department of Water and Sanitation (http://www.dwa.gov.za/Hydrology/). A total of eight river flow stations were selected for the study, see the characteristics of the selected stations as summarized in Table 9.3. The selected stations have been operational for over 3 decades, hence they provide reliable and continuous datasets. For the current study, the considered period for the daily observed streamflow data spanned from January 2016 to December 2017. The distribution of the selected streamflow stations is depicted in Fig. 9.1.

Table 9.3: Characteristics of streamflow stations

Station	Latitude	Longitude	Altitude (m)	No. of River Elements	Catchment Area (km^2)	Soil Texture	MAP (mm /yr)	MASF (m^3/s)
A2H053	-25.8093	27.4760	1266	9	1062.38	Clay loam	728	0.38
A2H106	-25.1321	27.8083	988	7	1135.75	Sandy loam	514	3.75
A6H035	-22.5502	27.7259	645	5	1441.96	Sandy loam	807	1.91
A3H029	-25.4618	26.3924	1036	7	732.408	Sandy loam	496	0.51
B3H025	-24.9586	29.3953	849	5	449.23	Sandy loam	667	4.14
B2H004	-25.9246	28.5859	1457	5	982.619	Sandy loam	668	0.81
B4H021	-24.9564	30.2679	1258	7	397.748	Sandy loam	637	0.75
B6H005	-24.5175	30.8317	592	7	294.299	Clay loam	524	6.81

9.5 Method of analysis

9.5.1 Global Climate Model ensembles

The Global Climate Model (GCM) used to force the ACRU (Agricultural Catchments Research Unit) modelling system (see below) is the ECHAM4.5-MOM3 coupled system (Beraki et al., 2014). This system runs at a T42 horizontal resolution (~2.5 deg.) and has 17 vertical levels. The hindcasts for this system was run from 1983-2009 with 10 ensemble members. The ensembles are created using a time lagged average approach where 10 daily atmospheric initial conditions (NCEP Reanalysis Version 2) prior to the start of each monthly model simulation (4^{th} of each month) is used for each ensemble member. For the ocean initial conditions only the latest pentad ocean analysis (obtained from the Global Ocean Data Assimilation System; GODAS) is used in the hindcasts, however in the operational model runs (starting from Oct 2015 to present), 4 ocean initial conditions are used (3 prior pentad analyses plus the latest) which gives an operational run of 40 ensemble members. For this study a two year period (2016-2017) of 1-month lead forecasts were stitched together to simulate an operational system in which the ACRU system obtains the latest forecasts for its simulations. In order to keep the simulations comparable with any future assessments with the total hindcast datasets, the operational members were restricted to 10. This is the same setup as the hindcast runs using 10 atmospheric initial conditions and the latest pentad ocean analysis.

9.5.2 ACRU agro-hydrological model

In this study we have used ACRU agro-hydrological modelling system (Schulze, 1995; Smithers and Schulze, 2004). The model is a physical-conceptual, multi-purpose, multi-soil-layered and daily time-step model, configured to be hydrologically sensitive to catchment land uses and respective changes thereof, such as influences of reservoirs, irrigation practices, urbanization, afforestation and sediment generation (Schulze, 1995; Schulze and Perks, 2000). The model has been effectively used in different categories of water resources related research such as hydrological impacts of wetlands and land use change on water resources (Le Maitre et al., 2014; Warburton et al., 2012; Kienzle et al., 1997), sediment yields (Kienzle et al., 1997), design flood estimation (Schulze et al., 1993) irrigation water demand and supply (Dent et al., 1988). The model requirements include input of known and measurable spatio-temporal variable factors that characterize the watershed. The minimum catchment information required to operate ACRU are the daily precipitation as well as maximum and minimum temperature datasets. Other catchment information that can be incorporated include the physical characteristics of the catchment (e.g. size, soils and altitude), bio-physical aspects (baseline land cover and present land use) and land use and management practices (i.e. irrigation and domestic demand/supply, industrial and livestock water abstraction). Some of the output information that can be derived from ACRU include, daily streamflow values, separated into stormflow and base-flow, peak discharge, reservoir status, recharge to groundwater, irrigation water supply and demand, crop yields, sediment yield. For a detailed description and theoretical background of the ACRU model, the reader is referred to Schulze (1995).

In the current study the simulated streamflow time series of each of the ensemble members was compared with the observed time series and differences in the statistical parameters were evaluated to investigate the uncertainties in the ensemble members that propagate into the streamflow forecasts. The schematic depicted in 9.3 summarizes the method of analysis considered in this study.

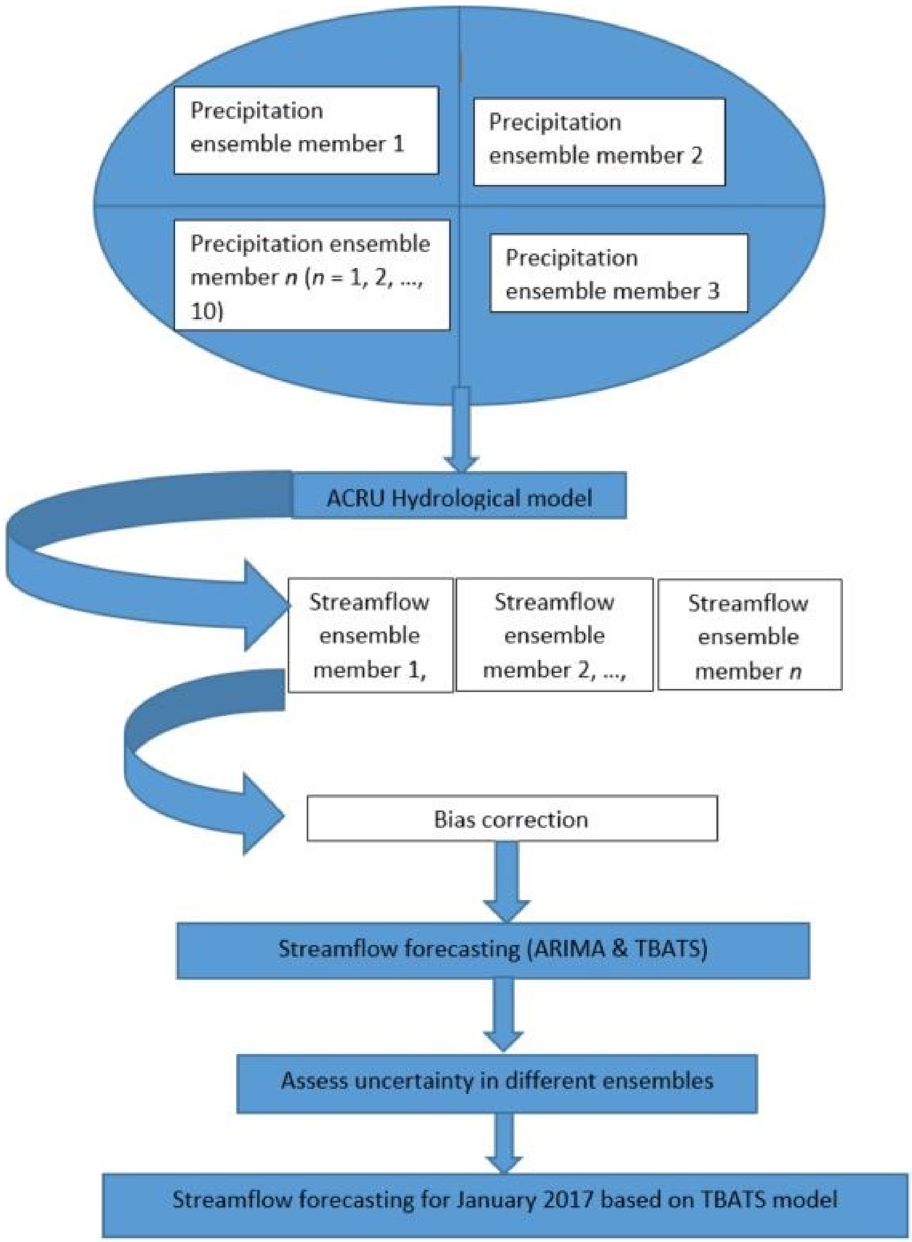

Figure 9.2: Proposed framework of streamflow forecasting

9.5.3 Precipitation elasticity of streamflow

Precipitation elasticity of streamflow, ε_p (also known as a sensitivity factor), is defined as proportional change in mean annual streamflow divided by proportional change in the mean annual precipitation (Sankarasubramanian et al., 2001). According to Sankarasubramanian et al. (2001), precipitation elasticity of streamflow can be estimated through a non-parametric estimator given by,

$$\varepsilon_p = median\left[\left(\frac{Q_t}{P_t} - \frac{\bar{Q}}{\bar{P}}\right)\frac{\bar{P}}{\bar{Q}}\right] \quad (1)$$

where Q_t and P_t correspond to streamflow and precipitation change, respectively. The mean values of precipitation and streamflow are denoted by $\bar{P}$ and $\bar{Q}$, respectively. The ε_p was used in this study to assess the sensitivity of streamflow to the changes in precipitation.

9.5.4 Bias corrections of simulated streamflow

Simulated streamflow outputs across the ten considered ensembles were bias-corrected to minimize systematic biases, using statistical bias correction method, also called the distribution mapping approach. The statistical distribution mapping bias correction method adjusts the distribution of the model simulated datasets such that their statistical distribution matches that of the observed datasets (Gudmundsson et al., 2012). Numerous approaches for statistical distribution mapping have been reported in the literature, e.g. probability mapping (Piani et al., 2010), empirical cumulative distribution function mapping (Iizumi et al., 2011), Q-Q map (Gudmundsson et al., 2012) and quantile mapping (Gudmundsson et al., 2012). In this study, the quantile mapping bias correction method described in Gudmundsson et al. (2012) was considered. This method estimates quantiles for both observed and simulated streamflow datasets and then generates a transfer function through interpolation between corresponding quantile values. The transformation can be formulated as (see for example, Gudmundsson et al., 2012)

$$SF_o = h(SF_s) \quad (2)$$

where SF_o and SF_s correspond to the distributions of daily observed and simulated streamflow, respectively, and *h* is a transfer function. Equation (2) can be restructured as follows,

$$SF_o = F_o^{-1}\left(F_s(SF_s)\right) \quad (3)$$

where F_s is the CDF of SF_s and F_o^{-1} is the inverse CDF of SF_o. Equation (3) defines a transformation of a variable with a known distribution. In this study, two methods of quantile mapping were considered, see Table 9.4 for the description of the methods.

Table 9.4: Summary of quantile mapping methods used for bias correction. (Source: Gudmundsson et al., 2012)

Method	Abbreviation	Application
Smoothing Spline	SSPLIN	adjusts the distribution of the modelled data to match the distribution of the observations using a spline function
Robust empirical quantiles	RQUANT	performs quantile mapping by interpolating the empirical quantiles using local linear least square regression

9.5.5 Streamflow forecasting

The streamflow forecasting was based on the Autoregressive Integrated Moving Average (ARIMA) stochastic model proposed by to Hipel and McLeod (1994) and the Trigonometric Box-Cox transform, ARMA errors, Trend and Seasonality (TBATS) model proposed by De Livera et al. (2011). The ARIMA model is a generalization of Autoregressive Moving Average (ARMA) model (Hipel and McLeod 1994) that takes into account non-stationarity behaviour. According to Hipel and McLeod (1994) the mathematical formulation of the ARIMA (*p,d,q)* model using lag polynomial can be described as per Equation (4)

$$\varphi(L)(1-L)^d y_t = \theta(L)\varepsilon_t \qquad (4)$$

where y_t and ε_t are the actual value and random error at time period *t*, respectively.

Equation (4) can be expanded or integrated by setting the integer *d* = 1, (*d* controls the level of referencing) as follows

$$\left(1-\sum_{i=1}^{p}\varphi_i L^i\right)(1-L)^d y_t = \left(1+\sum_{j=1}^{q}\theta_j L^j\right)\varepsilon_t \qquad (5)$$

where *p, d* and *q* are integers ≥ 0, corresponding to the order of the autoregressive, integrated and moving average parts of the model, respectively.

The TBATS model is basically a generalization of BATS (Box-Cox transformations, ARMA, Trend and Seasonality) model. The model assumes that the data is influenced by multiple seasonality factors and uses trigonometric regressors to model those complex seasonalities. A typical TBATS model is supplemented with arguments (ω,ø,*p*,*q*,{m_1,k_1},...,m_T,k_T}) and these indicate the Box-Cox parameter (ω), damping parameter (ø), ARMA parameters (*p* and *q*) and the trigonometric seasonal periods ({m_1,k_1},...,m_T,k_T}). For detailed information on the theoretical background of TBATS model, the reader is referred to De Livera et al. (2011).

9.5.6 Verification of forecasts

The accuracy performance of the different streamflow member ensembles and forecasts was measured based on the computation of the following metrics, mean bias, mean error, root mean square error (RMSE), and Spearman correlation coefficient. Streamflow forecasts were evaluated based on the differences in mean error, RMSE and mean absolute error statistical metrics. Details on how to calculate these metrics can be found in Agrawal and Adhikari (2013).

9.6 Results

9.6.1 Sensitivity of streamflow to the precipitation

Table 9.5 summarises the streamflow-precipitation relationship based on Spearman's correlation coefficient and the corresponding precipitation elasticity of streamflow values for the considered model ensemble members. Generally, the results indicate that individual model ensemble members have significant impacts on how streamflow responds to the changes in the precipitation. In particular, it is noticed that elasticity values vary across the ensemble members. This is attributed to the inherent uncertainties in the simulated streamflow ensemble members. Based on Table 9.5, the precipitation elasticity values for the Crocodile drainage region vary from 0.66 (rainfall – streamflow observations) to 0.95 (rainfall – ensembles). The highest precipitation elasticity values of streamflow are ~0.95 (R_{obs} – Ens1, R_{obs} – Ens3 and R_{obs} – Ens4) and ~0.98 (R_{obs} – Ens3 and R_{obs} – Ens4) for the Crocodile drainage region and Olifants drainage region, respectively. The results suggests that for a 1% change in mean annual precipitation, the simulated streamflow would change on-average by 0.95% and 0.98%, for the two Limpopo drainage regions, respectively. There's a strong statistically significant correlation between the observed precipitation and simulated streamflow across the ensemble members, for both the drainage regions. The highest correlation values between precipitation and simulated streamflow are 0.96 (R_{obs} – Ens2) and 0.93 (R_{obs} – Ens5) whereas the lowest values are 0.60 (R_{obs} – Ens10) and 0.63 (R_{obs} – Ens3), for Crocodile and Olifants drainage regions, respectively.

Table 9.5: Precipitation elasticity of streamflow across the model ensembles and observations for Crocodile and Olifants drainage regions of LRB

	Crocodile drainage region			Olifants drainage region		
	Elasticity	Correlation	*p*-value (%)	Elasticity	Correlation	*p*-value (%)
R_{obs} – SF_{obs}	0.66	0.71	1.0	0.26	0.51	8.9
R_{obs} – Ens1	0.95	0.76	0.4	0.92	0.83	0.1
R_{obs} – Ens2	0.71	0.96	0.0	0.81	0.88	0.0
R_{obs} – Ens3	0.94	0.44	14.7	0.97	0.63	3.0
R_{obs} – Ens4	0.95	0.63	2.7	0.98	0.75	0.5
R_{obs} – Ens5	0.77	0.80	0.2	0.80	0.93	0.0
R_{obs} – Ens6	0.87	0.84	0.1	0.77	0.77	0.3
R_{obs} – Ens7	0.90	0.75	0.5	0.88	0.81	0.1
R_{obs} – Ens8	0.81	0.80	0.2	0.69	0.90	0.0
R_{obs} – Ens9	0.95	0.77	0.3	0.95	0.88	0.0
R_{obs} – Ens10	0.81	0.60	3.8	0.86	0.69	1.4
R_{obs} – Avg. Ens.	0.86	0.77	0.4	0.87	0.85	0.0

9.6.2 Characteristics of statistical parameters of streamflow simulations

The streamflow simulations from each model ensemble member were assessed and characterized based on the following statistical parameters: the mean, standard deviation (STD), median, coefficient of variation (CV) as well as kurtosis and skewness coefficients. These parameters were calculated for both bias-corrected (RQUANTILE and SSPLINE methods of quantile-mapping bias correction approaches) and uncorrected simulations. The results are summarized in Table 9.6 for the Crocodile drainage region and for the Olifants drainage region. Based on the results in model ensemble 6, without bias correction, exhibits the highest mean (3.6 m^3/s), followed by model ensembles 1, 3 and 5 with mean value of approximately 3.3 m^3/s. On the other hand, model ensemble 10 exhibits the least mean value of 2.4 m^3/s. The mean values across the model ensembles significantly reduce after the bias-correction. In particular, the mean values after the RQUANTILE bias-correction are within 1.7 m^3/s range across the ensembles with only small fractional differences. For SSPLINE bias correction, the mean ranges between 1.7 m^3/s (ensembles 1, 3, 4, 6, 8, 9 and 10) and ~2.0 m^3/s for ensembles 2 and 5.

The STD varies across the ensemble members, with model simulation ensembles without bias correction depicting values ranging from the lowest value of 2.5 m^3/s (ensemble 8) to the highest mean value of 3.8 m^3/s (ensemble 1). The RQUANTILE bias corrected simulations depict STD values of approximately 3.1, across the ensembles (albeit small differences within the ensembles). On the other hand, when considering SSPLINE bias correction, the STD is high for ensembles 2 and 7, with values of

6.6 m^3/s and 4.1 m^3/s, respectively. Based on the median calculations, the uncorrected model ensembles overestimate the streamflow across the ensemble members. The results significantly improve after applying bias-correction, with the median values in the range of 0.85 m^3/s. The CV values are less variable for model simulations without bias correction, with the lowest value obtained for ensembles 6 and 8 (0.9%) and the highest for ensemble 4 (1.3%). The CV values increase after the bias correction to approximately 2.0% for the RQAUNTILE method and up to 3 for SSPILNE method. Simulated streamflow series exhibit positive coefficient of kurtosis, with the model ensembles showing a heavy-tailed distribution while the bias corrected ensembles depict extremely heavy and thick-tailed distribution. The distribution of streamflow is extremely skewed (< 1.0) across the ensembles, with the SSPLINE bias-corrected depicting the highest distribution whereas the ensembles without bias correction depict the least distribution. Similar pattern of the statistical parameter results is observed for the Olifants drainage region.

Table 9.6: Statistical parameters of streamflow simulations across the model ensembles in Crocodile drainage region

		SF-Obs.	SF-Ens1	SF-Ens2	SF-Ens3	SF-Ens4	SF-Ens5	SF-Ens6	SF-Ens7	SF-Ens8	SF-Ens9	SF-Ens10	SF-Ens11
Mean (m^3/s)	Model-Sim	1.669	3.319	2.761	3.219	2.545	3.303	3.613	2.74	2.646	2.768	2.401	2.931
	RQUANT BC	1.669	1.675	1.663	1.669	1.673	1.662	1.664	1.662	1.686	1.667	1.675	1.663
	SPLIN BC	1.669	1.655	1.988	1.675	1.663	1.904	1.684	1.773	1.709	1.696	1.679	1.755
STD (m^3/s)	Model-Sim	3.108	3.805	3.151	3.782	3.328	3.542	3.333	2.809	2.581	3.242	3.043	2.829
	RQUANT BC	3.108	3.124	3.049	3.078	3.119	3.051	3.082	3.042	3.175	3.089	3.114	3.034
	SPLIN BC	3.108	3.029	6.555	3.159	3.042	5.7	3.198	4.105	3.258	3.353	3.189	4.067
Median (m^3/s)	Model-Sim	0.853	1.696	1.541	1.804	0.447	1.55	2.77	1.371	1.648	0.912	0.656	1.743
	RQUANT BC	0.8535	0.8539	0.8536	0.8539	0.8539	0.8537	0.8539	0.8537	0.854	0.854	0.8541	0.8534
	SPLIN BC	0.8535	0.8579	0.8555	0.8579	0.8536	0.8534	0.854	0.8524	0.854	0.8543	0.8555	0.8534
CV	Model-Sim	1.862	1.146	1.141	1.175	1.307	1.072	0.922	1.025	0.975	1.171	1.267	0.965
	RQUANT BC	1.862	1.865	1.833	1.844	1.864	1.836	1.852	1.83	1.883	1.852	1.859	1.825
	SPLIN BC	1.862	1.83	3.298	1.886	1.829	2.994	1.898	2.314	1.906	1.977	1.9	2.317
Kurtos.	Model-Sim	37.86	4.52	9.73	6.32	3.3	6.93	3.64	3.09	4.43	4.27	3.78	2.18
	RQUANT BC	37.86	37.77	37.94	36.96	37.46	37.38	38.75	37.28	35.54	37.92	37.08	37.1
	SPLIN BC	37.86	37	137.39	36.77	40.69	138.95	37.64	86.09	35.85	43.51	40.3	97.4
Skew.	Model-Sim	5.48	1.47	2.11	1.89	1.23	1.64	0.93	1.11	1.33	1.3	1.39	0.84
	RQUANT BC	5.48	5.37	5.43	5.39	5.45	5.4	5.51	5.38	5.36	5.48	5.41	5.36
	SPLIN BC	5.48	5.41	10.86	5.44	5.64	10.72	5.51	8.13	5.35	5.96	5.66	8.56

Table 9.7: Statistical parameters of streamflow simulations across the model ensembles in the Olifants drainage region

		SF-Obs.	SF-Ens1	SF-Ens2	SF-Ens3	SF-Ens4	SF-Ens5	SF-Ens6	SF-Ens7	SF-Ens8	SF-Ens9	SF-Ens10	SF-Ens11
Mean (m^3/s)	Model-Sim	1.445	4.715	4.206	4.658	3.867	4.794	5.425	4.188	4.199	4.411	4.125	4.459
	RQUANT BC	1.445	1.439	1.441	1.437	1.438	1.435	1.436	1.444	1.45	1.444	1.449	1.45
	SPLIN BC	1.445	1.494	1.917	1.473	1.600	1.537	1.486	1.488	1.472	1.727	1.567	1.451
STD (m^3/s)	Model-Sim	2.816	4.912	4.144	4.778	4.285	4.453	4.871	3.945	3.743	4.699	4.411	3.879
	RQUANT BC	2.816	2.764	2.782	2.761	2.728	2.755	2.754	2.783	2.765	2.775	2.768	2.782
	SPLIN BC	2.816	3.197	7.842	2.300	3.304	3.621	3.206	3.169	3.962	6.148	3.299	2.856
Median (m^3/s)	Model-Sim	0.595	3.015	2.874	3.739	1.293	2.764	3.914	2.947	2.777	2.167	1.708	2.943
	RQUANT BC	0.595	0.5951	0.5948	0.5955	0.5952	0.5954	0.5944	0.5948	0.5956	0.5952	0.5948	0.596
	SPLIN BC	0.595	0.597	0.602	0.613	0.599	0.604	0.602	0.599	0.597	0.595	0.599	0.597
CV	Model-Sim	1.949	1.043	0.985	1.025	1.108	0.929	0.898	0.942	0.891	1.065	1.069	0.87
	RQUANT BC	1.949	1.921	1.931	1.921	1.914	1.901	1.919	1.928	1.919	1.922	1.921	1.929
	SPLIN BC	1.949	2.140	4.091	2.030	2.188	2.356	2.157	2.131	2.012	3.561	2.508	1.200
Kurtos.	Model-Sim	37.34	4.67	15.2	7.33	2.92	4.04	4.76	3.68	3.57	3.74	3.27	2.00
	RQUANT BC	37.34	36.76	37.05	36.77	36.43	36.41	37.18	36.75	45.81	36.27	36.45	36.51
	SPLIN BC	37.342	52.301	155.68	41.393	51.801	69.792	57.093	54.645	38.806	199.56	73.907	39.305
Skew.	Model-Sim	5.351	1.382	2.383	1.783	1.001	1.113	1.131	1.093	1.144	1.160	1.144	0.690
	RQUANT BC	5.35	5.27	5.31	5.29	5.25	5.22	5.3	5.28	5.21	5.23	5.26	5.28
	SPLIN BC	5.350	6.321	11.660	5.654	6.363	7.362	6.581	6.415	5.490	12.850	7.753	5.490

9.6.3 Uncertainty of streamflow simulations based on statistical metrics

Streamflow simulated across the 10 model ensemble members was evaluated based on four statistical metrics, namely: the mean bias (MB), mean error (ME), the root mean square-error (RMSE), mean square error (MSE) and Spearman correlation coefficient. Table 9.8 gives MB results across the ensembles and drainage regions. Based on the results, streamflow simulations without bias correction exhibit positive bias across all the 10 model ensemble members and drainage regions (see column 2). Model ensemble members 1, 3, 5 and 6 in the Crocodile drainage region exhibit the highest bias, exceeding 1000, whereas ensembles 4 and 10 exhibit the lowest bias errors. The bias-correction significantly reduces the MB in both drainage regions across the ensemble members. The MB values after the RQUANTILE bias correction range from 0.36 to 12.7 (positive) and -5.0 and -1.1 (negative). The SSPLINE bias correction slightly increases the MB values across the ensemble members with ensemble members 2 and 5 depicting the highest values and least values observed for ensemble members 1 and 4.

The Olifants drainage region depict the largest values in MB, almost double to those from the Crocodile drainage region. Bias correction based on RQUANTILE significantly reduces the MB, with negative values observed across all the ensemble members. On contrary, SSPLINE bias correction results in positive MB values across all the ensemble members, with ensemble members 2, 9 exhibiting the highest values while the averaged ensemble and ensembles 3 and 8 depict least MB values.

The ME measures the error between simulated streamflow and corresponding observations, given in terms of absolute difference, as a direct measurement of the model accuracy. Figure 9.3 depicts ME results across the ensembles and drainage regions. Positive ME values are observed for simulations without bias correction, suggesting potential overestimation of streamflow by the model ensembles. In both drainage regions, ensemble 6 (green) for uncorrected bias depicts the highest ME, followed by ensemble 5 and 1 (dark and light blue, respectively), while ensemble 4 exhibits the lowest ME (see the yellow bar). The ME values significantly reduce after bias-correction, resulting in some cases, negative values (e.g. underestimation of the model ensembles). In particular, the RQUANTILE mapping method applied to the model ensembles in the Crocodile region reduces the ME to almost zero in 6 model ensembles and -0.01 m^3/s in 4, while ME values in the Olifants region reduce to zero in half of the ensembles and -0.01 m^3/s in the other half of the ensembles. On the other hand, only two model ensembles (ensemble 1 and 4) exhibit negative ME in the Crocodile region, the rest of the ensembles (including those corresponding to the Olifants) exhibit positive mean error ranging from 0.01 m^3/s to 0.3 m^3/s.

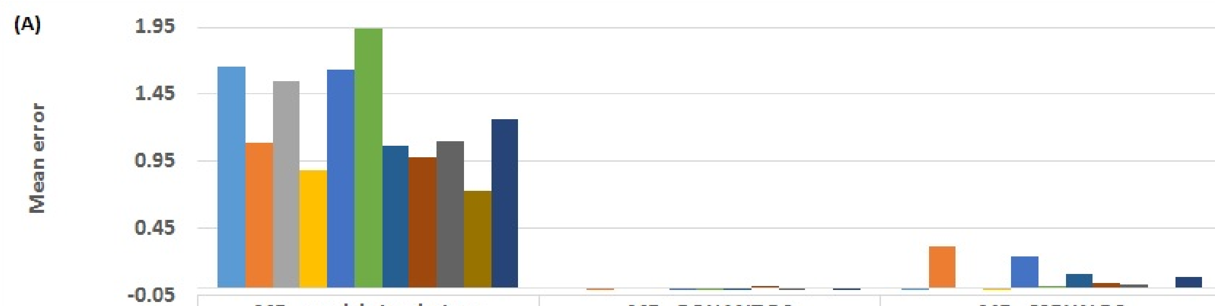

	ME - model simulations	ME - RQUANT BC	ME - SSPLIN BC
Ensemble 1	1.65	0.01	-0.01
Ensemble 2	1.09	-0.01	0.32
Ensemble 3	1.55	0.00	0.01
Ensemble 4	0.88	0.01	-0.01
Ensemble 5	1.64	-0.01	0.24
Ensemble 6	1.94	-0.01	0.02
Ensemble 7	1.07	-0.01	0.11
Ensemble 8	0.98	0.02	0.04
Ensemble 9	1.10	0.00	0.03
Ensemble 10	0.73	0.01	0.01
Avg Ensemble	1.26	-0.01	0.09

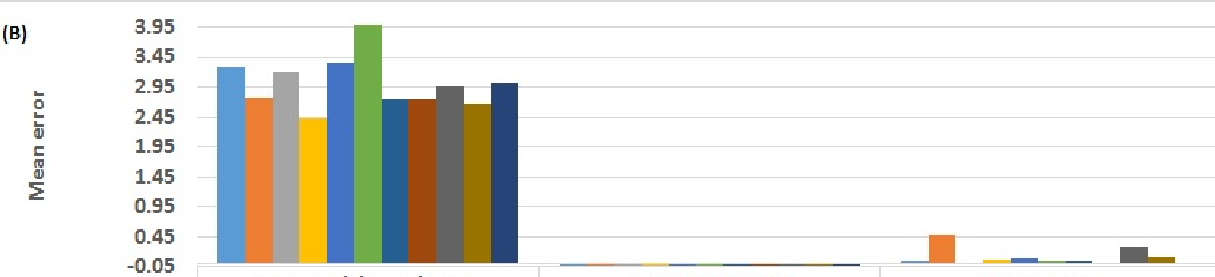

	ME - model simulations	ME - RQUANT BC	ME - SSPLIN BC
Ensemble 1	3.27	-0.01	0.05
Ensemble 2	2.76	0.00	0.47
Ensemble 3	3.21	-0.01	0.03
Ensemble 4	2.42	-0.01	0.07
Ensemble 5	3.35	-0.01	0.09
Ensemble 6	3.98	-0.01	0.04
Ensemble 7	2.74	0.00	0.04
Ensemble 8	2.75	0.00	0.03
Ensemble 9	2.97	0.00	0.28
Ensemble 10	2.68	0.00	0.12
Avg Ensemble	3.01	0.00	0.01

Figure 9.3: Mean error (ME): (A) corresponds to the Crocodile drainage and (B) to Olifants drainage of the LRB

Table 9.8: Characteristics of MB across ensemble members

Crocodile drainage (Limpopo Basin)			
Model	MB – model simulations	MB – RQUANT BC	MB – SSPLIN BC
Ensemble 1	1206.808	4.274	-10.227
Ensemble 2	798.702	-4.533	233.119
Ensemble 3	1133.276	0.363	4.599
Ensemble 4	640.259	3.415	-4.399
Ensemble 5	1194.86	-5.016	171.427
Ensemble 6	1421.019	-3.692	11.113
Ensemble 7	783.382	-4.703	76.545
Ensemble 8	714.734	12.7	29.424
Ensemble 9	803.963	-1.101	19.696
Ensemble 10	535.364	4.77	7.350
Avg. Ensemble	923.237	-4.43	62.804
Olifants drainage (Limpopo Basin)			
Ensemble 1	2390.875	-4.36	35.763
Ensemble 2	2018.191	-3.102	344.846
Ensemble 3	2348.813	-5.494	20.535
Ensemble 4	1770.573	-4.872	47.583
Ensemble 5	2447.992	-7.082	67.192
Ensemble 6	2909.166	-6.763	30.394
Ensemble 7	2005.182	-0.94	31.178
Ensemble 8	2013.032	-2.712	20.055
Ensemble 9	2168.352	-0.917	206.055
Ensemble 10	1958.995	-2.499	89.17
Avg. Ensemble	2203.117	-1.941	4.22

Figure 9.4 compares the RMSE values computed from streamflow simulations across the ensemble members, with and without bias correction. The results depict variation in the RMSE values across the ensemble members. Model ensemble 3 for simulations without bias correction in the Crocodile drainage region and ensemble 6 in the Olifants drainage region depict the highest RMSE values, followed ensemble 1. Lowest RMSE values are observed for Ensembles 2 and 8. The RQUANTILE bias correction simulations depict a slight decrease in RMSE values (with the exception of ensembles 4, 7, 8, and 10 in the Crocodile drainage region). On the contrary, the SSPLINE bias correction results in an increase in most of the ensembles, with ensemble 2 and 5 in the Crocodile and ensembles 2 and 9 in the Olifants drainage regions showing the highest RMSE values. Overall, the model ensembles with RQUANTILE bias correction depict reduced RMSE values as compared to the SSPLIE bias correction simulations.

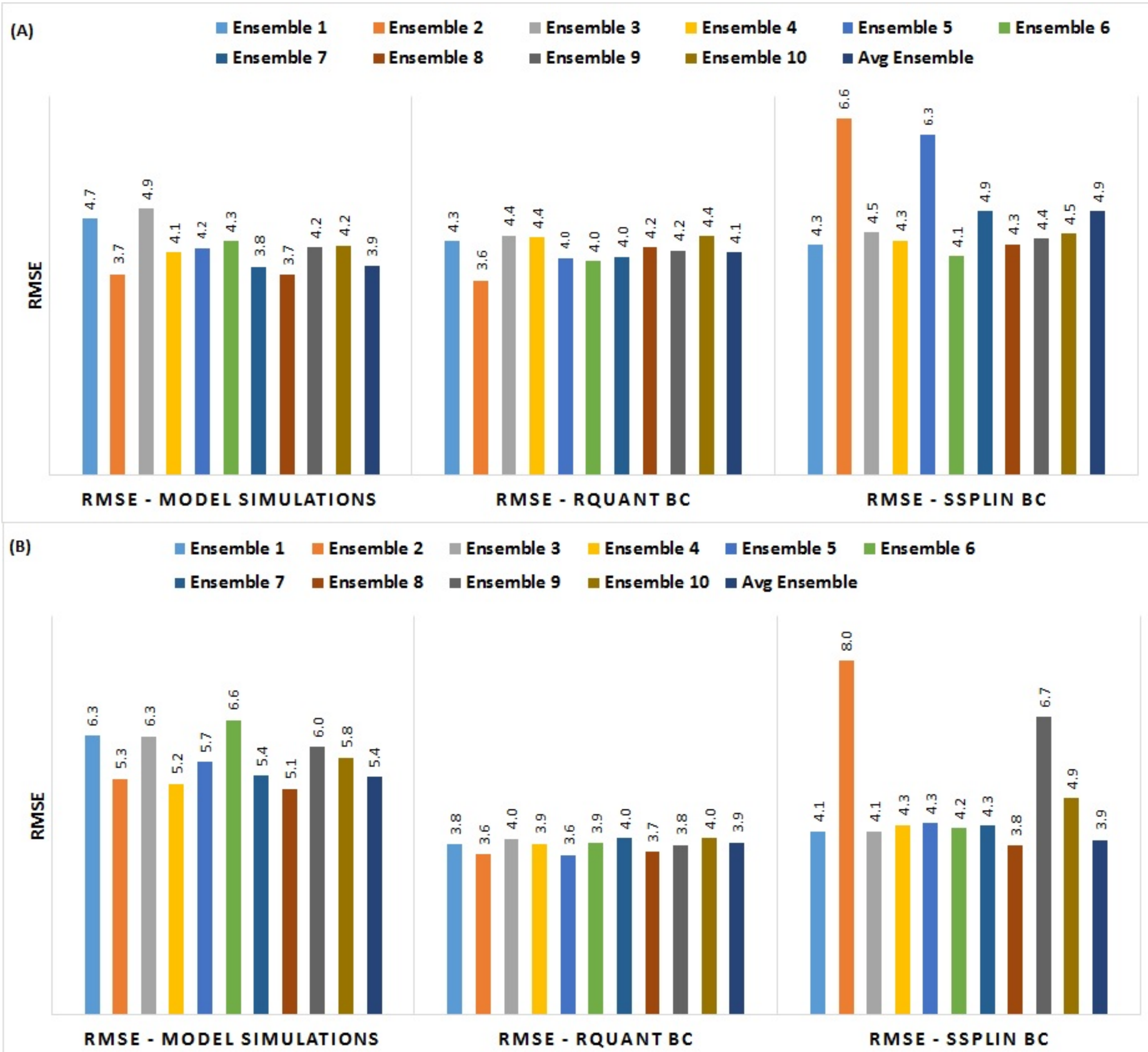

Figure 9.4: Same as Figure 9.3 but for root mean square error (RMSE)

Figure 9.5 compares uncertainties in model simulations in terms of the mean of the squared differences (i.e. MSE) between the observed and simulated streamflow across the model ensemble members, both with and without bias correction. In Figure 9.5 the blue bars depict MSE for ensemble members without bias correction, whereas the red and grey bars correspond to ensemble members with RQUANTILE and SSPLINE bias correction, respectively. Based on the results, ensembles 1 and 3 (without bias correction in the Crocodile region) exhibit the highest MSE (above 20 m^3/s), whereas ensembles 2 and 8 exhibit the lowest MSE values (below 15 m^3/s). The MSE values significantly increase after SSPLINE bias correction (particularly for ensembles 2, 5 and 7). For the Olifants drainage region, MSE from simulation without bias correction range from 20 m^3/s to 33 m^3/s. The RQUANTILE bias correction significantly reduces the MSE values across the ensembles, whereas the SSPLINE bias correction increases the MSE especially for ensemble members 2 and 9.

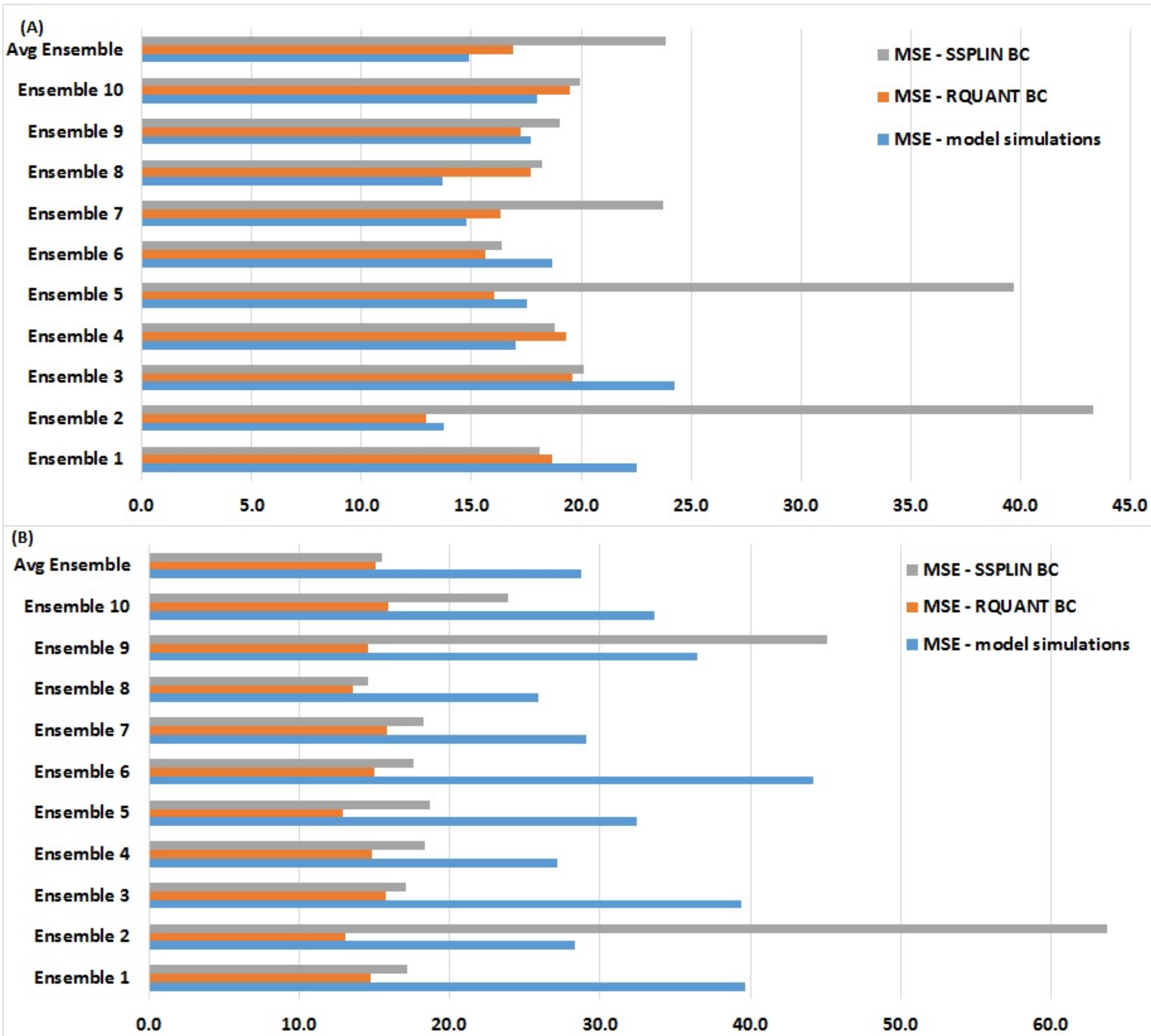

Figure 9.5: Same as Figure 9.3 but for mean square error (MSE)

Results for the Spearman correlation between the observed and simulated streamflow across the ensembles are depicted in Figure 9.6. Simulations without bias correction in both the Crocodile and Olifants drainage regions depict positive correlation across the ensembles. For Crocodile drainage region, high correlation is observed in ensembles 2, 5 and 6, whereas ensembles 3 and 10 show less correlation.

On contrary, ensembles 4 and 6 in Olifants drainage region depict high correlation while ensembles 3 and 10 exhibit less correlation compared to the Crocodile drainage region. The bias correction reduces the correlation between the observations and model simulations. In particular, two ensembles (3 and 10) and three ensembles (3, 7, and 10) in the Crocodile and Olifants drainage regions, depict negative correlation, respectively. The rest of the ensembles depict a positive correlation, with both RQUANTILE and SSPLINE bias correction methods recording high correlation for ensembles 2 and 6 and less correlation for ensemble 4. In terms of statistical significant test, over 90% of the correlations are found to be statistically significant at 95% confidence level.

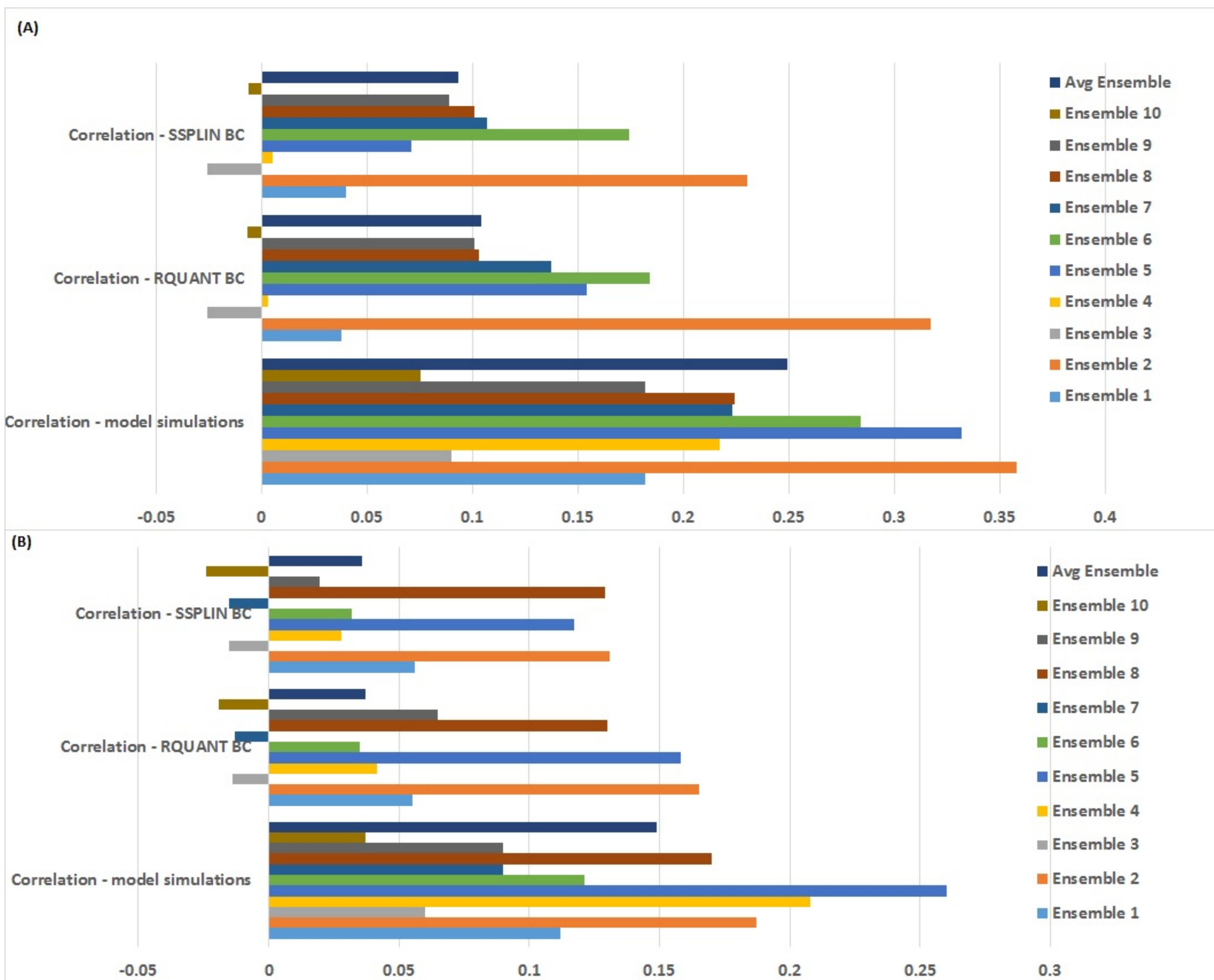

Figure 9.6: Same as Figure 9.3 but for Spearman correlation

9.6.4 Streamflow forecasting

Streamflow forecasting using all the ensemble members for both the Crocodile and Olifants drainage regions was based on ARIMA and TBATS models. The performance of the two models was assessed using ME, RMSE and MAE statistical metrics. The mean, STD, maximum and minimum values were calculated for each statistical metrics. The results are presented in Figure 9.7 (for mean), Figure 9.8 (STD), Figure 9.9 (maximum) and Figure 9.10 (minimum) across the observations and model ensemble members for both the Crocodile and Olifants drainage regions. In each figure, the first 3 sets of histogram bars on the left hand side correspond to ARIMA forecasts whereas the 3 sets on the right hand side correspond to TBATS forecast. In addition, (A) and (B) corresponds to the Crocodile and Olifants drainage regions, respectively. Based on these figures, it is noticed that the ARIMA model overestimate the streamflow forecasts across the ensembles and the drainage regions. On contrary, the TBATS model gives better forecasting results, particularly when assessment is based on the ME and MAE across the ensemble members and drainage regions. The uncertainty within the ensemble members varies, with ensemble members 1, 2, 3, 5 and 6 resulting in the highest uncertainty contrasts while on average, ensemble members 4, 7, 8, 9 and 10 result in less uncertainty contrasts. There are few cases where streamflow observations results in higher uncertainty contrasts than the model ensemble members. Based on the forecasting results obtained in this section, the TBATS model was further used to forecast streamflow for January 2017.

Figure 9.7: Streamflow forecasting statistical moments, expressed in terms of mean values, based on RIMA (A) and TBATS (B) methods.

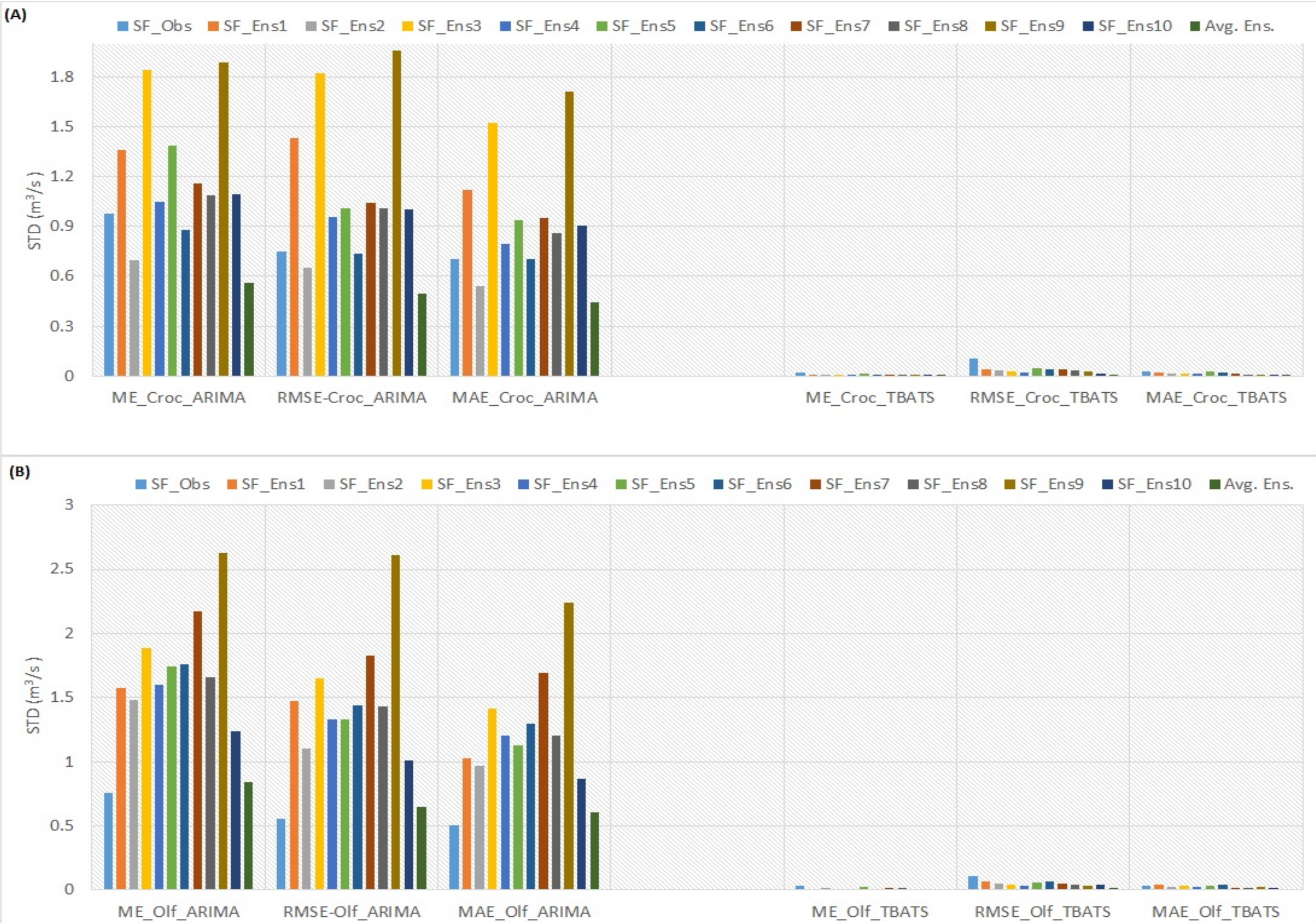

Figure 9.8: Same as Figure 9.7 but for the standard deviation

Figure 9.9: Same as Figure 9.7 but for the maximum values

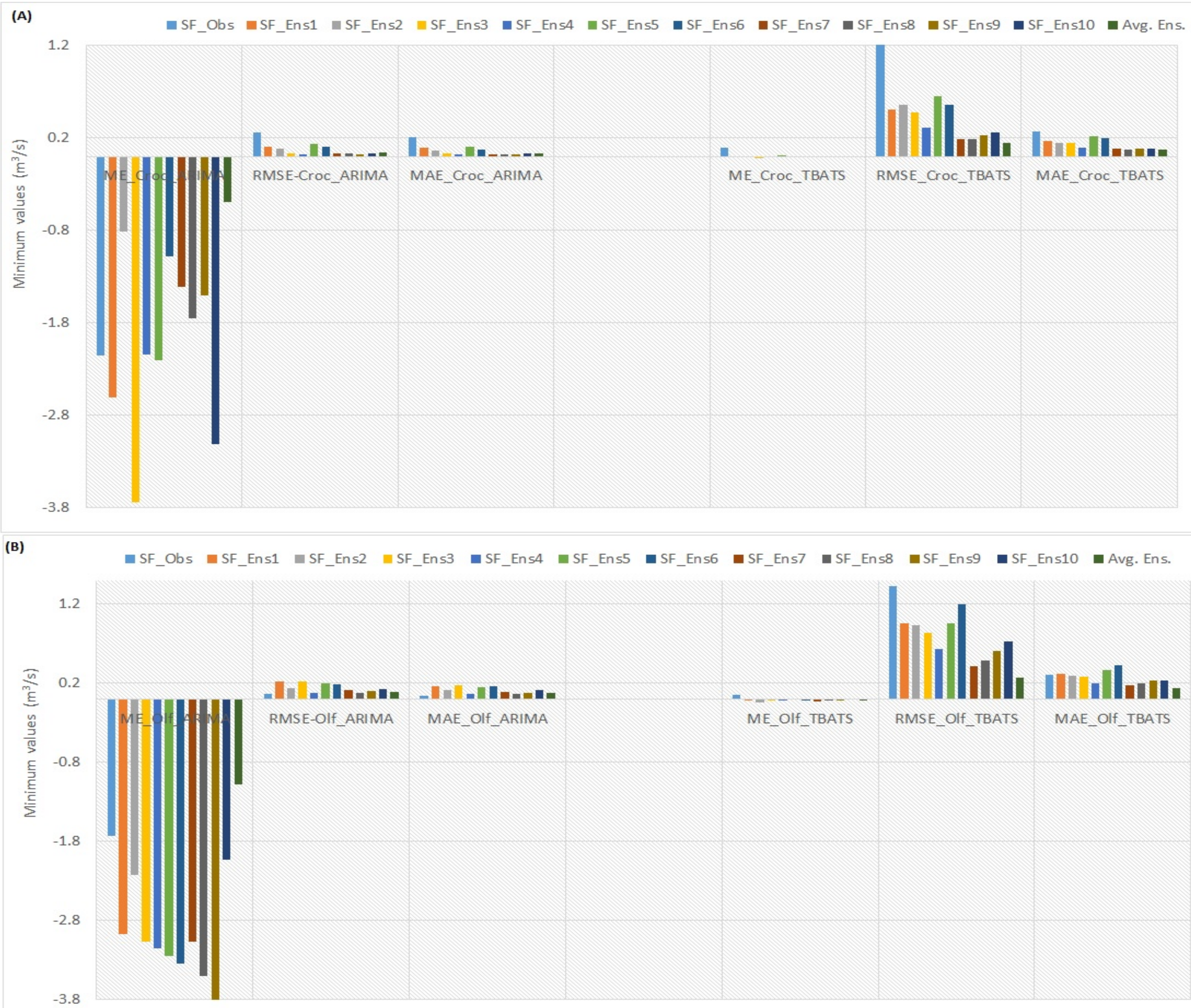

Figure 9.10: Same as Figure 9.7 but for the minimum values

9.6.5 Streamflow forecasting: A case study for January 2017

As a case study, January 2017 was selected because of the high precipitation received in the LRB. This high precipitation is characteristic of the CTLs. These elevated rainfall and streamflow observations are reflected in Figure 9.11. As noted in the figure, rainfall recorded in January ranged from 0 to approximately 60 mm in Crocodile and 0 to 40 mm in Olifants region. The streamflow ranged from 0.5 to 29 m^3/s and 1 to 18 m^3/s in Crocodile and Olifants drainage regions, respectively. The main aim of forecasting the streamflow during January 2017 is to understand how the uncertainties in simulated streamflow from different model ensemble members affect the accuracy of the streamflow forecasts in the LRB.

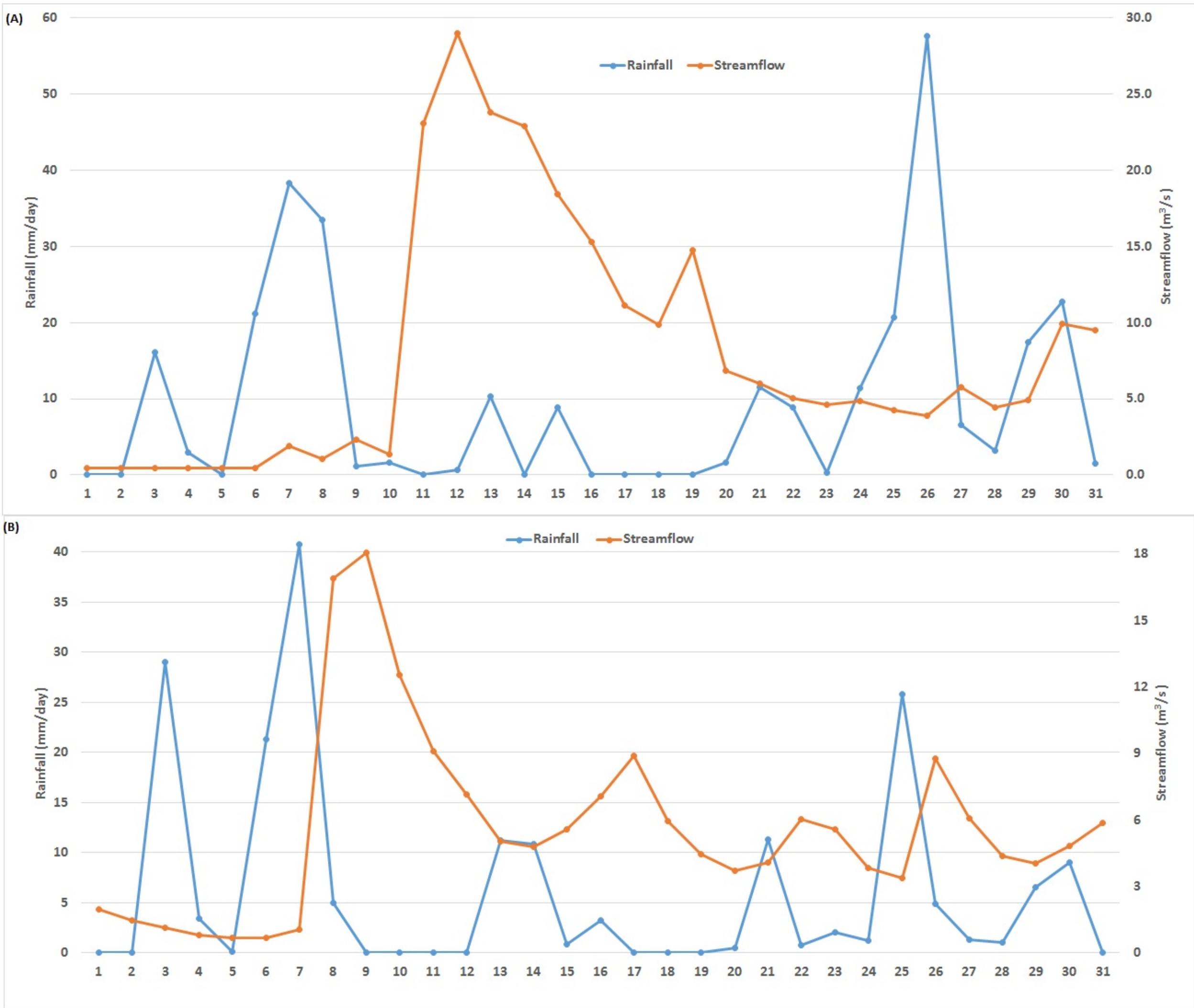

Figure 9.11: Rainfall and streamflow recorded during January 2017. (A) Crocodile and (B) Olifants

The characteristics of streamflow forecasts for January 2017, assessed using ME, RMSE and mean absolute error (MAE) metrics, are given in Figures 9.12-9.15. The forecasting consisted of two lead time epochs, 14 days (Figure 9.12) and 28 days (Figure 9.13). In addition, streamflow forecasting was performed on bias corrected times series, these results are presented in Figure 9.14 and Figure 9.15 for 14 and 28 days, respectively. In each of these figures, the light blue line represents streamflow observations, and it can be noted that the metrics are almost zero in both the drainage regions. For the 14 days lead time forecasts, ensemble members 2, 8 and 9 appear to be close to the observations while the rest of the ensembles significantly deviate from the observations, with ensemble members 3 and 6 showing pronounced uncertainties in the Crocodile drainage region. Similar patterns are observed for Olifants, with ensemble members 1, 3 and 6 depicting higher uncertainty contrasts.

Forecasting results for 28 days lead time (see for example, Figure 9.13) depict higher uncertainties from the following model ensemble members: 1, 3, 5, and 9 for both the Crocodile and Olifants drainage regions. Ensemble members that exhibit patterns similar to the observations include ensemble members 4, 7, 8 and 10. Generally, uncertainties derived from 28 days lead time forecasts are more amplified as compared to those derived from 14 days lead time. This confirms the notion that longer lead time forecasts have a tendency of producing larger uncertainties than short lead forecasts.

Streamflow forecasting for the SSPLINE bias correction time series also depict noticeable uncertainty variability across the ensemble members. Based on the statistical metrics derived from the 14 days lead time forecasts, ensemble members 2, 4, 5 and 9 depict less uncertainty, hence they are very close to the observations whereas ensemble members 1, 3, 6, and 10 as well as the averaged ensemble depict more pronounced uncertainty in both drainage regions. Similarly, for 28 days lead time forecasts, uncertainty from ensemble 9 in Olifants drainage is highly variable, with the RMSE and MAE values reaching 35, followed by ensembles 3, 6, and 10 in the same drainage region, and ensemble members 1, 3, 6, and 9 in the Crocodile drainage region. Overall, it can be inferred that the bias correction did not reduce the uncertainty of streamflow forecasts during January 2017. In some cases, the forecasted results appear to have been poorer than those obtained from unbiased corrected time series. This can be attributed to the short time span considered given that bias correction is assumed to work effectively for long-term data (over 20 years).

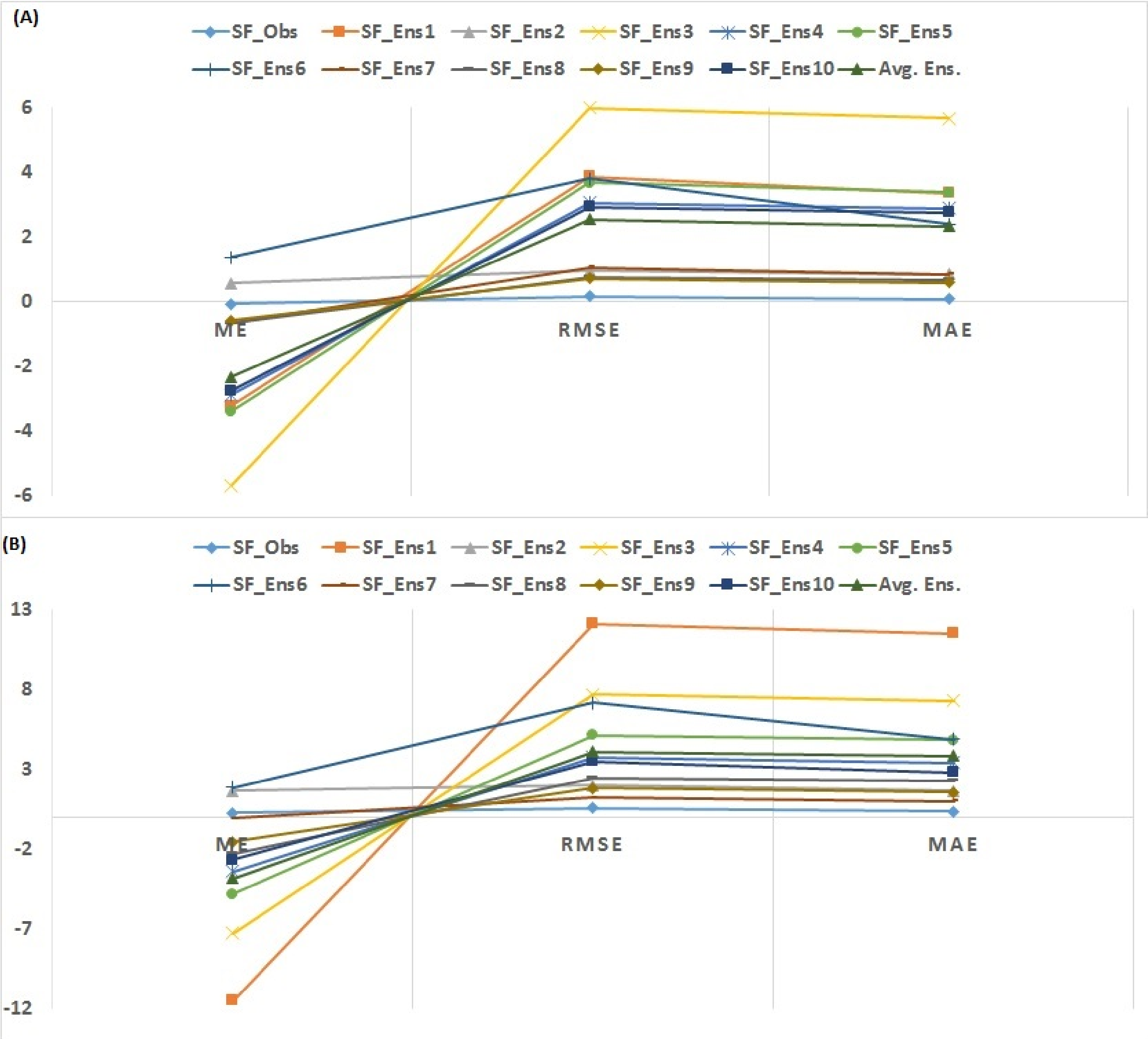

Figure 9.12: Fourteen (14) days streamflow forecasting statistical moments

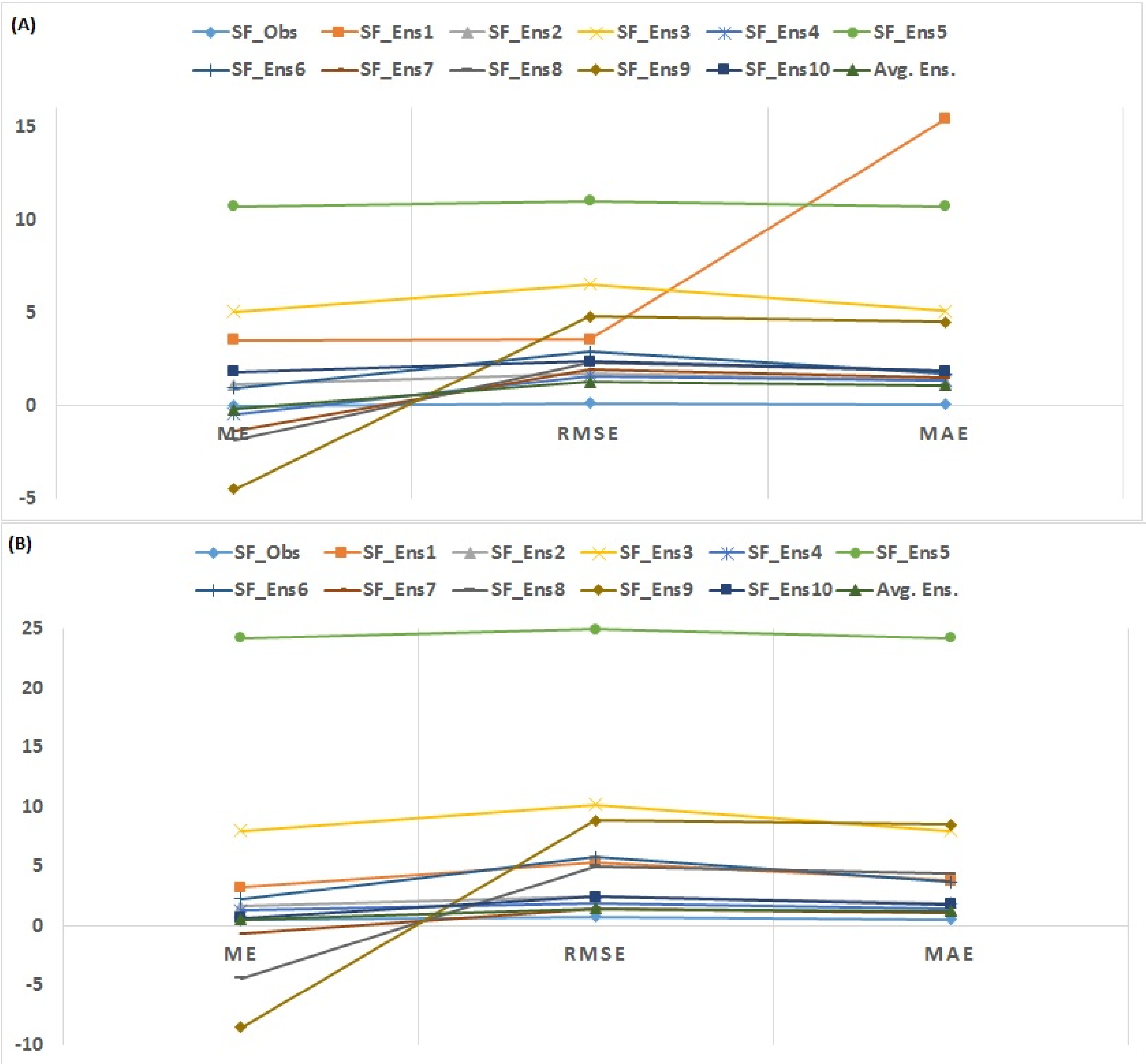

Figure 9.13: Same as Fig. 9.12 but for 28 days

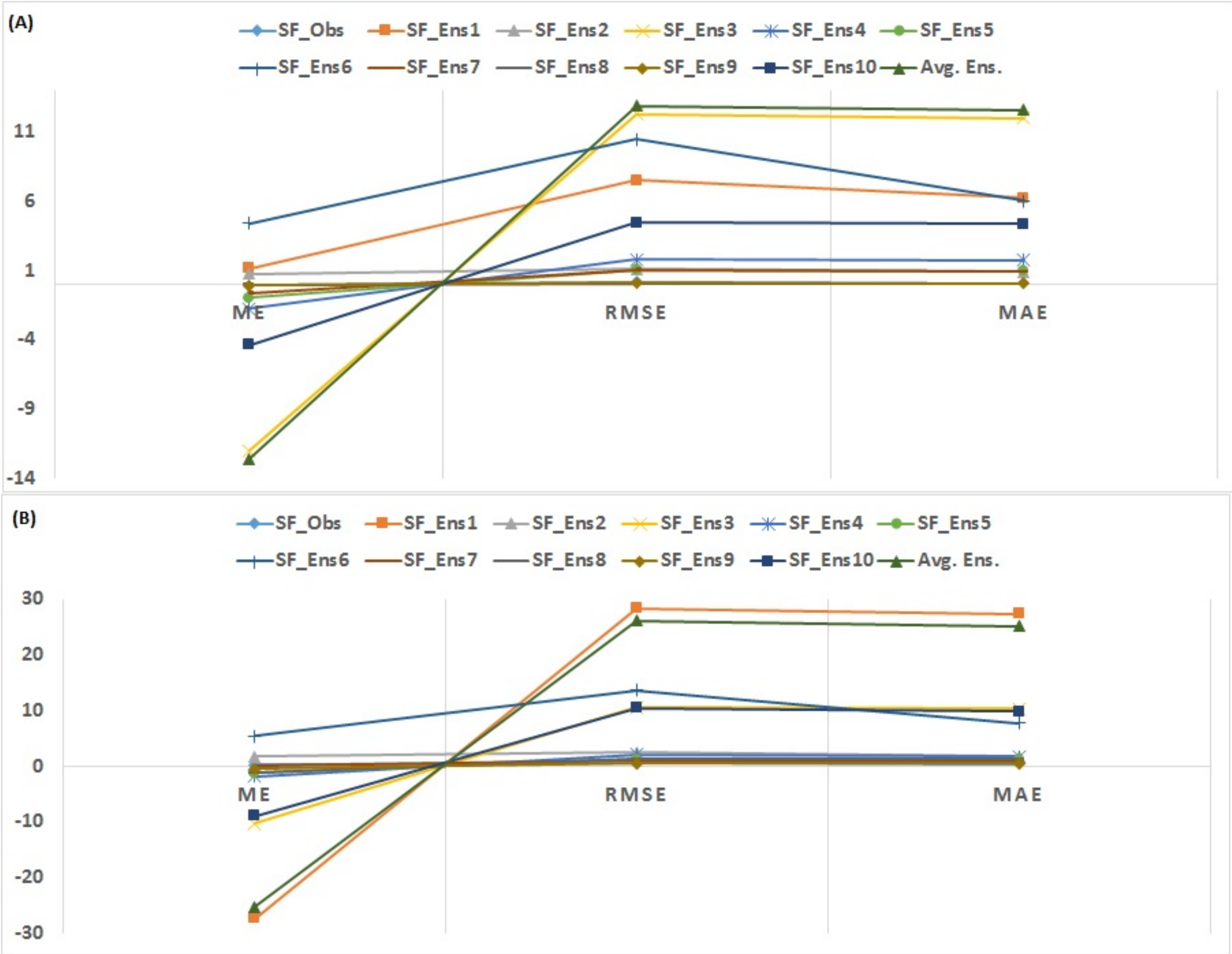

Figure 9.14: Fourteen (14) days streamflow forecasting statistical moments, after SSPLINE bias correction

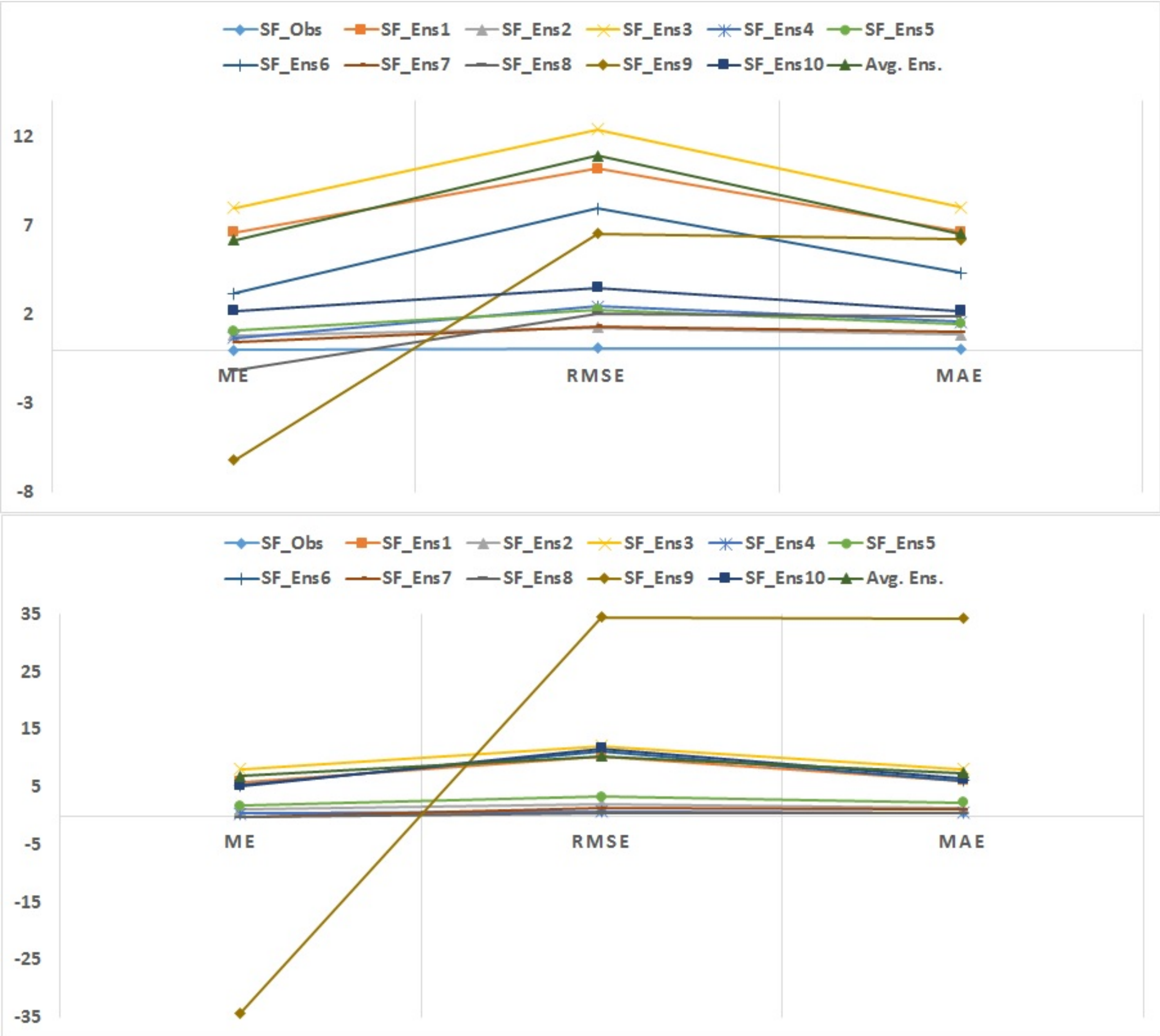

Figure 9.15: Same as Fig. 9.14 but for 28 days

9.7 Discussion

The aim of this study was to assess the effect the precipitation uncertainties has on streamflow forecasting, especially in the LRB. The LRB is prone to tropical systems such as cyclones, depressions, tropical lows, etc. These systems often contribute to local as well as widespread heavy rainfall events, causing severe floods and flash floods events that results in destruction to property, infrastructure and sometimes loss of lives. It is therefore crucial to develop forecasting systems that are capable to resolve the probable occurrences of these extreme events well in advance in order to help the society prepare and reduce any associated disasters. In this regard, we have used precipitation and temperature (minimum and maximum) from the 1-month lead time forecasts of 10 ECHAM4.5-MOM3 model ensemble members to drive the ACRU model to generate streamflow simulations. We have established that the uncertainties in the model ensembles are inherent in the streamflow simulations. Furthermore, streamflow forecasting for 14- and 28-days lead times were derived from the TBATS and the results demonstrating apparent contrasting uncertainties among the ensemble members with a strong dependence of the multi-day lead time forecasts. Understanding how to minimize these errors in streamflow forecasting could be helpful in deriving and achieving precise streamflow forecasts that can be used for flood risks management.

It is important to note that there are myriad of other factors not considered in the present study. For instance, in the present analysis the hydrological model parameters have not been varied and therefore not calibrated for low-flow and high-streamflow events that are characteristics of the LRB. Additionally, analysis of uncertainty propagation could be enriched if an assessment of how the different lead times (e.g. 2-, 3-, 6- months) of the model ensemble members influence the propagation of uncertainties. Similarly, additional insights on the propagation of uncertainties could be gained if more forecasting methods such as artificial neural networks are considered in addition to the ARIMA and TBATS methods. Lastly, it could be useful to investigate how the ensemble streamflow forecasts could perform under both low-and high-streamflow conditions modulated with contrasting hydrological model parameters.

Chapter 10: Conclusions

On 6 January 2017, a CTL was positioned over Botswana with cloud bands extending into the north-eastern parts of South Africa. This CTL resulted in the loss of at least seven lives, damage to numerous households in Phalaborwa, closure of many roads in the Kruger National Park and several cars were swept away due to the flood waters in Mpumalanga (SAWS, 2017). Even though this was a clear CTL, which in fact was the longest consecutive CTL during the study period, forecasters failed to acknowledge the presence of this weather system (SAWS, 2017). It is therefore evident that there is a lack of understanding and accurate identification of these weather systems over southern Africa even though the impacts caused as a result of the existence of a CTL are notoriously vast. The main contribution this research hopes to achieve is to create a better understanding of CTLs and the impacts they can have.

This project contributed to the understanding of synoptic scale circulation over southern Africa as it introduces and describes the character of Continental Tropical Lows. CTLs are not well recognised in southern African synoptic climatologies. CTLs are unique over southern Africa and no documentation is available on similar weather systems elsewhere in the world. This research developed a unique and strict set of criteria to objectively identify CTLs and then created a synoptic climatology of CTLs over southern Africa. In contrary, TTTs are well known and discussed over Africa and elsewhere around the globe (Hart et al., 2010). This is the first time such a study has been undertaken in southern Africa and provides information about a tropical low not previously available.

An objective method, applying very strict criteria was developed in order to identify CTLs over southern Africa. The method is new but builds on the work of others such as (Dyson and Van Heerden, 2002) who first described CTLs but also incorporates ideas of Engelbrecht et al. (2014), Berry and Reeder (2013), Hart et al. (2012), Malherbe et al. (2012) and Crétat et al. (2018). Tropical weather systems were also identified by Malherbe et al. (2012), Crétat et al. (2018) and Berry and Reeder (2013), while authors such as Engelbrecht et al. (2014) identified extratropical weather systems for example COLs and TTTs.

CTLs occur with high frequency in southern Zambia and Angola and less frequently over the central parts of Botswana, Namibia and Zimbabwe. It is rare for CTLs to invade South Africa and there is a return period of 78 years for this to happen. However, the influence of CTLs on rainfall is vast and CTLs located over central Botswana and Zimbabwe caused widespread and heavy rainfall over South Africa. Extreme rainfall may result when the circulation around the CTL encounters the escarpment. Most rainfall occurs to the east of the CTL but significant rainfall can occur some 500 km west of the low. Daily rainfall totals of more than 20 mm occurs regularly and more than 50 mm is also quite common. CTLs are slow moving with an average life span of 1-3 days, this results in the floods that are associated with CTLs not necessarily occurring because of the rainfall in a single day, but rather due to continual rainfall that falls over the same area for several days.

CTLs may sometimes be associated with tropical temperate troughs, but this is not always the case. The temperate trough helps to draw tropical moisture southwards causing thunderstorms over the southern parts of South Africa. However, CTLs are also responsible for heavy rainfall in the absence of a westerly/temperate trough.

The case study demonstrated that the location of the NCEP CTL and the actual position as on the satellite image is not always the same, although it is in close proximity. Even though NCEP reanalysis data is of a high quality and have been used in similar studies, it remains an approximation of reality and therefore can misplace the position of the low.

Numerical weather predictions deals relatively well with CTLs with the forecast uncertainty significantly smaller than for COLs. Weather forecaster can use the NWP forecast of position and depth of a CTL with a large degree of confidence. However, forecast uncertainty increases with increasing lead time and this impacts on hydrological modelling as slight changes in position of the CTL can have a significant influence on the rainfall distribution.

There is predicted to be a general increase in warm cored mid-tropospheric lows over South Africa towards the end of the century. The ensemble average of five CCAM climate projections shows that the number of warm lows over Zambia and Angola is expected to decrease with a slight increase in lows over Namibia. Botswana and north-eastern South Africa. Over the central coast of Namibia there is predicted to be a 40% increase in the number of lows towards the end of the century. The increase in the number lows at this grid point could lead to an increase in the number of heavy rainfall events over northern Limpopo an especially the escarpment.

Streamflow simulations from 10 ECHAM4.5-MOM3 model ensemble members were evaluated to assess the impact of precipitation uncertainty in streamflow forecasting. The results depict a potential 1:1 influence of mean annual precipitation changes to the changes in mean annual streamflow across the model ensemble members. There exists a substantial variation in streamflow simulations across the model ensemble members and across the drainage regions of LRB, with the majority of the model ensemble members overestimating the simulated streamflow. The observed variations in streamflow simulations can be attributed to the differences in model ensemble members' structures. In addition, 14-days and 28-days lead time streamflow forecasts during January 2017 show apparent contrasting uncertainties among the ensemble members, with the longer lead time forecasts depicting more pronounced uncertainty. Overall, the results have important scientific and practical applications. From the scientific perspective, this study points to the need for a holistic consideration of hydrometeorological model parameterization, catchment initial conditions, meteorological inputs, as well as coupling of both climatic and non-climatic drivers. For practical purposes, this study could be seen as a precursor to the development of multi-model rainfall-runoff streamflow forecasting applications or services in an operationally realistic scenario. If such a system is tested and calibrated, then it could be useful to water resources managers in the LRB, for aiding policy planning for future practices, as well as to the South African water management agencies in general.

References

AGRAWAL, R.K., ADHIKARI, R. An introductory study on time series modeling and forecasting. CoRR, 2013

AMOO, O.T., DZWAIRO, B. Hydrological characterization of a watershed for streamflow prediction. International

ANTHES, R.A. (1982). Tropical Cyclones-Their Evolution, Structure and Effects. National Centre for Atmospheric Research, Meteorological Monographs, 19(41). ISBN 0-933876-54-8.

ANWENDER, D., P. HARR, and S. JONES (2008). Predictability associated with the downstream impacts of the extratropical transition of tropical cyclones: Case studies. Mon. Wea. Rev., 136, 3226-3247.

ASNANI, G.C. (2005). Tropical Meteorology. Revised Ed. Pashan, Pune, India, Indian Institute of Tropical Meteorology, 1. ISBN 81-900400-7-3.

BAWDEN, A.J., LINTON, H.C., BURN, D.H., PROWSE, T.D. A spatiotemporal analysis of hydrological trends and variability in the Athabasca River region, Canada. Journal of Hydrology, 2014. 509: p. 333-342.

BERAKI, A. F., DEWITT, D. G., LANDMAN, W. A., OLIVIER, C. Dynamical seasonal climate prediction using an ocean-atmosphere coupled climate model developed in partnership between South Africa and the IRI. Journal of Climate, 2014; 27(4): 1719-1741.

BERRY, G. and REEDER, M.J. (2013). Objective Identification of the Intertropical Convergence Zone: Climatology and Trends from the ERA-Interim. Journal of Climate, 27, pp. 1894-1909.

BLAMELY, R.C. and REASON, C.J.C. (2012). The Role of Mesoscale Convective Complexes in Southern Africa Summer Rainfall. Journal of Climate, 26, pp. 1654-1668.

BOTAI, C.M., BOTAI, J.O., DLAMINI, L.C., ZWANE, N.S., PHADULI, E. (2016). Characteristics of Droughts in South Africa: A Case Study of Free State and North West Provinces. Water MDPI, 8, 439, DOI: 10.3390/w8100439.

BOUGEAULT, P., TOTH, Z., BISHOP, C., BROWN, B., BURRIDGE, D., CHEN, D. H., ... & WORLEY, S. (2010). The THORPEX interactive grand global ensemble. Bulletin of the American Meteorological Society, 91(8), 1059-1072.

CRETAT, J., POHL, B., DIEPPOIS, B., BERTHOU, S., PERHAUD, J. (2018). The Angola Low: relationship with southern African rainfall and ENSO. Clim. Dynamics.

CHAN, J.C.L. and KEPERT, J.D. (2010). World Scientific Series on Asia-Pacific Weather and Climate, Volume 4. Global Perspectives on Tropical Cyclones. From Science to Mitigation. World Scientific Publishing Co.

CHIKOORE, H., VERMEULEN, J.H. and JURY, M.R. (2015). Tropical Cyclones in the Mozambique Channel: January-March 2012. Natural Hazards, 77, pp. 2081-2095. DOI: 10.1007/s11069-015-1691-0.

CLIMATE PREDICTION CENTRE INTERNET TEAM (2018). Cold & Warm Episodes by Season, NOAA, National Centre for Environmental Prediction, Maryland, http://origin.cpc.ncep.noaa.gov/products/analysis_monitoring/ensostuff/ONI_v5.php.

CONCEPTUAL MODELS FOR SOUTHERN HEMISPHERE (2015). Tropical Lows in Southern Africa.https://sites.google.com/site/cmsforsh/CoE-South-Africa/continental-tropical-lows

CRIMP, S.J., VAN DEN HEEVER, S.C., D'ABRETON, P.C., TYSON, P.D. and MASON, S.J. (1997). Mesoscale Modelling of Tropical-Temperate Troughs and Associated Systems over Southern Africa. WRC Report 595/1/97, 395pp.

DE LIVERA, A.M., HYNDMAN, R.J., SNYDER, R.D. Forecasting time series with complex seasonal patterns using exponential smoothing. J. Am. Stat. Assoc. 2011; 106(496), 1513-1527.

DE LIVERA, A.M., HYNDMAN, R.J., SNYDER, R.D. Forecasting time series with complex seasonal patterns using exponential smoothing. J. Am. Stat. Assoc. 2011; 106(496), 1513-1527.

DYSON, L.L. (2000). A Dynamical Forecasting Perspective on Synoptic Scale Weather Systems over southern Africa. Unpublished M.Sc. Thesis, University of Pretoria, South Africa.

DYSON, L.L. and VAN HEERDEN, J. (2001). The heavy rainfall and floods over the north-eastern interior of South Africa during February 2000. S. Afr. J. Sci. 97, pp. 80-86.

DYSON, L.L. and VAN HEERDEN, J. (2002). A model for the identification of tropical weather systems over South Africa. Water SA, 28(3), pp. 249-258.

DYSON, L.L., VAN HEERDEN, J. and MARX, H.G. (2002). Short Term Weather Forecasting techniques for Heavy Rainfall. WRC Report 1011/1/02.

DYSON, L.L. (2009). Heavy daily-rainfall characteristics over the Gauteng Province. Water SA 35: 627-638, DOI: 10.4314/wsa.v35i5.49188.

DYSON, L.L., VAN HEERDEN, J. and SUMNER (2015). A baseline climatology of sounding-derived parameters associated with heavy rainfall over Gauteng, South Africa. International Journal of Climatology, 35, pp. 114-127. doi:10.1002/joc.3967

DE VILLIERS, M.P., LAING, M., RAE, K., QUINN, S., GILL, T. and HUNTER, I. (2000). Two Heavy Rain and Flooding Events Over the North-Eastern Part of South Africa during February 2000. Weather Bureau, Department of Environmental Affairs and Tourism, Republic of South Africa, Directorate Forecasting, Internal Report No FOR/18.

ENGELBRECHT, C.J., ENGELBRECHT, F.A. and DYSON, L.L. (2013). High resolution model projected changes in tropospheric closed-lows and extreme rainfall events over southern Africa. International Journal of Climatology, 33(1), pp. 173-187.

ENGELBRECHT, C.J., LANDMAN, W.A., ENGELBRECHT, F.A. and MALHERBE, J. (2015). A Synoptic Decomposition of Rainfall over the Cape south coast of South Africa. Clim. Dynamics. DOI 10.1007/s00382-014-2230-5

ENGELBRECHT, F., ADEGOKE, J., BOPAPE, M.M., NAIDOO, M., GARLAND, R., THATCHER, M., MCGREGOR, J., KATZFEY, J., WERNER, M., ICHOKU, C. and GATEBE, C. (2015). Projections of rapidly rising surface temperatures over Africa under low mitigation. Environmental Research Letters.

ENGELBRECHT, F.A., LANDMAN, W.A., ENGELBRECHT, C.J., LANDMAN, S., BOPAPE, M.M., ROUX, B., MCGREGOR, J.L. and THATCHER, M. (2011). Multi-scale climate modelling over Southern Africa using a variable-resolution global model. Water SA 37 647-658.

ENGELBRECHT, F.A., MCGREGOR, J.L. and ENGELBRECHT, C.J. (2009). Dynamics of the conformal-cubic atmospheric model projected climate-change signal over southern Africa. Int J Climatol 29 1013-1033.

ENGELBRECHT, E.H. and LANDMAN, S. (2015) Utilizing Standardized Anomalies to predict Heavy Rainfall Producing Synoptic Scale Systems over South Africa. Unpublished Honours Research Project, University of Pretoria, South Africa.

FAO. Drought Impact Mitigation and Prevention in the Limpopo River Basin: A Situation Analysis. Land and Water Discussion Paper; Food and Agricultural Organization (FAO): Rome, Italy, 2004.

FAVRE, A., HEWITSON, B., TADROSS, M., LENNARD, C. and CEREZO-MOTA, R. (2012). Relationships between cut-off lows and the semiannual and southern oscillations. Clim. Dynamics 38, pp. 1473-1487.

FAVRE, A., HEWITSON, B., LENNARD, C., CEREZO-MOTA, R. and TADROSS, M. (2013). Cut-off lows in the South Africa region and their contribution to precipitation. Clim. Dynamics 41, pp. 2331-2351.

FETTER, C.W. Applied Hydrogeology. 1988, New Jersey: Prentice Hall, Upper Saddle River.

GERMANN, U., BERENGUER, M., SEMPERE-TORRES, D., ZAPPA, M. REAL: ensemble radar precipitation estimation for hydrology in a mountainous region. Q. J. Royal Meteorol. Soc., 2009; 135, 445-456.

GUDMUNDSSON, L., BREMNES, J.B., HAUGEN, J.E., ENGEN-SKAUGEN, T. Technical Note: Downscaling

RCM precipitation to the station scale using statistical transformations – a comparison of methods. Hydrology and Earth System Sciences, 2012, 16, 3383-3390.

HART, N.C.G., REASON, C.J.C. and FAUCHEREAU, N. (2010). Tropical-Extratropical Interactions over Southern Africa: Three Cases of Heavy Summer Season Rainfall. Mon. Wea. Rev., 138, pp. 2608-2623

HART, N.C.G., REASON, C.J.C. and FAUCHEREAU, N. (2012). Building a Tropical-Extratropical Cloud Band Metbot. American Meteorological Society. DOI: 10.1175/MWR-D-12-00127.1

HARRISON, M.S.J. (1984). A generalized classification of South African summer rain-bearing synoptic systems. Journal of Climatology, 4, pp. 547-560.

HARRISON, M.S.J. (1986). A synoptic climatology of South African rainfall variations. Unpublished PhD Thesis. University of the Witwatersrand, 341pp.

HARRISON, M.S.J. (1988). Rainfall and Precipitable Water Relationships over the Central Interior of South Africa. South African Geographical Journal 70(2), pp. 100-111.

HIPEL, K.W., MCLEOD, A.I. Time Series Modelling of Water Resources and Environmental Systems. Amsterdam, Elsevier 1994.

HOLTSLAG, A.A.M. and BOVILLE, B.A. (1993). Local versus non-local boundary layer diffusion in a global climate model. *J. Climate* **6** 1825-1842.

HOLTON, J.R. (2004). An introduction to dynamic meteorology. 4th edition. Academic Press, San Diego. 535pp.

HUSCHKE, R.E. (1959). Glossary of Meteorology. American Meteorological Society. Boston. 638pp.

IIZUMI, T., NISHIMORI, M., DAIRAKU, K., ADACHI, S.A., YOKOZAWA, M. (2011). Evaluation and intercomparison of downscaled daily precipitation indices over Japan in present day climate: Strengths and weaknesses of dynamical and bias correction-type statistical downscaling methods. Journal of Geophysical Research, 116: D01111. doi:10.1029/2010JD014513.

IRENE, B.G., CONSUELO, V.O., DAVID, R.P. Integrated assessment of policy interventions for promoting sustainable irrigation in semi-arid environments: A hydro-economic modeling approach. Journal of Environmental Management, 2013; 128: 144-160.

JURY, M.R. and PATHACK, B. (1991). A study of climate and weather variability over the tropical southwest Indian Ocean. Meteorology and Atmospheric Physics. 47, pp. 37-48.

KALNAY, E. and co-authors (1996). The NCEP/NCAR 40-year reanalysis project, Bulletin of the American Meteorological Society 77:437-470. DOI:http://dx.doi.org/10.1175/1520-0477 (1996)077<0437:TNYRP>2.0.CO;2

KAROLY, D.J. and VINCENT, D.G. (1998). Meteorology of the Southern Hemisphere 27 (49). American Meteorological Society. Boston. 410pp.

KATZFEY, K.K., MCGREGOR, J.M., NGUYEN, K. and THATCHER, M. (2009). Dynamical downscaling techniques: Impacts on regional climate change signals. 18th World IMACS/MODSIM Congress, Cairns, Australia, July 2009.

KERKMANN, J. (2005). RGB composites with channels 01-11 and their interpretation, Accessed on 15 October 2018. http://oiswww.eumetsat.org/WEBOPS/msg_interpretation/msg_channels.php

KIENZLE, S.W., LORENTZ, S.A., SCHULZE, R.E. (1997). Hydrology and Water Quality of the Mgeni Catchment. Water Research Commission, Pretoria, RSA. Report TT 87/97. pp88.

KNAFF, J.A., CRAM, T.A., SCHUMACHER, A.B., KOSSIN, J.P. and DEMARIA, M. (2008). Objective Identification of Annular Hurricanes. American Meteorological Society. DOI: 10.1175/2007WAF2007031.1

KOWALCZYK, E.A., GARRATT jr, and KRUMMEL, P.B. (1994). Implementation of a soil-canopy scheme into the CSIRO GCM-regional aspects of the model response. CSIRO Div. Atmospheric Research Tech. Paper No. 32. 59 pp

LBPTC. Joint Limpopo River Basin Study Scoping Phase: Final Report; Limpopo Basin Permanent Technical Committee: Southern Africa Development Community (SADC), Gaborone, Botswana, 2010.

LAING, A.G. and FRITSCH, M.J. (1993). Mesoscale Convective Complexes in Africa. Monthly Weather Review, 121, pp. 2254-2263.

LAING, A. and EVANS, J.L. (2016). Introduction to Tropical Meteorology. 2nd Edition. A comprehensive Online and Print Textbook. Version 4.0. Accessed on 15 October 2018. https://www.meted.ucar.edu/tropical/textbook_2nd_edition/

LANDMAN, W.A. and MASON, S.J. (1999). Change in the association between Indian Ocean sea-surface temperatures and summer rainfall over South Africa and Namibia. International Journal of Climatology, 19, pp. 1477-1492.

LANDMAN, S., ENGELBRECHT, C.J., MASON, S.J. and PEGRAM, G.G.S. (2016). Evaluation of the Predictability of Rainfall over South Africa by Regional and Global Weather Prediction Models. Reprints of the 32nd Annual Conference of South Africa Society for Atmospheric Sciences held at Cape Town, South Africa.

LE MAITRE, D.C., KOTZEE, I.M., O'FARRELL, P.J. Impacts of land-cover change on the water flow regulation ecosystem service: Invasive alien plants, fire and their policy implications. Land Use Policy 36, 2014: 171-181.

LI, H., HUANG, H., WIGMOSTA, M.S., KE, Y., COLEMAN, A.M., LEUNG, L.R., WANG, A., RICCIUTO D.M. Evaluating runoff simulations from the Community Land Model 4.0 using observations from flux towers and a mountainous watershed. Journal of Geophysical Research: Atmospheres, 2011. 116(D24).

LYON, B., MASON, S.J. (2007). The 1997-98 Summer Rainfall Season in Southern Africa. Part I: Observations. Journal of Climat. 20, pp. 5134-5148

MALHERBE, J., ENGELBRECHT, F.A., LANDMAN, W.A. and ENGELBRECHT, C.J. (2012). Tropical systems from the southwest Indian Ocean making landfall over the Limpopo River Basin, southern Africa: a historical perspective. International Journal of Climatology DOI: 10.1002/joc.2320.

MALHERBE, J., ENGELBRECHT, F.A. and LANDMAN, W.A. (2013). Projected changes in tropical cyclone climatology and landfall in the Southwest Indian Ocean region under enhanced anthropogenic forcing. Clim Dyn 40 2867-2886.

MILLY, P.C., DUNNE, K.A., VECCHIA, A.V. Global pattern of trends in streamflow and water availability in a changing climate. Nature, 2005; 438(17): 347-350.

MULENGA, H.M. (1998). Southern African Climatic Anomalies, Summer Rainfall and the Angola Low. Dissertation, University of Cape Town, South Africa.

MCGREGOR, J.L. (2003). A new convection scheme using a simple closure. In: Current Issues in the Parameterization of Convection. BMRC Research Report 93. 33-36.

MCGREGOR, J.L. (2005). C-CAM: Geometric aspects and dynamical formulation. CSIRO Atmospheric Research Tech. Paper No 70, 43 pp.

MCGREGOR, J.L. and DIX, M.R. (2001). The CSIRO conformal-cubic atmospheric GCM. In: Hodnett, P.F. (ed.) Proc. IUTAM Symposium on Advances in Mathematical Modelling of Atmosphere and Ocean Dynamics. Kluwer, Dordrecht. 197-202.

MCGREGOR, J.L. and DIX, M.R. (2008). An updated description of the Conformal-Cubic Atmospheric Model. In: Hamilton K and Ohfuchi W (eds.) High Resolution Simulation of the Atmosphere and Ocean. Springer Verlag. 51-76.

MCGREGOR, J.L., GORDON, H.B., WATTERSON, I.G., DIX, M.R. and ROTSTAYN, L.D. (1993). The CSIRO 9-level atmospheric general circulation model. CSIRO Div. Atmospheric Research Tech. Paper No. 26. 89 pp

PIANI, C., HAERTER, J. and COPPOLA, E. (2010). Statistical bias correction for daily precipitation in regional climate models over Europe, Theor. Appl. Climatol., 99, 187-192.

PATIl, S., STIEGLITZ, M. Controls on hydrologic similarity: role of nearby gauged catchments for prediction at an ungauged catchment. Hydrol. Earth Syst. Sci., 2012; 16(2): 551-562.

PRESTON-WHYTE, R.A. and TYSON, P.D. (1993). The Atmosphere and Weather of Southern Africa. Oxf. Univ. Press. 374pp.

POOLMAN, E. and TERBLANCHE, D. (1984). Tropiese Siklone Domoina en Imboa. South African Weather Bureau Newsletter. 420, pp. 37-45.

QUINN, S.J. (1988). The weather of February 1988. Weather Bureau Newsletter, February 1988, No. 467.

RAMAGE, C.S. (1995). Forecasters Guide to Tropical Meteorology AWS TR 240 Updated. Air Weather Service.

REASON, C.J.C. and KEIBEL, A. (2004). Tropical Cyclone Eline and Its Unusual Penetration and Impacts over the Southern African Mainland. Weather and Forecasting, 19, pp. 789-805.

REASON, C.J.C., LANDMAN, W. and TENNANT, W. (2006). Seasonal to Decadal Prediction of Southern African Climate and its Links with Variability of the Atlantic Ocean. Bulletin American Meteorological Society, 8.7, pp. 941-955.

REKACEWICZ, P. and BOURNAY, E. (2005). Southern Africa, topographic and political map, UNEP/GRID-Arendal, http://www.grida.no/resources/5305.

RICHARD, Y., FAUCHEREAU, N., POCCARD, I, ROUAULT, M., TRZASKA, S. (2001). 20th Century Droughts in Southern Africa: Spatial and Temporal Variability, Teleconnections with Oceanic and Atmospheric Conditions. International Journal of Climatology, 21, pp. 873-885. DOI: 10.1002/joc.656.

RIEHL, H. (1979). Climate and Weather in the Tropics. Academic Press. 611pp.

ROTSTAYN, L.D. (1997). A physically based scheme for the treatment of stratiform clouds and precipitation in large-scale models. I: Description and evaluation of the microphysical processes. Quart. J. Roy. Meteor. Soc. 123 1227-1282.

SANKARASUBRAMANIAN, A., VOGEL, R.M., LIMBRUNNER J.F. Climate elasticity of streamflow in the United States. Water Resour. Res., 2001; 37: 1771-1781.

SCHNEIDER, U., BECKER, A., FINGER, P., MEYER-CHRISTOFFER, A., RUDOLF, B., ZIESE, M. (2011). GPCC Full Data Reanalysis Version 6.0 at 0.5°: Monthly Land-Surface Precipitation from Rain-Gauges built on GTSbased and Historic Data. DOI: 10.5676/DWD_GPCC/FD_M_V7_050.

SCHULZE, R.E., PERKS, L.A. Assessment of the impacts of climate change on hydrology and water resources in South Africa. Report to SA Country Study for Climate Change Programme. School of Bioresources Engineering and Environmental Hydrology, University of Natal, Pietermaritzburg, South Africa, p. 118.

SCHULZE, R.E. Hydrology and Agrohydrology: A Text to Accompany the ACRU Agrohydrological Modelling System. Water Research Commission, Pretoria, RSA. Technology Transfer Report TT 69/95. 1995: p. 552.

SCHULZE, R.E., SCHMIDT, E.J., SMITHERS, J.C. SCS-SA User Manual. Department of Agricultural Engineering, University of Natal, Pietermaritzburg, RSA. ACRU Report, 1993; 40. p 78.

SINGLETON, A.T. and REASON, C.J.C. (2006). A Numerical Model Study of an Intense Cutoff Low Pressure System over South Africa. Mon. Wea. Rev., 135, pp. 1128-1150.

SINGLETON, A.T. and REASON, C.J.C. (2007). Variability in the characteristics of cut-off low pressure systems over subtropical southern Africa. International Journal of Climatology, 27, pp. 295-310.

SIVAPALAN, M., THOMPSON, S.E., HARMAN, C.J., BASU, N.B., KUMAR, P. Water cycle dynamics in a changing environment: Improving predictability through synthesis. Water Resources, 2011; 47(10).

SOUTH AFRICAN WEATHER SERVICE (2017). Climate Summary of South Africa, January 2013. ISSN 1992-2566. Volume 28, No.1.

TALJAARD, J.J. (1985). Cut-off Lows in the South African Region. South African Weather Service Technical Paper, 14, South African Weather Service, Private Bag X97, Pretoria, 0001. 153pp.

TALJAARD, J.J. (1986). Change of rainfall distribution and circulation patterns over southern Africa in summer. Journal of Climatology, 6, pp 579-592.

TALJAARD, J.J. (1994). Atmospheric Circulation Systems, Synoptic Climatology and Weather Phenomena of South Africa. Part 1 Controls of the Weather and Climate of South Africa. South African Weather Service Technical Paper, 27, South African Weather Service, Private Bag X97, Pretoria, 0001. 45pp.

TALJAARD, J.J. (1995). Atmospheric Circulation Systems, Synoptic Climatology and Weather Phenomena of South Africa. Part 2 Atmospheric Circulation Systems in the South African Region. South African Weather Service Technical Paper, 28, South African Weather Service, Private Bag X97, Pretoria, 0001. 65pp

TALJAARD, J.J. (1996). Atmospheric Circulation Systems, Synoptic Climatology and Weather Phenomena of South Africa. Part 6 Rainfall in South Africa. South African Weather Service Technical Paper, 32, South African Weather Service, Private Bag X97, Pretoria, 0001. 98pp

TENNANT, W.J. and HEWITSON, B.C. (2002). Intra-seasonal rainfall characteristics and their importance to the seasonal prediction problem. International Journal of Climatology, 22, pp. 1033-1048. DOI: 10.1002/joc.778.

TRIEGAARDT, D.O., VAN HEERDEN, J. and STEYN, P.C.L. (1991). Anomalous precipitation and floods during February 1988. South African Weather Service Technical Paper 23, South African Weather Service, Private Bag X97, Pretoria, 0001. 25pp

VAN DEN HEEVER, S.C., D'ABRETON, P.C. and TYSON, P.D. (1997). Numerical simulation of tropical-temperate troughs over southern Africa using the CSU RAMS model. South African Journal of Science, 93, pp. 359-365.

VILLARINI, G., KRAJEWSKI, W.F. Empirically based modelling of radar-rainfall uncertainties for a C-band radar at different timescales. Q.J.R. Meteorol. Soc., 2009; 1438: 1424-1438.

XU, X., SCANLON, B.R., SCHILLING, K., SUN, A. Relative importance of climate and land surface changes on hydrologic changes in the US Midwest since the 1930s: implications for biofuel production. Journal Hydrology, 2013; 497(8): 110-120.

WARBURTON, M.L., SCHULZE, R.E., JEWITT, G.P. Hydrological impacts of land use change in three diverse South African catchments. Journal of Hydrology, 2012, 414: 118-135.

WARD, F.A., LYNCH, T.P. Integrated River Basin Optimization: Modeling economic and hydrologic interdependence1. 1996, Wiley Online Library.

WASHINTON, R. and TODD, M. (1999). Tropical-temperate links in southern African and southwest Indian Ocean satellite-derived daily rainfall. International Journal of Climatology, 19, pp. 1601-1616.

WEATHER BUREAU (1991). Caelum – A History of Notable Weather Events in South Africa: 1500-1990. Department of Environmental Affairs.

WILLIAMS, F.R., RENARD, R.J., JUNG, G.H., TIMKINS, R.D. and PICARD, R.R. (1984). Forecasters Handbook for the Southern African Continent and Atlantic/Indian Ocean Transit. Department of Meteorology Naval Postgraduate School. Monterey, California

WILKS, D.S. (2011). Statistical Methods in the Atmospheric Sciences. Third edition. Elsevier Academi

WINSEMIUS, H.C., DUTRA, E., ENGELBRECHT, F.A., ARCHER VAN GARDEREN, E., WETTERHALL, F., PAPPENBERGER, F. and WERNER, M.G.F. 2(014). The potential value of seasonal forecasts in a changing climate in southern Africa. Hydrol. Earth Syst. Sci. 18 1525-1538.c Press. 265 California, USA.

WORLD METEOROLOGICAL ORGANIZATION (WMO). Limpopo River Basin: A Proposal to Improve the Flood Forecasting and Early Warning System. World Meteorological Organization (WMO) with the Support of Limpopo Water Course Secretariat and the Riparian States of Botswana, Mozambique, South Africa and Zimbabwe; WMO: Geneva, Switzerland, 2012.

ZAGAR, N., SKOK, G. and TRIBBIA, J. (2011). Climatology of the ITCZ Derived From ERA Interim Reanalyses. Journal of Geophysical Research, 116. DOI:10.1029/2011JD015695.